SYNTHESIS OF EARTH ABUNDANT, NON-TOXIC MIXED-METAL OXIDE CATALYSTS FOR CONVERSION OF RENEWABLE CARBON SOURCES TO DROP-IN FUELS

by

JUSTIN WILLIAM WEBER

(Under the Direction of James Kastner)

ABSTRACT

A 2-stage catalytic process for converting bio-oil oxygenates to higher value compounds for drop-in fuels was proposed. Ketonization using iron oxide catalysts prepared from red mud was implemented in a packed bed reactor system using model compounds. High levels of acetone (15-25 g/L), 2-butanone (~5 g/L), and cyclic ketones (9-13 g/L) were observed. Time-on-stream studies (8 h) indicated no measurable decline in conversion of acetol, formic acid, and levoglucosan, and only a 4% decline in acetic acid conversion. The effect of reduction pretreatment temperature on activity and surface properties of red mud was studied. Hydrogenation of ketonization products was conducted in continuous reactions using iron oxides and Pd-C catalysts. The best results were achieved in reactions using Pd-ACM (monoliths) at 180°C and 300 psi (H_2), which converted ketones to alcohols at ~60-80%. Pd-C monoliths achieved higher space time yields and conversions compared to Pd-C granules.

INDEX WORDS: Catalysis, Iron Oxides, Red Mud, Monoliths, Pyrolysis Oil, Ketonization, Hydrogenation, Continuous

SYNTHESIS OF EARTH ABUNDANT, NON-TOXIC MIXED-METAL OXIDE CATALYSTS FOR CONVERSION OF RENEWABLE CARBON SOURCES TO DROP-IN FUELS

by

JUSTIN WILLIAM WEBER

B.S. in Biochemical Engineering, University of Georgia, 2014

A Thesis Submitted to the Graduate Faculty of The University of Georgia in Partial Fulfillment of the Requirements for the Degree

MASTER OF SCIENCE

ATHENS, GEORGIA

2016

SYNTHESIS OF EARTH ABUNDANT, NON-TOXIC MIXED-METAL OXIDE CATALYSTS FOR CONVERSION OF RENEWABLE CARBON SOURCES TO DROP-IN FUELS

by

JUSTIN WILLIAM WEBER

Major Professor:	James Kastner
Committee:	Sudhagar Mani
	Aaron Thompson
	Eric Ferreira

Electronic Version Approved:

Suzanne Barbour
Dean of the Graduate School
The University of Georgia
May 2016

Table of Contents

List of Figures

List of Tables

List of Equations

Chapter 1 Project Summary

As increasing global energy demand and depleting fossil fuel reserves become growing concerns, alternative fuels derived from renewable biomass are gaining significant interest. The Environmental Sciences Division at Oakridge National laboratory conducted an analysis of all land resources available for bioenergy crop production. According to this study, there are 672 million acres of forest land and 448 million acres of agricultural land available in the United States that can be used for bioenergy crops. Utilizing this land, it was found that 1.367 billion tons of bioenergy crops for can be produced each year. This equates to over 100 billion barrels of biofuels that could be produced per year, which is approximately a third of the fuel consumption of the United States in 2005 (Perlack et al., 2005). In order to fully utilize this vast renewable resource as fuel source, technologies that convert biomass to useful fuels must be researched and further developed.

Fast pyrolysis is one of the main processes by which solid biomass is converted to liquid hydrocarbons. This process is highly favorable because it can generate oil at yields of up to 80% (Pham et al., 2013). In addition, many types of biomass can be used as feedstocks for fast pyrolysis, including woody biomass, grasses, and crop waste. Much research in the United States has focused on the use of Loblolly pine because of its abundance in the southeastern U.S. (Steele et al., 2012). However, pyrolysis oil contains highly acidic and reactive oxygenates (particularly carboxylic acids and aldehydes), that cause low energy density, poor stability, and make the oil difficult to store. These

characteristics make pyrolysis oil unsuitable for use as a liquid transportation fuel or co-processing with petroleum in existing refining infrastructure. Currently, the direct use of bio-oil is limited to boiler fuel. In order to utilize pyrolysis oil as a drop-in fuel, the reactive oxygenates that it contains must first be removed or converted to less reactive intermediates.

Many catalytic strategies for accomplishing this goal have been proposed in the literature, including hydrotreating, cracking, esterification, and aqueous phase processing. It is possible to remove nearly all of the oxygen in bio-oil through hydrodeoxygenation (HDO) at high temperatures and H_2 pressure (~400 °C, 1000 psi), but these conditions lead to extremely high processing cost, making them unfeasible (Zacher et al., 2014). Most catalytic upgrading strategies suffer from critical issues such as high processing cost (from high pressure H_2 requirements) or deactivation of expensive catalysts (through coke formation/poisoning). For these reasons, an inexpensive catalytic upgrading strategy that is effective and resistant to deactivation is needed.

Aqueous phase processing is one bio-oil treatment method that involves the separation of bio-oil into two phases through the addition of water. The problematic oxygenates partition into the aqueous phase, while heavy lignin components partition into the organic phase. Oxygenates in the aqueous phase can then be treated separately. Catalytic ketonization is a process by which reactive oxygenates in the aqueous phase can be treated. This reaction involves the coupling of two carboxylic acids to produce a ketone, carbon dioxide, and water. Unlike other aqueous phase treatments such as mild hydrotreating, ketonization produces compounds with longer carbon chain length and does not lose carbon through the formation of C_2-C_3 gases. Products from ketonization

have greater energy density and can be further upgraded to gasoline/diesel fuel through subsequent hydrogenation reactions to form alcohols and alkanes.

Ketonization of oxygenates in aqueous extracted bio-oil has been demonstrated using iron oxide catalysts, which are much less expensive than noble metals and other metal oxides. Kastner et al. (2015) demonstrate that iron oxide catalysts prepared from red mud bauxite refining waste can be used to selectively upgrade oxygenates in aqueous extracted pyrolysis oil to more stable compounds in a continuous process without the need for expensive hydrogen or noble metal catalysts. The primary products from ketonization reactions (acetone, 2-butanone, and cyclic ketones) can be further upgraded via hydrogenation to alcohols or alkanes. Catalysts prepared from red mud are highly stable in hydrogenation reactions, because they are not susceptible to poisons (Sushil & Batra, 2008). However, there has been little research investigating the hydrogenation of products formed from ketonization of water extracted bio-oil. Red mud catalysts typically exhibit lower activity than commercial catalysts because of poor surface properties, but these surface properties can be enhanced via physical or chemical pretreatments such as reduction via hydrogen. Thus, it is proposed that a detailed study on the effects of pretreatment and surface properties of iron catalysts for both ketonization and hydrogenation of bio-oil oxygenates would greatly expand the knowledge in the field of biofuel upgrading. In addition to iron oxides, palladium catalysts will be studied in the hydrogenation of ketone products in order to demonstrate the production of alcohols from aqueous extracted bio-oil in a 2-stage process. Findings in this study may help develop an economically feasible catalytic strategy for upgrading

oxygenates in pyrolysis oil, which would help transition away from non-renewable petroleum.

Chapter 2 Background and Literature Review

2.1 Fast Pyrolysis

Pyrolysis is the thermal decomposition of biomass that takes place in the absence of oxygen. Pyrolysis can be carried out using a wide range of reaction temperatures and residence times, and can produce liquids, gases, and coal. Fast pyrolysis, which takes place at shorter residence times (under 2 seconds) and at mild temperatures (approximately 500 °C), is of particular interest because it favors the production of liquid bio-oil and can achieve yields of up to 75% (Bridgwater, 2011). This oil contains a wide distribution of complex products, such as carboxylic acids, ketones, aldehydes, sugars, phenolics, furans, and lignin components. There has been a considerable amount of research focused on the use of fast pyrolysis oil directly, or as an intermediate that can be further processed for the production of chemicals, heat, and power.

While nearly any type of biomass can be used as a feedstock for fast pyrolysis, research in the United States often focuses on the use of Loblolly pine because it is highly abundant in the southeastern U.S. (Steele et al., 2012). For wood and most other feedstocks, grinding and drying operations are required before biomass is pyrolyzed to ensure proper heat transfer and to reduce the water content of the oil product.

Fast pyrolysis requires a reactor system that can provide high rates of heat transfer to ensure that thermal decomposition of the biomass takes place at around 500 °C, which maximizes liquid yield. Short residence times are also required to minimize unwanted

secondary reactions. For these reasons, continuous fluidized bed (CFB) reactors are commonly used to carry out fast pyrolysis. These reactor systems provide rapid heat transfer through the circulation of inert packing material, which contacts and rapidly heats the biomass feed. This rapid thermal heating results in a mixture of condensable vapors (~75%), solid biochar (~12%), and incondensable gases (~13%) (Bridgwater, 2011). Solid char particle byproducts are capable of catalyzing the cracking of the pyrolysis vapors. Because these cracking reactions are undesirable, the immediate separation of char from the vapor stream is important, and is typically accomplished through the use of cyclones or gas filters. This char contains a significant amount of energy (roughly 25% of the total biomass feed), and can be combusted to generate heat energy that can be recycled back into the process. Finally, the hot vapor stream is rapidly cooled and condensed to collect the liquid bio-oil product.

2.1.1 Treatment of Pyrolysis Oil

Currently, the end use of untreated or minimally treated pyrolysis oil is limited mainly to boiler fuel. There are many challenges associated with the use of pyrolysis oil for other purposes, such as transportation fuels. When using raw bio-oil directly as a liquid transportation fuel, studies have reported combustion difficulties, corrosion, clogging, coking, and engine seizure (Hossain & Davies, 2013). Pyrolysis oil has high water content (~25%) and has about half of the energy density of conventional fuel oil (~17 MJ/kg versus 40 MJ/kg) (Bridgwater, 2011). Also, pyrolysis oil contains a complex mixture of oxygenates, particularly carboxylic acids, aldehydes, ketones, sugars, phenolics, furans, guaiacols, and lignin oligomers. The presence of these oxygenates, especially the reactive acids, result in an oil that is acidic, corrosive, unstable, and is

unsuitable to be stored or processed using existing petroleum refining infrastructure. In addition, bio-oil is dissimilar to petroleum-derived fuel oil, with significantly higher viscosity (15-35 cp versus 3.0-7.5 cp), lower carbon content (56% versus 85%) and higher density (1.1-1.3 kg/L versus 0.89 kg/L) (Zacher et al., 2014). For these reasons, a significant portion of bio-oil research has been focused on bio-oil upgrading strategies that allow the bio-oil to be processed using existing petroleum refining infrastructure, specifically focusing on acidity, oxygen content, and stability of the bio-oil. There are many proposed strategies for integrating bio-oil and petroleum oil refining. One logical upgrading strategy is high temperature, high pressure hydrodeoxygenation (HDO) of bio-oil followed by hydrocracking to produce light fuel products. Deoxygenation values of up to 99.5% have been reported at 400 °C and 1000 psi of H_2 (Elliott et al., 2012). However, high temperature and pressure requirements translate to extremely high processing costs, making this strategy unfeasible. Instead, the extent of completeness of hydroprocessing needs to be balanced with the requirements of different insertion points into existing refinery infrastructure. Figure 2.1 shows some of the possible integration strategies and the generally accepted elements that are necessary to produce a liquid transportation fuel product.

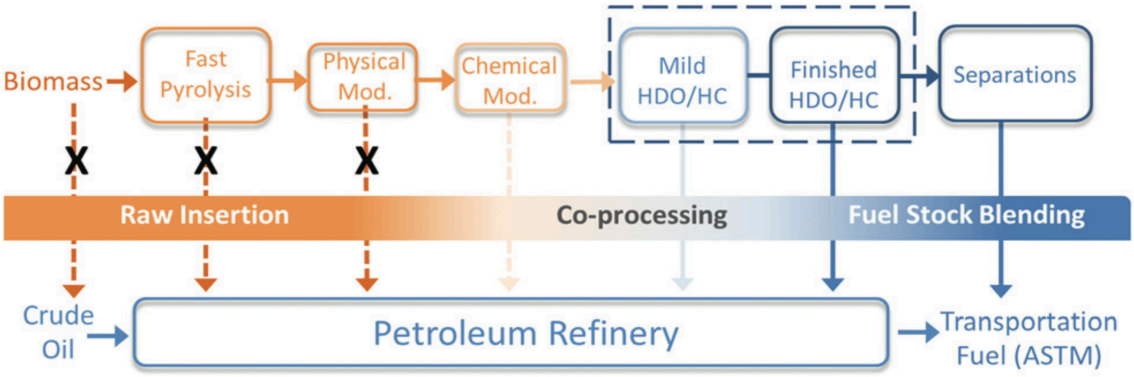

Figure 2.1 Integrating bio-fuels and petroleum refining (Zacher et al., 2014)

Figure 2.1 shows that the complexity of the bio-oil upgrading process depends on the targeted insertion point into the petroleum refinery, with early insertion being the least extensive. Theoretically, early insertion strategies would require the least amount of additional bio-oil processing and thus seem favorable. However, early insertion of raw or minimally processed bio-oil has been shown to cause major issues, even in robust unit operations such as fluidized catalytic crackers (FCC). One study reports clogging of nozzles, excessive coke deposition on the FCC catalyst, and lower gasoline yield when only 3% raw pyrolysis oil was co-fed into a FCC pilot unit (Bryden & Habib, 2013). Even early insertion strategies require treatment of the bio-oil feed. Upgrading strategies targeting insertion typically involve physical modification, chemical (catalytic) modification, or some combination of both.

Physical upgrading methods include solvent addition, filtration, emulsion, and phase separation unit operations. Solvent addition aims to decrease viscosity while increasing stability and homogenizing the oil. This is usually accomplished through the direct addition of methanol or ethanol, which has been shown to decrease the rate of secondary reactions that cause increases in viscosity over time (Bridgwater, 2011). This

method may allow for long-term storage of bio-oil. However, the large quantities of solvent required make this strategy less attractive. Filtration is a physical treatment that aims reduce the solid/char contaminates in the bio-oil. Filtering out char particles drastically reduces the concentration of alkali metals, which are concentrated within the char particles (Zacher et al., 2014). Removal of solid contaminants reduces secondary reactions that lead to low yields and unwanted byproducts. Filtration typically takes place in situ (before pyrolysis vapor is condensed) because filtration of the condensed viscous liquid is much more difficult due to high pressure drop and filter plugging. Gas filtration of pyrolysis oil has been shown to effectively reduce the ash content of the oil to less than 0.01%, which in turn increased the quality and yield of the liquid product (Bridgwater, 2011).

While physical treatments have been shown to increase the quality and usefulness bio-oil, physical treatments alone do not fully address the problems associated with the presence of oxygenates. Chemical and catalytic treatments better address these problems because they focus on the direct conversion of oxygenations to stabilize the bio-oil before final hydrotreating. Examples include esterification, ketonization, and catalytic transfer hydrogenation. Esterification aims to neutralize carboxylic acids by forming esters, typically with ethanol or methanol. Esterification activity has been demonstrated using acid, base, and ion exchange resin catalysts (Zacher et al., 2014). However, catalyst deactivation due to coke formation is a major concern.

2.1.2 Aqueous Phase Processing of Pyrolysis Oil

Phase separation of bio-oil can be induced by adding water, which separates the pyrolytic lignin (typically 15-25 wt% of the original bio-oil) from the alcohols,

aldehydes, ketones, acids, sugars, and lignin monomers which all partition into the aqueous phase (Zacher et al., 2014). The main advantage of phase separation is that the aqueous phase can be treated separately from the organic phase. Studies have demonstrated conversion of the organic phase to liquid hydrocarbons at high yields (78%) using HDO over commercially available sulphided CoMo catalysts (Piskorz et al., 1989). The aqueous phase containing the problematic oxygenates has been the focus of several studies. One study demonstrates that hydrogen and alkanes can be generated from aqueous extracted bio-oil (Vispute & Huber, 2009). In this study, water was added to fast pyrolysis oil to induce phase separation. The aqueous phase containing sugars, acetic acid, acetol, furfural, and trace amounts of guaiacols was then subject to a series of catalytic reactions using supported metal catalysts. The aqueous phase was first subject to low temperature hydrogenation with Ru/C catalyst, which converted aldehydes, acids, and sugars to corresponding alcohols as well as diols and sorbitol. These hydrogenated products were then used to produce hydrogen via aqueous phase reforming (APR) or alkanes via aqueous phase dehydration/hydrogenation (APD/H). APR was performed using 1 wt% Pt/Al_2O_3. This catalyst cleaves C-C bonds, generating CO, which is then converted to H_2 and CO_2 through the water-gas shift reaction. Hydrogen selectivity of 60% was achieved. APD/H was performed using 4 wt% Pt/SiO_2-Al_2O_3, a bi-functional catalyst containing metal sites (for hydrogenation activity) and acid sites (for dehydration activity). When hydrogen was co-fed, APD/H generated alkanes ranging from C_1-C_6 at selectivity of 77%. APD/H was then combined with APR, which provided an internal source of hydrogen, resulting in alkane selectivity of 45% (Vispute & Huber, 2009).

Vispute & Huber (2009) state that thermally unstable sugars such as levoglucosan and glucose must be converted to thermally stable compounds prior to aqueous phase processing, or they will cause coke formation that will deactivate the catalyst. This was achieved through the initial low temperature hydrogenation step. However, this low temperature hydrogenation resulted in loss of carbon through the production of unwanted methane gas, and consumed significant amounts of hydrogen. Converting all types of sugars and anhydrosugars to alcohols was cited as a major challenge of aqueous phase processing (Vispute & Huber, 2009). These challenges demonstrate the need for an improved catalytic strategy for converting oxygenates in the aqueous phase while retaining carbon, minimizing hydrogen consumption, and avoiding catalyst deactivation and coke formation.

2.1.3 Ketonization of Water Extracted Pyrolysis Oil Using Metal Oxides

Catalytic ketonization is an attractive strategy for upgrading oxygenates in aqueous extracted bio-oil that may address some of the challenges cited in Vispute & Huber (2009). Ketonization involves the coupling of two carboxylic acids to form a longer-chain ketone, releasing carbon dioxide and water. Ketonization removes oxygen without requiring a source of hydrogen and does not result in carbon loss via C_2-C_3 gases, making it a favorable alternative to the mild hydrogenation. Ketonization reactions produce compounds with higher chemical energy, lower oxygen content, and greater stability. In addition, ketones products have much greater flexibility for downstream processing than organic acids, and distillation of ketone products from water is economically feasible (Albrecht et al., 2015). Figure 2.2 shows several downstream processing options for further upgrading ketone products, including acid/base catalyzed

aldol condensation to fuel range hydrocarbons and noble metal catalyzed hydrogenation to alcohols or light olefins.

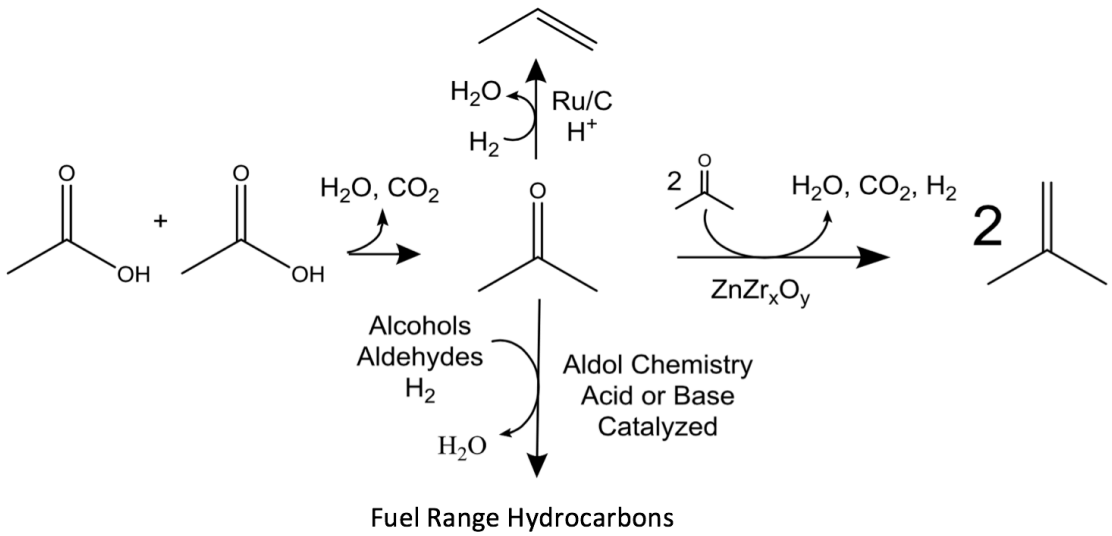

Figure 2.2 Downstream processing options of ketones (Albrecht et al., 2015)

Many oxide catalysts have been found to be active in ketonization reactions, including Fe_3O_4, Al_2O_3, MgO, TiO_2, ThO_2, UO_2, CdO, Bi_2O_3, ZnO, SnO_2 Cr_2O_3 (R. Pestman et al., 1997). There is still some debate in the literature concerning ketonization reaction mechanisms for different oxide catalysts. Several mechanisms have been proposed that involve either the formation of alkylidene or ketene intermediates (Karimi et al., 2012; R. Pestman et al., 1997). For iron oxide catalysts, ketonization is believed to take place through the initial dehydration of a carboxylic acid to its corresponding ketene, which reacts quickly with another carboxylic acid to form a ketone as shown in Figure 2.3 (Karimi et al., 2012). It is theorized that the Lewis acid sites stabilize surface

carboxylates (Resasco, 2011). Thus, reducibility and density of Lewis acid sites are important characteristics of metal oxides used for ketonization.

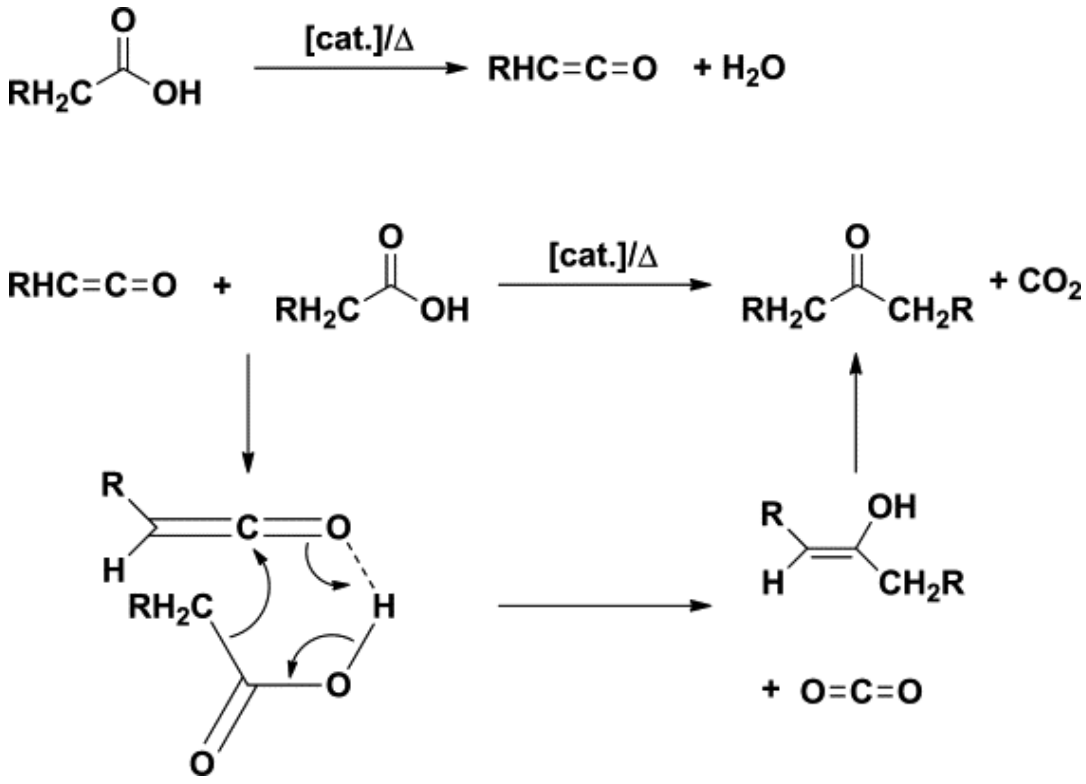

Figure 2.3 Ketonization reaction mechanism (Karimi et al., 2012)

Several metal oxides have been studied for ketonization of oxygenates in water extracted bio-oil including CeO_2, TiO_2, Fe_3O_4, and La_2O_3/ZrO_2 (Albrecht et al., 2015; Hakim et al., 2013; Kastner et al., 2015). The use of these metal oxides for bio-oil upgrading is especially attractive because of their significantly lower cost than noble metals. In addition, metal oxides are generally more resistant to deactivation than noble metals (Sushil & Batra, 2008). However, a major challenge of the use of metal oxides is that they generally suffer from lower activity and selectivity than more expensive

commercial catalysts. A recent study conducted at Pacific Northwest National Laboratory evaluated a series of catalysts for ketonization activity. Reactions were conducted in a packed bed reactor system at 300°C, 1350-1400 psi, and WHSV= 0.13-0.37 hr^{-1}. Out of 25 catalysts evaluated, La_2O_3/ZrO_2 achieved the highest reaction rate (0.15 mmol/g-cat/hr), conversion (25-40%), selectivity (45%) over the course of a 150-hour continuous reaction using acetic acid in water (Albrecht et al., 2015). However, lower activity was reported using "real feed" derived from biomass.

In another recent study, $CeZrO_x$ catalyst was used to ketonize a model compound mixture of acetic acid, acetol, furfural, and levoglucosan in a continuous reactor system (Hakim et al., 2013). The study explores how the presence of CeO_2, TiO_2, and ZrO_2 affect the activity and stability of the catalyst. Lewis sites on both CeO_2 and TiO_2 served as catalytic centers by stabilizing surface carboxylates, allowing them to pair. The addition of ZrO_2 disrupted the crystal structure of CeO_2, increasing the reducibility and thus the activity of the CeO_2. The presence of ZrO_2 also gives rise to aldol condensation activity and stabilizes the catalyst, which would otherwise deform at high temperatures. High levels of ZrO_2 may decrease the Lewis site density to a point at which carboxylate species do not pair, decreasing activity. Based on these theories, a ceria zirconia catalyst with composition $Ce_{.5}Zr_{.5}O_2$ was selected for optimal ketonization activity, aldol condensation activity, and catalyst stability. This catalyst showed nearly 100% conversion of carboxylic acids and 40% selectivity in a packed bed reactor system (Hakim et al., 2013). Results demonstrated how the presence of promoting metals increased catalyst stability, conversion, and ketone selectivity. However, levoglucosan

caused severe plugging of the reactor system due to thermal polymerization and had to be diluted to maintain operation of the packed bed reactor system.

2.1.4 Iron Oxide Catalysts Prepared from Red Mud

Iron oxides have also gained significant interest as catalysts for bio-oil upgrading. Iron oxide catalysts are made of earth-abundant materials, making them much less expensive than noble metals and most other metal oxides. One iron oxide catalyst that is of particular interest for ketonization of bio-oil oxygenates is red mud waste from bauxite refining. Red mud is a highly alkaline solid waste product generated in the manufacture of alumina by the Bayer process. This process consists of washing, grinding, and dissolving ore in sodium hydroxide at high heat and pressure. The resulting sodium aluminate liquor is further processed into aluminum, and the remaining solid waste (red mud) is disposed of in holding ponds (shown in Figure 2.4). Over 70 million tons of red mud waste is generated worldwide each year (Karimi et al., 2010). The use of this industrial waste as a replacement for commercial catalysts may drastically reduce the costs associated with catalytic upgrading of bio-oil to useable fuel.

Figure 2.4 Red mud holding pond near Stade, Germany (Boe, 2012)

Red mud is rich in metal oxides, particularly iron, aluminum, and titanium, and contains smaller amounts of silicon, calcium, and sodium. The applications of red mud as a catalyst have been presented in an extensive review by Sushil & Batra (2008). High concentrations of iron oxides (ranging from 15-40 wt%) can serve as catalytic centers for several reactions of interest including ketonization, hydrogenation, Fischer-Tropsch synthesis, and water gas shift reactions. Evidence has shown that red mud is highly stable and is not susceptible to catalyst poisons that deactivate noble metal catalysts such as sulfur. Pretreatment methods such as H_2 reduction or HCl activation can be used to activate the iron phase or increase surface area. Even after these minor treatments, red mud is still much cheaper than both noble metals and traditional metal oxides (Sushil &

Batra, 2008). This means that if irreversible deactivation by coke formation occurs, red mud can act as a sacrificial catalyst that is simply discarded and replenished.

Studies have been conducted using red mud to convert model compound mixtures of acetic acid, formic acid, and levulinic acid (Karimi et al., 2010; Karimi et al., 2012). It was demonstrated that hydrogen can be supplied internally via thermal decomposition of formic acid to CO and H_2O, followed by water gas shift forming CO_2 and H_2. Ketonization of carboxylic acids followed by iterative aldol condensation, hydrogenation, and deoxygenation reactions led to the formation of C_3-C_{10} hydrocarbons. Additional studies have demonstrated the potential advantages of co-processing whole bio-oil with red mud (Jollet et al., 2014; Karimi et al., 2014). Batch reactions using externally supplied hydrogen increased the value of both feed materials by reducing the oxygen content of the pyrolysis oil from 43.1% to 3.5% and simultaneously neutralizing the red mud, transforming it into a less hazardous waste product.

The studies mentioned have all used small batch reactor systems to study red mud as a catalyst for bio-oil upgrading. At present, there is insufficient research in the literature investigating the use of red mud for converting bio-oil oxygenates in continuous reactor systems. A continuous study using red mud has emerged in the literature only very recently (Kastner et al., 2015). In this recent study, red mud catalyst was used in a series of ketonization reactions in a packed bed reactor using a model compound mixture (acetic acid, formic acid, levoglucosan, and acetol) to represent key functional groups found in water-extracted bio-oil. In addition to high conversions, high levels of acetone (15-25 g/L), 2-butanone (~5 g/L), and cyclic ketones (9-13 g/L) were observed. Moreover, total ketone yields ranged from 16-27%, space time yields ranged from 40-70

g/L-cat/h, and oxidative thermogravimetric analysis indicated little coke formation on the recovered catalyst (Kastner et al., 2015). Red mud achieved lower acetone selectivity than $CeZrO_x$ in a similar study (18% vs 40%), but did not experience reactor plugging from levoglucosan (Hakim et al., 2013). It is postulated that this resistance to coke formation is due to the presence of alkali metals. Evidence in the literature indicates that iron oxides doped with K, Ca, and Na generate highly active and stable catalysts for CO and CO_2 hydrogenation to hydrocarbons (Dorner et al., 2009). These alkali metals promote the formation of iron nanoparticles without sintering, prolonging activity and shifting selectivity to $>C_2$ hydrocarbons. Additional studies on the stability of iron oxides catalysts prepared from red mud in continuous upgrading of bio-oil oxygenates are needed.

2.2 Hydrodeoxygenation (HDO)

Most of the undesirable properties of bio-oil stem from its high oxygen content. Even when treatment methods discussed earlier are utilized, ultimately fast pyrolysis oil requires hydrodeoxygenation (HDO). Hydrodeoxygenation (the removal of oxygen using hydrogen) involves the following 6 key classes of reactions.

(1) **Hydrogenation**: The hydrogenation of C=O bonds producing alcohols. Noble metals, Ni, Cu, and Co exhibit high hydrogenation activity. Aldehydes, ketones, esters, and carboxylic acids can all be hydrogenated (listed in order of decreasing activity). Catalysts that contain metal and acid sites can also hydrogenate C=C bonds, producing stable alkanes, making them extremely useful in bio-oil upgrading reactions (Nakagawa et al., 2015). See Figure 2.5-a.

(2) **Dehydration of Alcohols**: The dehydration of alcohols dissociates C-O bonds, producing alkenes. Strong Brønsted acid sites catalyze the dehydration of alcohols (Nakagawa et al., 2015). See Figure 2.5-b.

(3) Acid-catalyzed conversion of ethers: The dissociation of C-O bonds in ethers is possible using acid catalysts, although these reactions are rarely utilized because of harsh conditions that can cause dissociation of C-C bonds. See Figure 2.5-c.

(4) Metal Catalyzed C-O dissociation: The dissociation of C-O bonds in both alcohols and ethers can be catalyzed on metal sites (Pt-Re, Pt-W, Rh-Mo, Pt, Ru). The noble metal activates H_2, while a group 6 or 7 element activates the substrate (Nakagawa et al., 2015). See Figure 2.5-d.

(5) C-C Dissociation (Hydrocracking): C-C dissociation can take place via carbocation formation or direct metal-catalyzed C-C dissociation (Ru, Ir, Rh). In many cases, C-C dissociation is unfavorable, because decreasing the length of the carbon chain is not desired. Some C-C dissociation is inevitable when conducting acid-catalyzed reactions at high temperatures (Nakagawa et al., 2015). See Figure 2.5-e.

(6) **Decarboxylation and decarbonylation:** These reactions involve C-C dissociation in a functional group at a terminal position. Decarboxylation can take place on carboxylic acids, esters, and lactones, and produces CO_2. Decarbonylation takes place on aldehydes and produces CO. CO_2 and CO can be interchanged via the water-gas shift reaction that takes place on metal catalysts. In addition, metal catalysts may reduce CO_x in the presence of H_2 to methane gas. Acids, bases, or transition metals can catalyze decarboxylation, whereas

decarbonylation is typically catalyzed by a metal surface (Nakagawa et al., 2015). Both reactions are typically more desirable in fuel upgrading than hydrocracking reactions because they remove oxygen without a significant loss of carbon chain length. See Figure 2.5-f.

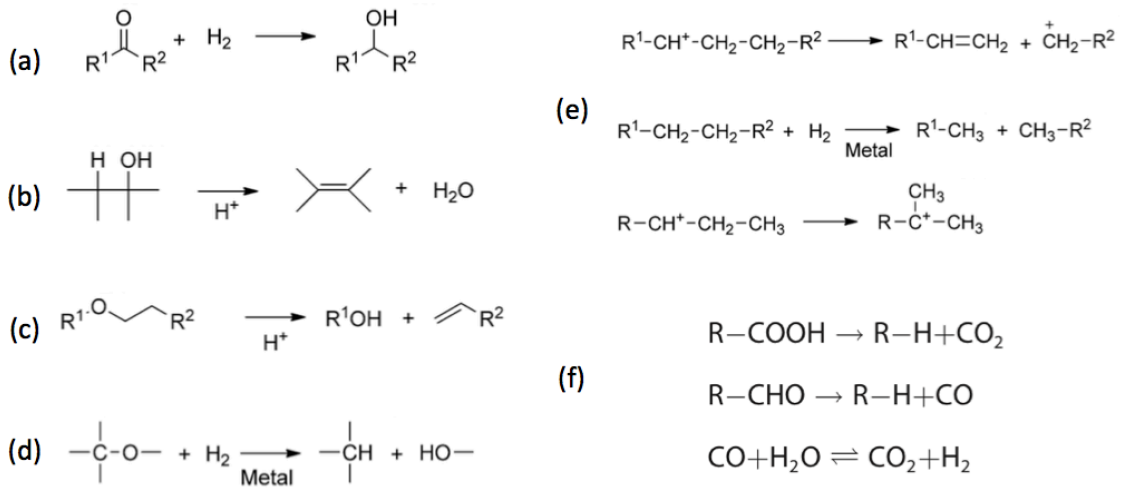

Figure 2.5 HDO reaction mechanisms (Nakagawa et al., 2015)

2.2.1 HDO Using Iron-Based Catalysts

One of the main challenges of upgrading bio-oil through HDO is catalyst deactivation through coke formation and poisoning. Coke formation is common when dealing with highly unsaturated substrates, like those found on bio-oil. Increasing H_2 pressure generally reduces coke formation, but can significantly increase processing costs. In addition, the presence of inorganics in bio-oil, particularly sulfur and phosphorous can poison noble metal catalysts (Nakagawa et al., 2015). Iron oxides are of significant interest because they are far less expensive than noble metals and more

resistant to deactivation. Many studies have demonstrated the activity of iron-based catalysts for hydrodeoxygenation. One study demonstrates the selective hydrogenation of acetic acid over a series of non-reduced and pre-reduced iron oxide catalysts. Pre-reduction of pure Fe_2O_3 catalyst using H_2 at 450 °C resulted in partial reduction of Fe_2O_3 (hematite) to metallic (zerovalent) Fe, which increased selectivity for acetaldehyde formation from acetic acid (R. Pestman et al., 1998). It is theorized that the reaction takes place on the oxide phase via the reverse Mars-van Krevelen mechanism (see Figure 2.6). First, hydrogen reduces the metal oxide resulting in oxygen vacancy sites. A carboxylic acid then binds to a vacancy site. The vacancy site is re-oxidized by an oxygen atom on the binding carboxylic acid. Activated hydrogen chemisorbed on the metal surface reduces the carboxylic acid and the resulting aldehyde desorbs. Hydrogen can then re-reduce the metal oxide, regenerating the vacancy site. Thus, reactions following the reverse Mars-van Krevelen mechanism require reducible oxide sites, hydrogen to reduce and regenerate oxygen vacancy sites, and metal sites that can activate hydrogen on the surface in close proximity to oxygen vacancy sites.

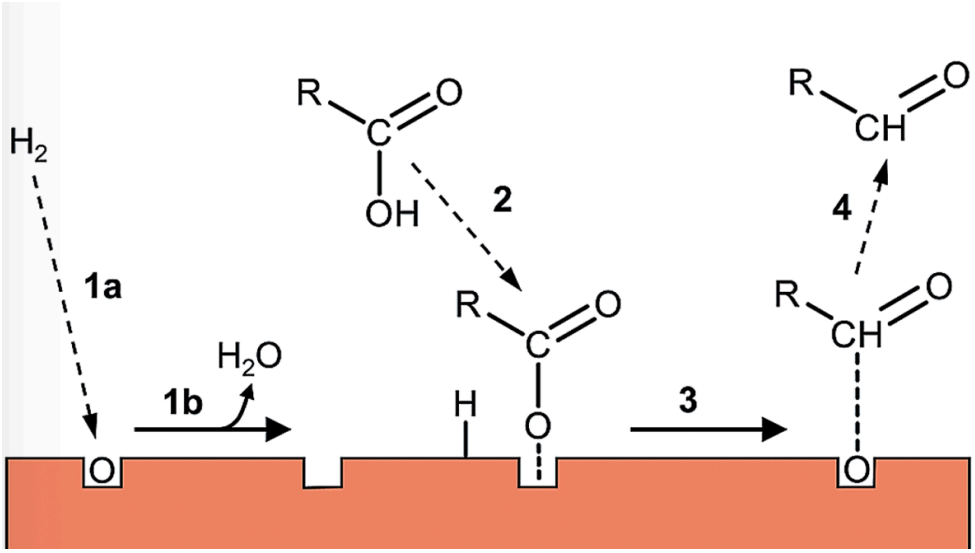

Figure 2.6 Reverse Mars-van Kevelen Mechanism. Hydrogen reduces the metal oxide site (1a) releasing water and creating an oxygen vacancy site (1b). The vacancy site is re-oxidized by an oxygen atom on the binding carboxylic acid (2). Hydrogen chemisorbed on the surface binds to the carbon atom (3), relasing the aldehyde (4) (Hargus et al., 2014).

Additional studies have demonstrated the activity of iron-based catalysts for hydrodeoxygenation of lignin pyrolysis vapors (R. Olcese et al., 2013; R. N. Olcese et al., 2013). In one study, Fe/SiO_2 (15 wt%) and Fe/AC (10 wt%) were used to improve the quality of pyrolysis oil by catalyzing hydrodeoxygenation reactions of pyrolysis vapor in-line (before condensation of pyrolysis products) (R. N. Olcese et al., 2013). The Fe catalysts were pre-reduced at 500 °C, and then subsequently re-reduced in-situ at 400 °C. Hydrogenated products from lignin included benzene, toluene, xylenes, phenol and cresols. Fe/SiO_2 selectively catalyzed hydrogenolysis of C-O bonds while avoiding unwanted cracking and hydrogenation of C-C bonds. The overall quality of the condensed bio-oil was improved significantly. As expected, significant coke formation on the catalyst was observed. Olcese et al. (2013) argue that deactivation of the catalyst is not of significant concern, because iron-based catalysts are environmentally friendly

and inexpensive. However, the need to frequently regenerate or replace catalysts is considered to be unfavorable.

2.3 Simultaneous Ketonization/Hydrogenation of Aqueous Oxygenates using Iron-Based Catalysts

In the previous section, water extraction followed by catalytic ketonization of oxygenates in the aqueous phase as a bio-oil upgrading strategy was explored. The ketone products of catalytic ketonization can then be hydrogenated to form alcohols and alkanes using a catalyst that exhibits hydrogenation activity. It is theorized that the same iron-based mixed metal oxide catalyst used to ketonize aqueous phase oxygenates in Kastner et al. (2015) could exhibit hydrogenation activity necessary to hydrogenate the ketone products. Similar iron oxide catalysts that contained zero valent iron successfully catalyzed the hydrogenation of acetic acid (R. Pestman et al., 1998). Hydrogenation of the ketone products from Kastner et al. (acetone, 2-butanone, cyclopentatones) should be easier to hydrogenate, since ketones typically show higher hydrogenation activity than carboxylic acids (Nakagawa et al., 2015). For these reasons, it is hypothesized that a reduction treatment resulting in a mixture of magnetite and zero valent iron could result in an iron catalyst that is capable of simultaneously ketonizing carboxylic acids and then hydrogenating ketone products. Such a catalyst would provide an inexpensive and effective strategy for upgrading aqueous extracted bio-oil to alcohols and alkanes while retaining carbon and minimizing catalyst deactivation.

2.4 Heterogeneous Catalysis Using Monolith Technology

Slurry reactors (batch) and fixed-bed reactors (continuous) are the two most commonly used reactor systems for heterogeneously catalyzed reactions in industry today. Continuous packed bed systems have several obvious advantages over batch systems, such as the low operating cost, simple design, and no catalyst separation required. However, larger catalyst particle sizes that are required in fixed-bed reactors are often less desirable for reactions rates and selectivity. In addition, multiphase-flow and turbulence in porous media are often difficult to model and lead to unpredictability. Monolith catalysts aim to address some of these issues. Monoliths are made up of a large number of parallel channels, resulting in laminar flow that is easy to model, and maximizes mass transfer. Monoliths can be formed using a wide variety of materials, such as carbon, ceramic, and metals. High transport rates can be achieved without using small particle catalysts, which result in pressure drop issues. These high transport rates often translate to more selective catalysts (Moulijn et al., 2014). Figure 2.7 shows a typical design of a monolith catalyst.

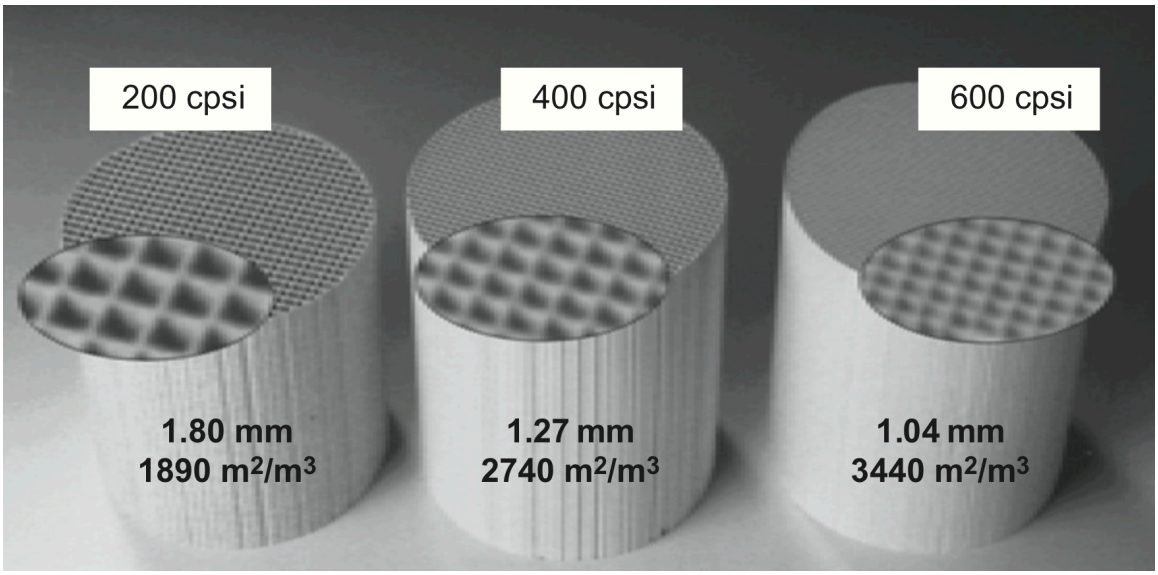

Figure 2.7 Monolith catalysts (Moulijn et al., 2014)

Reactions involving gas-liquid mixtures using monoliths can exhibit a variety of flow patterns depending on the ratio of gas to liquid flow (see Figure 2.8). The two flow patterns of most interest are Taylor flow and film flow. In Taylor flow, gas and liquids move through monolith channels in segments, resulting plug-flow behavior. Film flow occurs at high gas flow rates when liquid coats the channel walls, allowing gas to flow through at higher velocities.

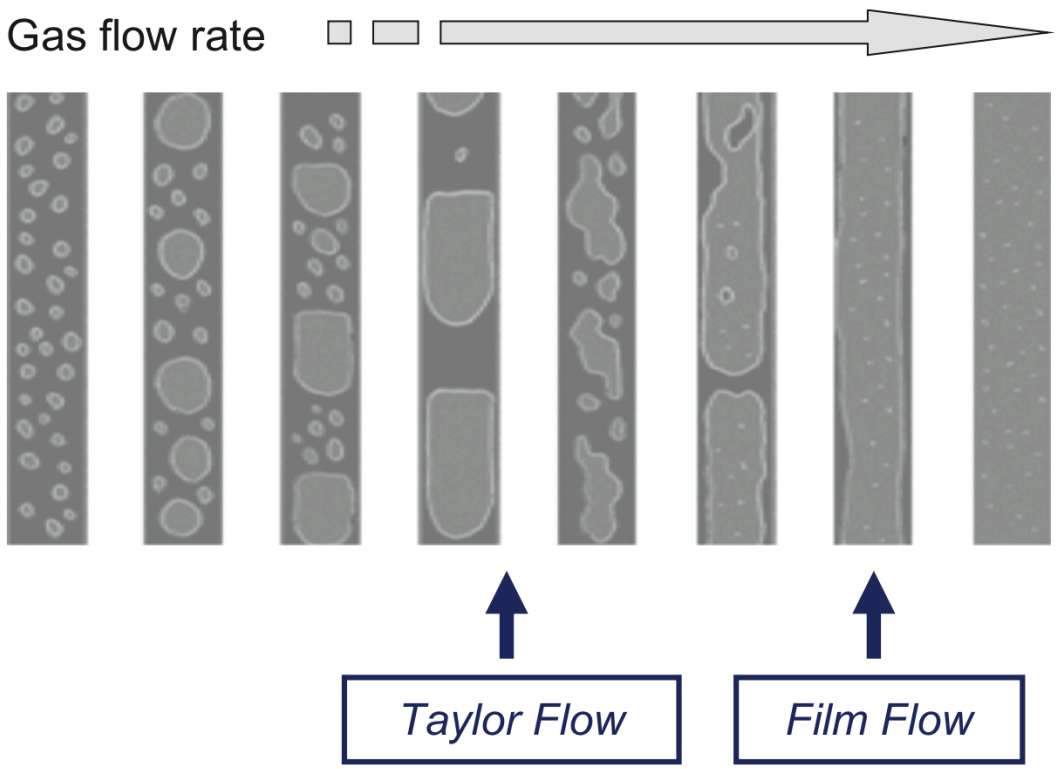

Figure 2.8 Flow regimes inside monolith channels (Moulijn et al., 2014)

Chapter 3 Rationale

In the previous chapter, several challenges that limit the direct use of pyrolysis oil as a liquid fuel were discussed. These challenges such as low energy density, high oxygen content, high acidity, and poor stability are caused mainly by the oxygenates present (particularly carboxylic acids and aldehydes). A catalytic strategy for converting these oxygenates into useful products is needed. Many strategies for accomplishing this goal have been proposed in literature, but most of these upgrading strategies suffer from at least one of the critical issues mentioned earlier, such as high processing cost (from high pressure H_2 requirements), deactivation of expensive catalysts (through coke formation/poisoning), or inadequate conversion to desired products (from poorly active/selective catalysts). Catalytic ketonization of water extracted bio-oil using metal oxide catalysts is one upgrading strategy that is of particular interest, because this process converts oxygenates to stable, higher value products without expensive noble metals or hydrogen requirements. Several studies have demonstrated that inexpensive iron oxide catalysts prepared from red mud can convert bio-oil oxygenates to more valuable products with greater energy density and stability (Karimi et al., 2010; Karimi et al., 2014; Karimi et al., 2012). Previous studies with red mud have been conducted in small batch reactors, and there is insufficient research in the literature investigating the use of red mud to convert bio-oil oxygenates in continuous systems.

One recent study has demonstrated ketonization of aqueous extracted bio-oil using red mud in a continuous reactor system (Kastner et al., 2015). In this study, red mud

showed ketonization activity similar to that of $CeZrO_x$, and did not experience significant coke formation and reactor plugging due to the presence of levoglucosan (Hakim et al., 2013). The stability, cost, and abundance of iron oxide catalysts prepared from red mud provide rationale for further study of these catalysts in continuous reactor systems.

The ketone products formed via ketonization of aqueous extracted bio-oil can be further upgraded via hydrogenation to alcohols and olefins for drop-in fuels. Continuous hydrogenation studies have been conducted using a variety of metal oxide catalysts (Cr, Fe, Co, Ni, Cu, and Pd, supported on SiO_2 and Al_2O_3) (Narayanan & Unnikrishnan, 1998; Witsuthammakula & Sooknoi, 2015). These studies have focused on hydrogenation of individual model compounds (acetone, 2-butanone, cyclohexanone). Additional research is needed investigating hydrogenation of mixtures of these ketones, which are more representative of the actual liquid products from ketonization of water extracted bio-oil.

It has been demonstrated in the literature that catalysts prepared from red mud are highly stable in hydrogenation reactions, because they are not susceptible to poisons (Dorner et al., 2009; Sushil & Batra, 2008). Yet there has been little research investigating the hydrogenation of products formed from ketonization of water extracted bio-oil in continuous systems. Simultaneous ketonization and hydrogenation of the ketone products (acetone, 2-butanone, and cyclopentatones) using iron oxide catalysts may be possible if (1) the catalyst possesses an optimal ratio of magnetite to zerovalent iron, which are required to stabilize surface carboxylates and activate hydrogen, respectively, and (2) hydrogen partial pressure is sufficient [supplied externally or internally via transfer hydrogenation of formic acid, as demonstrated by Karimi et al. (2010)]. Red mud catalysts typically exhibit lower activity than commercial catalysts

because of poor surface properties, but these surface properties can be enhanced using a variety of chemical pretreatments including hydrogen reduction, which activates the iron phase for hydrogenation (Sushil & Batra, 2008).

Thus, there is motivation to explore the use of iron oxides for ketonization and hydrogenation of aqueous extracted bio-oil in a continuous process. A detailed study focusing on the effects of reduction pretreatment and surface properties of red mud catalysts for both ketonization and hydrogenation of bio-oil oxygenates is presented. In addition, this study includes hydrogenation of ketone product mixtures using commercial noble metal catalysts, including activated carbon monoliths, which have not been previously studied in continuous reactions with aqueous extracted bio-oil.

Obtaining continuous catalytic transformation data is essential in order to evaluate the feasibility of using metal oxides for catalytic upgrading of bio-oil at the industrial scale. The knowledge gained in this study may contribute to the development of a continuous 2-stage ketonization/hydrogen process to convert bio-oil oxygenates to more valuable products in a manner that is efficient, inexpensive, and avoids catalyst deactivation. This catalytic strategy has the potential to increase the economic feasibility of lignocellulosic-derived bio-fuels as a replacement to non-renewable petroleum. Transitioning from non-renewable fuel sources to renewable biomass-derived fuels carries broad impacts such as increased economic competitiveness of the United States, improved national security, and improved well being of individuals in society.

Chapter 4 Experimental Approach

4.1 Experimental Plan

4.1.1 Ketonization Studies Using Red Mud

Studies were conducted in order to investigate the catalytic properties of mixed metal oxide catalyst synthesized from red mud for ketonization of bio-oil oxygenates. Model compound mixtures of acetic acid, formic acid, acetol, and levoglucosan (4% each in H_2O) were prepared to represent key oxygenates in water extracted fast pyrolysis oil. Reactions were then carried out in a continuous packed bed reactor system (outlined in section 4.2.2) using red mud that was pre-reduced at 300 °C (RRM-300). Catalysts were characterized before reduction, after reduction, and after use in continuous reactions using methods outlined in section 4.2.4. The effect of temperature on catalytic ketonization of the model compound mixture was studied by varying the reaction temperature from 350 °C to 425 °C. The effect of catalyst weight to flow ratio (W/F) was studied by varying the mass of catalyst used from 5- 20 g. Gas and liquid products of the reactions were collected and analyzed according to procedure outlined in section 4.2.3.

4.1.2 Longevity Studies Using Red Mud

A catalyst longevity (time-on-stream) study was conducted using RRM-300 and the best conditions for ketonization determined in the previous study. The purpose of this

study was to investigate any changes in ketonization activity or surface properties of red mud throughout the course of its use in ketonization reactions. The reaction lasted approximately 400 minutes (6.67 hours) at 400 °C using 20 grams of RRM-300. Liquid and gas products were sampled every 100 minutes. Liquid and gas products were then analyzed according to the procedure described in section 4.2.3. The catalyst was characterized before and after the reaction using the methods in section 4.2.4.

4.1.3 The Effect of Reduction Pretreatment Temperature on Activity and Surface Properties of Red Mud

The effect of hydrogen reduction pre-treatment temperature on the activity and surface properties of red mud were investigated. Evidence in the literature suggests that the presence of zero valent iron in reduced red mud may promote hydrogenation activity (R. Pestman et al., 1998). In addition, decomposition of formic acid may provide an internal source of hydrogen needed for hydrogenation reactions to take place (Karimi et al., 2010). Thus, it was theorized that simultaneous ketonization and hydrogenation may be possible using red mud reduced at higher temperatures. Three different catalysts were prepared from red mud (RRM-300, RRM-400, RRM-500) via reduction in pure hydrogen at 300, 400, and 500 °C. Catalysts were characterized before and after reduction to determine the effect of reduction temperature on iron valence state, reducibility, base site density, and surface area. Each catalyst was used in a series of ketonization reactions using the model compound mixture and best conditions determined in section 5.2.1 (T= 400 °C, P= atm (N_2), 5 g catalyst). In addition to red mud reduced at three different temperatures, Fe_2O_3 supported on carbon nanoparticles and HCl-treated red mud were tested for comparison.

4.1.4 The Effect of Pressure and Externally Added Hydrogen on Ketonization/Hydrogenation Activity of Red Mud

It has been demonstrated that hydrogen can be produced internally via decomposition of formic acid to H_2O and CO followed by water gas shift to form CO_2 and H_2 (Karimi et al., 2010). Internally generated hydrogen may have a role in the formation of several major products including 2-butanone, 2-pentanone, and cyclopentanone. However, it is unlikely that low hydrogen partial pressure at atmospheric conditions would lead to significant hydrogenation of ketones. It was theorized that increasing hydrogen availability may lead to simultaneous hydrogenation of ketone products to alcohols, and increase selectivity for 2-butanone, 2-pentanone, and cyclopentanones.

In order to test this hypothesis, ketonization studies using red mud were conducting at elevated pressures. First, reactions using RRM-300 (T= 400 °C, LHSV= 5.646 1/hr) at varying N_2 pressure (1 atm-600 psi) were conducted. In addition, reactions where hydrogen was added externally (at 1 atm) were also conducted. These purpose of these reactions using RRM-300 was to first understand the effect of total pressure and hydrogen availability on the formation of ketonization products (particularly 2-butanone, 2-pentanone, and cyclopentanones).

Subsequent ketonization reactions were conducted using RRM-400 and RRM-500 in pure hydrogen. Due to the presence of zero valent iron in red mud reduced at 400 and 500 °C, it was hypothesized that ketone products (acetone, 2-butanone, and cyclic ketones) could be simultaneously hydrogenated to alcohols. These reactions were

conducted at atmospheric pressure, 150 psi, and 300 psi (H_2) using the following conditions: T= 400 °C, WHSV = 0.89 g/g-cat/hr, LHSV= 5.65 hr^{-1}.

4.1.5 Ketonization using Fe-SiAl

The high yields of acetone, 2-butanone, and cyclic ketones that were achieved in ketonization using red mud provided reason to test other iron oxide catalysts with similar elemental composition. Commercial iron oxides are known to have much higher surface area than iron oxides prepared from red mud (Sushil & Batra, 2008). In addition, the use of chemically-defined iron oxides may be favorable over catalysts prepared from ill-defined media, which can have varying properties depending on the source.

Thus, defined iron oxide catalysts were synthesized on silica alumina support (outlined in section 4.2.1.3). Silica alumina was chosen as a supporting material to represent to high concentrations of silicon dioxide and aluminum oxides found in red mud. Ketonization activity of Fe-SiAl was determined in a packed bed reactor system using the optimal reaction conditions determined in ketonization studies using red mud (section 5.2.1). The following reaction conditions were used: T= 400 °C, P = atm (N_2), WHSV= 5.646 1/hr. The Fe-SiAl catalyst was reduced at 300 °C in situ for 20 hours prior to reactions.

4.1.6 Hydrogenation Studies using Pd-C Monoliths

Hydrogenation studies were conducted to demonstrate that the mixture of ketone products generated in the previously described ketonization reactions can be further upgraded to higher value chemicals in a continuous reactor system. The advantages of monoliths over traditional granular catalysts are numerous (Moulijn et al., 2014).

However, few studies have focused on the use of monoliths for upgrading of oxygenates in water extracted bio-oil. Thus, the use of Pd supported on activated carbon monoliths (Pd-ACM) was chosen for hydrogenation studies. Pd-C monolith cores (0.8 wt% Pd loading, 1-inch diameter) were provided by Applied Catalysts (further described in section 4.2.1.5). Model compound mixtures representing the primary products from ketonization reactions were prepared. This mixture consists of acetone (2%), 2-butanone (0.5%), cyclopentanone (0.75%) and 2-cylcopenten-1-one (0.75%) in water. Model compounds and their concentrations were selected based on the products generated in ketonization reactions using RRM-300 (in section 5.2.1).

The effects of pressure and temperature on hydrogenation activity of Pd-ACM catalysts were tested. Six 1-inch cores (21.8 g) were loaded into the packed bed reactor vessel and used for all hydrogenation experiments without replacement. A thin layer of quartz wool was wrapped around the circumference of each core prior to loading to ensure tight packing and minimize any bypassing around the outside of the cores. The catalyst was then reduced in situ at 500°C in pure H_2 for 20 hours. Reactions were conducted using the following conditions: T= 130-180 °C, P= 1 atm-300 psi (H_2), WHSV= 0.0538 hr^{-1}, LHSV 0.389 hr^{-1}.

4.1.7 Hydrogenation Studies Comparing Pd-ACM and Granular Pd-C

Reactions were conducted in order to compare the hydrogenation activity of Pd-C monoliths (Pd-ACM) with that of granulated Pd-C. Granulated Pd-C (5 wt% Pd loading, particle size <0.5mm) was purchased from Alfa Aesar. Each catalyst was tested in a series of continuous reactions at varying liquid hour space velocity (LHSV). Reactions were conducted using the best reaction conditions determined in section 5.3.1 and section

5.3.2 (180 °C, 300 psi), using ketone model compound mixtures (acetone, 2-butanone, cyclopentanone). Liquid hourly space velocity was varied by varying the reactant feed rate from 0.5 mL/min to 8.0 mL/min.

4.1.8 Hydrogenation Studies Using Red Mud and Fe-SiAl

Studies described in sections 4.1.3 - 4.1.4 explored RRM and Fe-SiAl for simultaneous ketonization/hydrogenation of acetic acid, formic acid, acetol, and levoglucosan. Additional reactions were conducted with RRM and Fe-SiAl using ketone model compounds (acetone, 2-butanone, and cyclopentanone) in order to study hydrogenation only. Red mud and Fe-SiAl were pre-reduced at 400°C and 500°C and used in hydrogenation reactions using the following conditions: P= 300 psi (H_2), reaction temperature= 400 °C, WHSV= 0.1262 hr^{-1}.

4.1.9 2-stage Ketonization/Hydrogenation Studies

The previously mentioned hydrogenation reactions used aqueous model compound mixtures of acetone, 2-butanone, and cyclopentanones to represent the primary products formed in ketonization reactions. 2-stage experiments were then conducted that used actual liquid products generated in ketonization reactions as feedstocks for hydrogenation reactions. The best reaction conditions determined from ketonization studies in section 5.2.1 were used for stage 1 (RRM-300, T= 400°C, P= atm (N_2), WHSV = 0.21 g/g-cat/hr, LHSV= 1.41 hr^{-1}). A model compound mixture (150 g) containing acetic acid, formic acid, acetol, and levoglucosan (4% each) was fed into the continuous reactor for 5 hours. The catalyst was previously shown to be stable over this length of time (in section 5.2.2). Liquid products from the reaction were collected and

stored overnight. A subsample was analyzed via GC-FID and HPLC. Liquid products were then fed into 2nd stage hydrogenation reactions using Pd-C and Pd-ACM at the best reaction conditions determined in sections 5.3.2 and 5.3.3 (T= 180 °C, P= 300 psi (H_2), LHSV= 0.78 hr^{-1}). Conducting ketonization and hydrogenation in one continuous process using two catalyst beds is desired. However, this was not possible using the available facilities, because reaction temperature and pressure could not be controlled for each catalyst bed independently.

4.2 Methodology and Experimentation

4.2.1 Catalyst Preparation

4.2.1.1 Red Mud

Red mud was obtained from Rio Tinto (Alcan, Canada). The wet slurry was dried at 105 °C for 20 hours, and then crushed using a hammer. The resulting granules were sieved into two fractions (0.5-2.0 mm and <0.05mm).

4.2.1.2 HCl-Treated Red Mud

Acid pretreatment was conducted by The Energy and Resources Institute (TERI) using the following procedure. Red mud from Belgaum, India (10 g) was dried and sieved (< 200 μm) and then mixed with 190 mL of distilled water. The mixture was stirred for 5 minutes using a magnetic stirrer. HCl (34 mL, 37%) was then added and stirring was continued at 95 °C for approximately 8 hours (until white residue was obtained). The liquid was separated from the residue and aqueous ammonia was added to the liquid drop-wise while stirring until a pH of 8 was reached. The resulting precipitate

was centrifuged and washed with warm distilled water to remove residual chlorine. The separated precipitate was dried at 95-110 °C in an oven for 12 hours.

4.2.1.3 Fe-SiAl (10 %wt Fe)

Nonahydrate $Fe(NO_3)_3$ (36.17 g) was dissolved in 10 mL of deionized water. The dissolved solution was then added drop wise to 45 g of SiAl catalyst support (calcined, fine particles provided by Sigma Aldrich). Deionized water (47 mL) was then added and allowed to soak for 24 hours. The wet slurry was then dried at 105 °C for 24 hours. The resulting solid was crushed into a fine powder and calcined at 300 °C using an air flow rate of 100 mL/min for 18 hours.

4.2.1.4 Fe_2O_3-C (Fe on Activated Carbon)

Fe_2O_3-C catalyst was prepared by deposition of iron oxide nanoparticles on carbon support using the supercritical water method described in the literature (Xu & Teja, 2006). A solution of $Fe(NO3)3.9H2O$ (Sigma-Aldrich) was prepared in deionized water (0.5 M). Activated carbon pellets (30.3 g, Sigma-Aldrich) were added to 150 mL of the iron salt solution, followed by sonication for 45 minutes at room temperature. The mixture was then allowed to soak for 5 days. The mixture was then treated under helium gas in a high-pressure reactor system (Parr Instrument Company). The reactor was loaded at 750 psi and 17 °C. Temperature was then increased to 355 °C, resulting in a final pressure of 4050 psi. These conditions were maintained for 90 minutes, followed by cooling to 33 °C. The solid activated carbon pellets were then separated and washed with deionized water and then dried at 105 °C overnight.

4.2.1.5 Pd-C Monolith (Pd-ACM)

All monolith catalysts were supplied by Applied Catalysts with the following properties: diameter = 1 in, core length = 1 in, 529 cells/in^2, wall thickness = 0.01 in, cell spacing= 0.0435 in, geometric surface area= 70.84 in^2/in^3, open frontal area = 0.593 in^2, Pd loading= 0.8 wt%. Figure 4.1 shows three unused Pd-ACM cores.

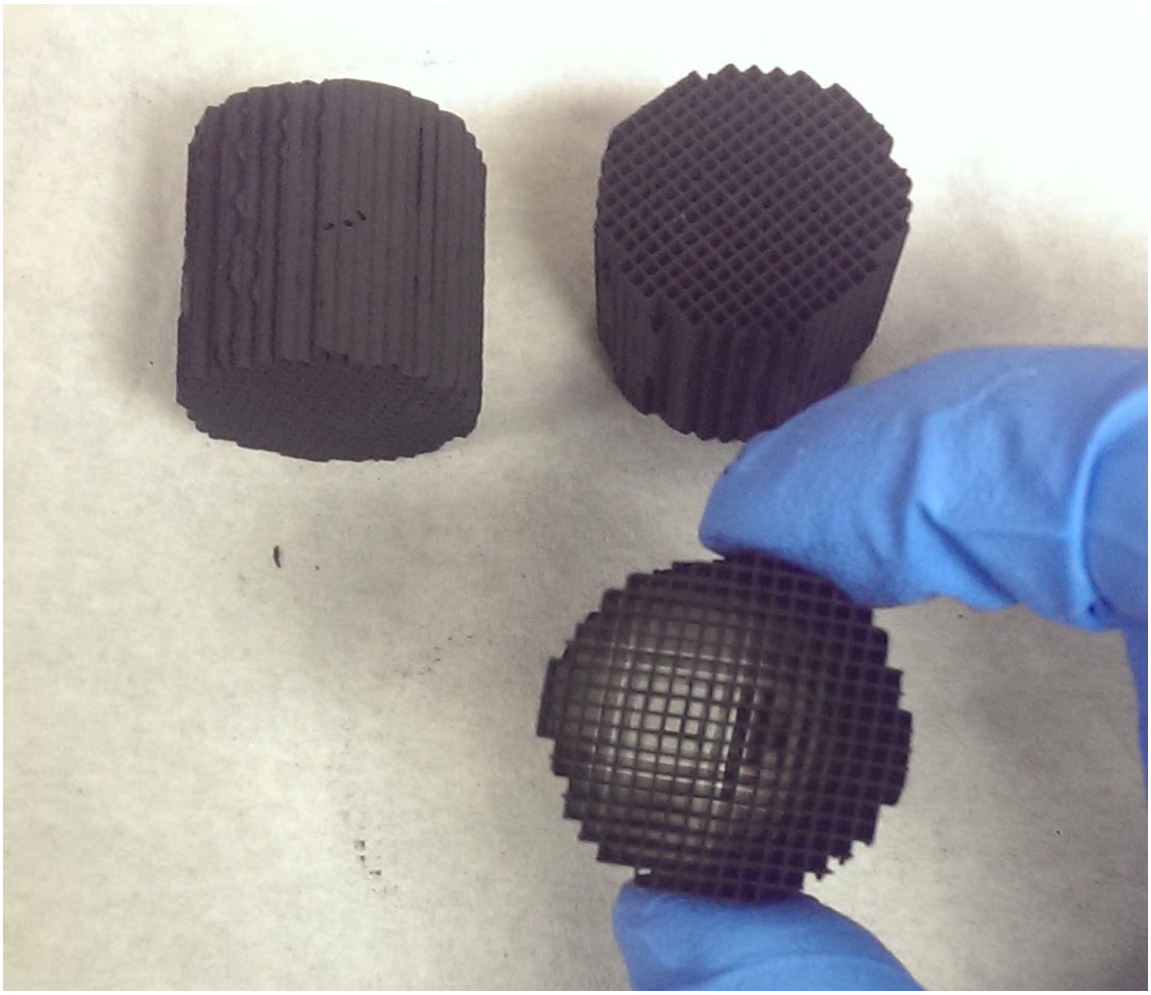

Figure 4.1 Pd-C Monoliths Supplied by Applied Catalysts

4.2.1.6 Catalyst Reduction

Catalysts were loaded into a Parr packed bed reactor system, supported by quartz wool or a steel screen, depending on particle size. Catalysts were then reduced in-situ at 300, 400, or 500 °C using H_2 flow of 100 mL/min for 20 hours prior to use. The mass of catalyst reduced was between 5 -20 grams, according to the corresponding reaction.

4.2.2 Operation of Continuous Packed Bed Reactor System

Ketonization and hydrogenation reactions were performed in a continuous packed bed reactor system custom designed by Parr Instrument Company (Figure 4.2-A). The reactor consists of a stainless steel tube with inner diameter of 2.4 cm and length of 38 cm. Catalysts were loaded into the top of the reactor, supported by a stainless steel screen and quartz wool. The reaction temperature was controlled by a Thermcraft Lab-Temp 1760-watt tube furnace (Figure 4.2-D) powered by a Parr 4875 Power Controller (Figure 4.2-G). When applicable, reduction/pretreatment of the catalyst was conducted for 20 hours (in-situ) prior to the reaction. Aqueous model compound mixtures were injected downward into the reactor tube at a rate of 0.5-1.5 mL/min using a Lab Alliance HPLC pump (Figure 4.2-B). A total of 50 grams of liquid feedstock was injected for each reaction, resulting in a total reaction time between 33-100 minutes. Nitrogen/hydrogen were supplied as carrier gases to the reactor head at a rate of 100 mL/min using a Brooks Delta II Smart Mass Flow Controller (Figure 4.2-C). Pressure was maintained by an in-line back pressure regulator system. The operator controlled all reactions from a safe location (an isolated control room) using SpecView software. A condenser vessel (Figure 4.2-E) chilled to 7 °C by a Brookfield TC-602 water bath (Figure 4.2-F) was used to capture liquid products, which were collected at the end of each reaction for analysis.

Gas products were collected for analysis from the reactor exhaust line using 1 L Tedlar bags.

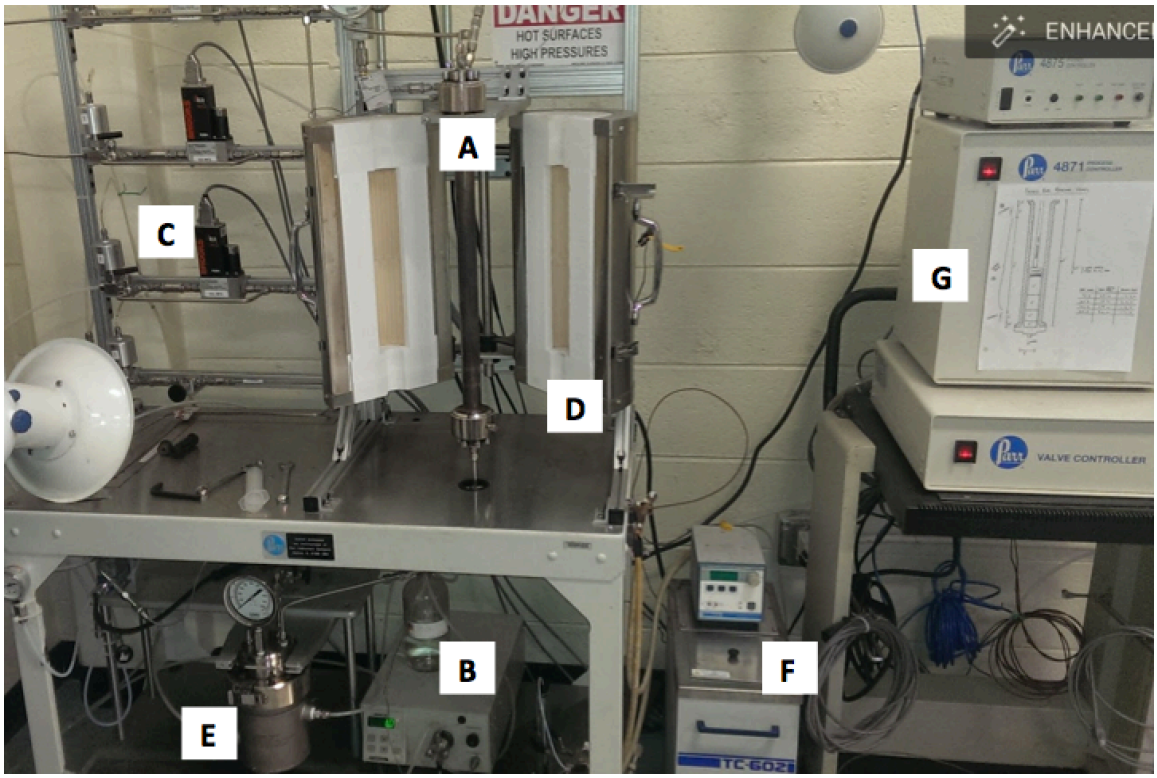

Figure 4.2 Packed Bed Reactor System (Parr Instrument Company). A) Tubular reaction vessel, 1 inch diameter, 20.5 inch length. B) Lab Alliance HPLC Pump C) Brooks Delta II Smart Mass Flow Controller D) Thermcraft Lab-Temp 1760-watt tube furnace E) Parr condenser vessel F) Brookfield TC-602 water bath G) Parr 4871 Process Controller interfaced with Specview software

4.2.3 Analysis of Liquid and Gas Products

4.2.3.1 Gas Chromatography/ Mass Spectrometry (GC/MS)

The composition of the liquid products collected from each reaction was determined by GC-MS analysis using a Hewlett-Packard (model HP-6890) gas chromatograph coupled with a Hewlett-Packard mass spectrometer (Model HP-5973).

An HP-5 MS column (30 m length with 25 mm internal diameter and 0.25 μm film thickness) was used with the following method: inlet temperature of 230 °C and detector temperature of 280 °C, He flow of 1 mL/min, starting oven temperature of 40 °C for 3 minutes followed by an 8 °C/min ramp to 250 °C, then held for 5 minutes. The injection volume used was 1 μL and the spectrometer scan range was 10-350 mass units. Compounds were identified using MSD ChemStation D.03.00.611 and the NIST 2008 database. For select compounds (methylated cyclic ketones, 2-pentanone, 3-pentanone) concentrations were estimated using quantitative GC/MS analysis using hexanol as an internal standard. A standard stock solution was prepared by adding 30 μL of hexanol (106.17 g/L) to a 200 μL mixture of acetone and methanol (1:1 by volume). A series of 3 standard stock solutions were then prepared by adding 5, 10 and 20 μL of the analyte and 6 μL of hexanol stock solution to a 1:1 acetone/methanol mixture, resulting in a final volume of 611 μL. Standard stock solutions contained 1.043 g/L of hexanol and between 0.7 and 10 g/L of the analyte. Stock solutions were injected in triplicate using the method described above. Three-point standard curves were developed that relate the analyte/hexanol peak area ratio to analyte concentration. In order to quantify analytes in liquid product mixtures that were collected from each reaction, 6 μL of hexanol stock solution was added to 605 μL of the liquid product mixture resulting in a hexanol concentration of 1.043 g/L. The ratio of analyte to hexanol peak area measured via GC/MS was then used to calculate the concentration of analyte in the liquid product mixture using the three-point standard curves. The concentrations of 2-pentanone and 3-pentanone were estimated using the standard curve for 2-butanone. The fragmentation

patterns of linear pentanones and 2-butanone were found to be similar, which provided confidence in the accuracy of this quantification method.

4.2.3.2 Gas Chromatography- Flame Ionization Detection (GC-FID)

For certain compounds (acetone, 2-butanone, isopropanol, 2-butanol, cyclopentanone, cyclopentanol), a GC-FID was used for quantitative analysis using an HP Innowax column (30 m x 0.25 mm x 0.25 mm) and an HP 5890 Series II detector using the following method: inlet temperature 230 °C, detector temperature 240 °C, initial oven temperature of 45 °C for 2.5 minutes followed by a ramp of 10 °C/min for 15.5 minutes and then held at 200 °C for 3 minutes. Four-point standard curves (run in triplicate) were generated for each of the compounds listed above. When necessary, liquid samples were diluted to ensure that the measured peak areas fall within the range of the standard curves for each compound (typically 1-10 g/L).

4.2.3.3 High Pressure Liquid Chromatography (HPLC)

Sugars and some organic acids such as levoglucosan, formic acid, and acetic acid were quantified via high pressure liquid chromatography using a Shimadzu LC-20 AT. This instrument uses a RID-10A refractive index detector and a Coregal 64-H transgenomic analytic column (7.8 x 300 mm). The flow rate, sample size, and run time were 0.6 mL/min, 5 μL, and 55 minutes, respectively. The mobile phase was 4 mN sulfuric acid. Samples were analyzed at 6.89 MPa at 60 °C. Samples were injected using an LC-20 AT Shimadzu auto-injector. Four-point standard curves (run in triplicate) were generated for acetic acid, levoglucosan, formic acid, and other water-soluble bio-oil oxygenates. Samples were diluted as needed to ensure that the measured peak area falls within the range of the standard curves for each compound (typically 1-10 g/L).

4.2.3.4 Gas Chromatography-Thermal Conductivity Detection (GC-TCD)

Gas products were collected from the reactor exhaust in 1 L Tedlar bags and quantified using a GC-TCD (Hewlett Packard 5890 Series II) using the following method: inlet temperature 100 °C, detector temperature 140 °C, initial oven temperature 35 °C for 5 minutes, followed by a ramp of 20 °C/min for 8.25 minutes and held at 200 °C for 26.75 minutes. Standard curves for CO, CO_2, CH_4, and H_2 were generated (4-point standards, run in triplicate).

4.2.4 Catalyst Characterization Methods

4.2.4.1 Catalyst Rinsing

Catalyst samples were rinsed by washing 2.5 grams of sample with an acetone-toluene-methanol mixture (1:1:1 by weight) and filtering using Whatman #4 filter paper under a vacuum. Washed samples were then dried at 105 °C for 1 hour. Percent tar accumulation on the catalyst was determined by subtracting pre-rinse weight from post-rinse weight then dividing by post-rinse weight.

4.2.4.2 Thermal Gravimetric Analysis (TGA)

Coke formation was determined via Thermo gravimetric analysis using a Mettler-Toledo TGA/SDTA 851e. Samples (0.5 mg) were heated to 800 °C at 10 °C/min in air (flow rate = 50 mL/min). Coke accumulation was determined by the change in mass of the sample relative to fresh unreacted catalyst.

4.2.4.3 BET/BJH

Catalyst samples were degassed for 3-4 hours at 250-300 °C prior to analysis. 7-point Brunauer-Emmet-Teller (BET) analysis was used to determine the surface area of catalysts. N_2 adsorption was measured over a relative pressure (P/P_0) of 0.05-0.35 using

a Quantachrome Austosorb-1C. Pore size distribution, total pore volume, and average pore radius were estimated using N_2 desorption curves using the Barrett, Joyner, and Halenda (BJH) method.

4.2.4.4 Elemental analysis

Elemental composition analysis was conducted at WestCHEM School of Chemistry at the University of Glasgow. Fe, Na, Al, Si, Ca, and Ti were quantified using ICP-MS in scan mode. Catalysts were digested in sealed Teflon containers using hydrofluoric and nitric acid in a 400 W microwave for 25 minutes.

4.2.4.5 Temperature Programmed Reduction (TPR)

Hydrogen temperature programmed reduction was used to study the valence state of active metals (Pd and Fe). TPR was conducted using a Quantachrome Austosorb-1C. Approximately 0.25 grams of catalyst sample was suspended in a U-tube between two layers of quartz wool. Samples were subject to nitrogen flow at 185 °C for 30 minutes in order to desorb any adsorbed gases. Samples were then heated from 60 °C to 800 °C at a rate of 20 °C per minute in H_2 (3-5 mol% H_2 in N_2 at 80 mL/min). TCD signal response versus temperature plots were then used to determine the hydrogen consumption as a function of temperature.

4.2.4.6 Pulse Titration

Dispersion of active metals was determined via pulse titration using a Quantachrome Austosorb-1C. Approximately 0.2 g of catalyst sample was loading into a U-tube, suspended by quartz wool on both sides. Adsorbed gases were desorbed by flowing helium across the catalyst at 140 °C for 30 minutes. The furnace was then set to the titration temperature (40 °C for Pd, 100 °C for Fe). Nitrogen was then allowed to

flow for 20 minutes at the titration temperature. Titrations were then performed by injecting 100 μL of pure H_2. Between 6-12 injections were made until the resulting peaks indicated that hydrogen was no longer being adsorbed. For select iron oxide catalysts, an in-situ reduction step was added (hydrogen flow for 60 minutes at the desired reduction temperature).

4.2.4.7 CO_2/NH_3 Temperature Programmed Desorption (TPD)

CO_2 and NH_3 temperature programmed desorption were used to estimate the strength of acid and base sites, respectively. TPD was conducted using a Quantachrome Austosorb-1C. Catalysts were degassed at 250-300 °C for 3 hours prior to analysis. Approximately 0.2 g of catalyst sample was loaded into a U-tube, packed between the layers of quartz wool. Samples were then degassed at 185 °C in helium followed by saturation with the adsorbate. For CO_2-TPD, samples were saturated with 100% CO_2 at 30 °C for 10 minutes. For NH_3-TPD, samples were saturated in 100% electronic grade ammonia at 40 °C for 15 minutes. Samples were then desorbed with helium (80 mL/min) from 30 – 800 °C at a rate of 10 °C per minute. Desorbed NH_3 and CO_2 were detected using a TCD.

4.2.4.8 Mössbauer Spectroscopy

Catalyst samples were analyzed via ^{57}Fe Mössbauer Spectroscopy in order to determine the relative abundance of iron redox states (hematite, magnetite, and zero valent iron). This method is further outlined in Tishchenko et al. (2015). Approximately 0.5 grams of each catalyst was loaded and spectra were taken at 295 K, 140 K, 77 K, and 4 K for approximately 24 hours. The relative abundance of each iron phase was extracted from the spectral fittings as a fraction of the total iron spectral area. This analysis

assumes equal Mössbauer recoilless fractions of all detected phases (Tishchenko et al., 2015).

Chapter 5 Results

5.1 Catalyst Characterization Studies

5.1.1 Brunauer-Emmet-Teller and Barret-Joyner-Halenda (BET/BJH) Analysis

BET/BJH analysis was conducted for red mud, Fe-SiAl, Pd-ACM, and Pd-granules using methods described in section 4.2.4.3. Calculations involved are detailed in section 7.3. Analysis was conducted on untreated, pre-reduced, and spent catalysts (see Table 5.1). Reduction of Fe-SiAl in H_2 for 20 hours had little effect on surface area, but lead to reduced pore volume and pore diameter. Red mud was found to have significantly lower surface area than all other catalysts tested (≈30 m^2/g) vs. 400-600 m^2/g). Reduction of red mud at 300 °C for 20 hours lead to increases in surface area (from 13.30 to 30.7 m^2/g), average pore size (from 27.16 to 31.26 Å), and pore volume (from 0.0091 to 0.024 cm^3/g). Figure 5.1 shows the pore size distribution for unreduced red mud and red mud reduced at 300, 400 and 500 °C. Reduction at 300°C leads to a significant increase in pores with diameter ≈37 Å. Reduction of red mud at 400 and 500 °C also increased surface area, but led to significantly lower pore volume and average pore diameter (shown in Table 5.1). It is possible that this decrease in pore volume is due to sintering or agglomeration of iron nanoparticles that blocks a fraction of the pores. Sintering of iron nanoparticles is known to occur at high temperatures or long reduction times in pure H_2 (K. D. Chen et al., 1997). RRM-300 had significantly reduced surface area and pore

volume (shown in Figure 5.2) after use in a 6.6-hour longevity study (detailed in section 5.2.2). Untreated Pd-ACM (0.8 wt% Pd) catalyst had similar surface area, pore volume, and pore size distribution as granular Pd-C. This suggests that the surface properties of the activated carbon were not significantly affected by processing and extrusion into monolith supports. Pd-ACM catalyst samples were analyzed after use in approximately 40 hydrogenation reactions over the course of 5 months (detailed in section 5.3.1). Only a small decrease in surface area (from 608.2 to 592.2 m^2/g) was observed. Average pore size of spent Pd-ACM catalyst was significantly lower (11.80 versus 29.77 Å), and average pore volume decreased from 0.453 to 0.175 cm^3/g. This decrease in pore size and pore volume is likely due to accumulation of a thin organic layer that penetrated into the porous structure but did not block entire pores.

Table 5.1 Surface area, pore size distribution, and pore volume determined by BET/BJH

Catalyst	Treatment	Surface Area (m^2/g)	Avg Pore Diameter (Å)	Pore Volume (cm^3/g)
Fe-SiAl	untreated	405.5	24.20	0.2454
	reduced 400°C	405.5	13.37	0.1355
Red Mud	untreated	13.30	27.16	0.0091
	reduced 300°C	30.70	31.26	0.0240
	reduced 400°C	27.00	11.54	0.0078
	reduced 500°C	22.76	11.48	0.0065
	spent [a]	19.10	8.95	0.0043
Pd-ACM (monolith)	untreated	608.2	29.77	0.4530
	spent[b]	593.2	11.80	0.1750
Pd-C (granular)	untreated	686.2	27.54	0.4725

[a] Analyzed after use in packed bed with the following conditions T= 400 °C, P=atm (N2), WHSV = 0.21 g/g-cat/hr, LHSV= 1.41 hr^{-1}, feedstock= carboxylic acid mixture. [b] Analyzed after approximately 40 hydrogenation reactions over 5 months using acetone, 2-butanone, and cyclopentanones.

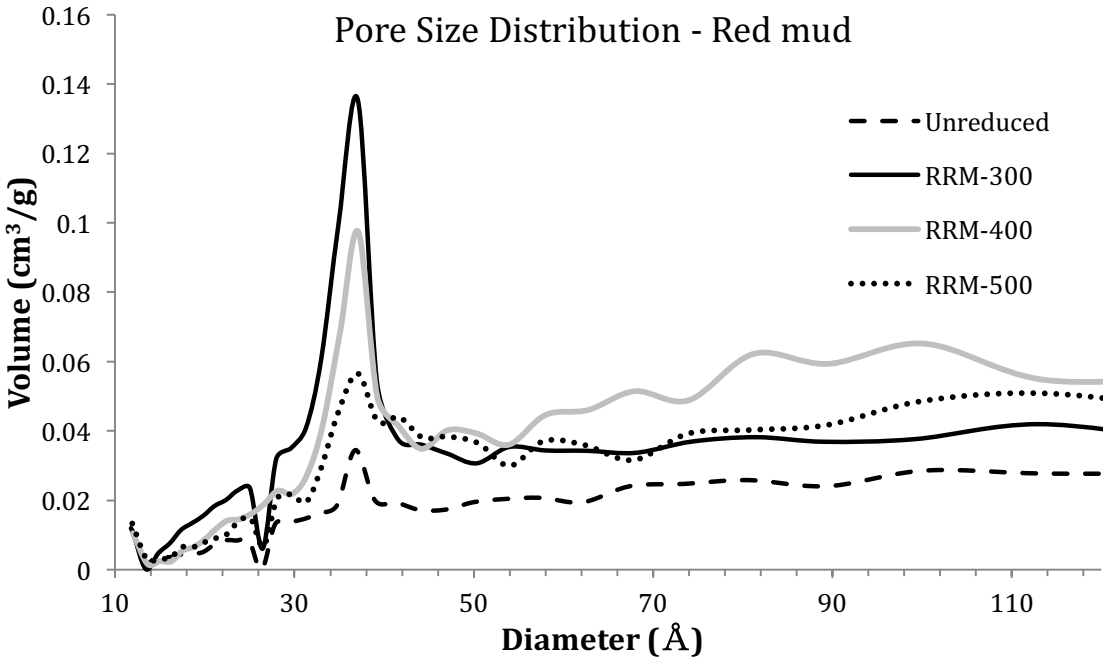

Figure 5.1 Pore size distribution of red mud reduced at different temperatures. RRM- indicates reduced red mud and the temperature at which it was reduced at for 20 hours in pure H_2. Unreduced red mud shown for comparison.

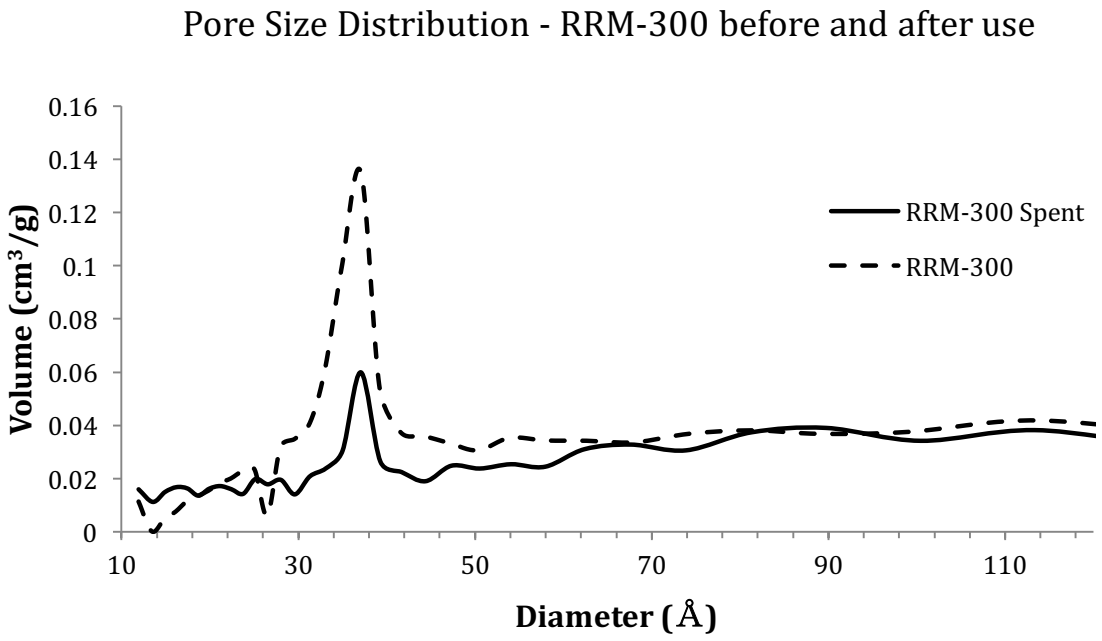

Figure 5.2 Pore size distribution of RRM-300 before and after use. Red mud was pre-reduced at 300°C for 20 hours. "Spent" indicates use in a 6.6 hour reaction with acetic acid, formic acid, acetol, and levoglucosan with the following conditions T= 400 °C, P=atm (N_2), WHSV = 0.21 g/g-cat/hr, LHSV= 1.41 hr^{-1}

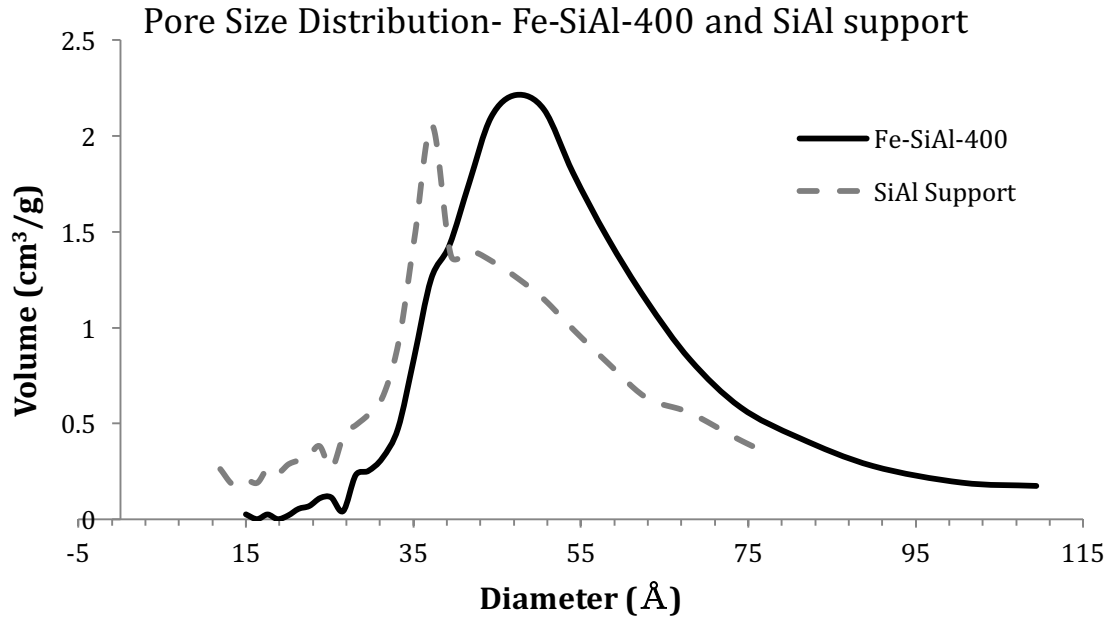

Figure 5.3 Pore size distribution of Fe-SiAl-400 compared to SiAl support. Fe-SiAl (10 wt%) was prereduced at 400 °C in H_2 for 20 hours. SiAl support indicates untreated support material that was not impregnated with Fe.

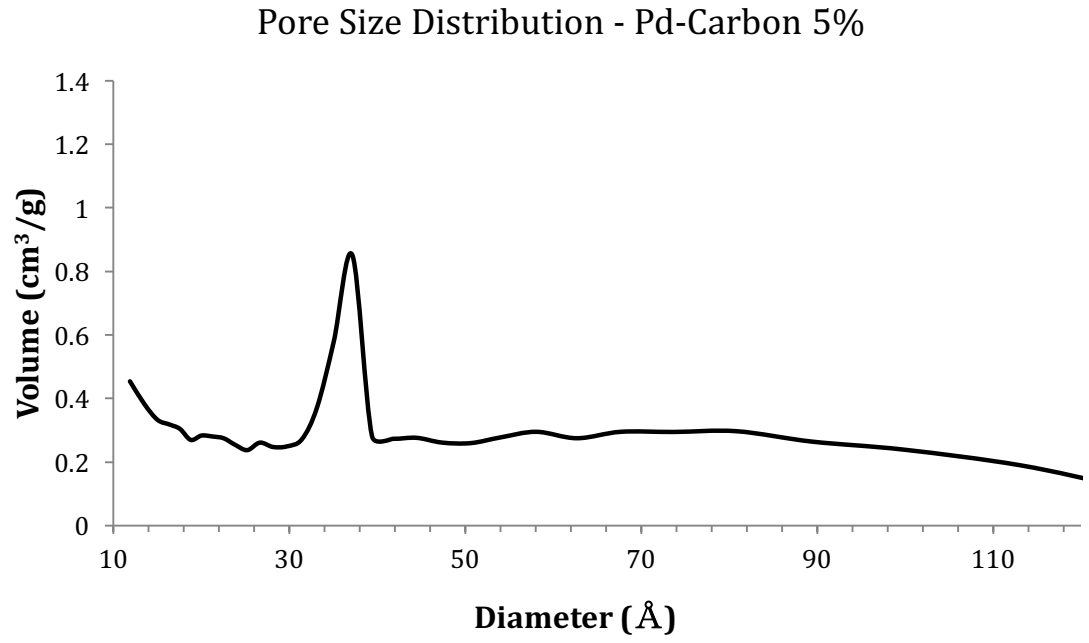

Figure 5.4 Pore size distribution of Pd-C granules (5 wt%) without pretreament

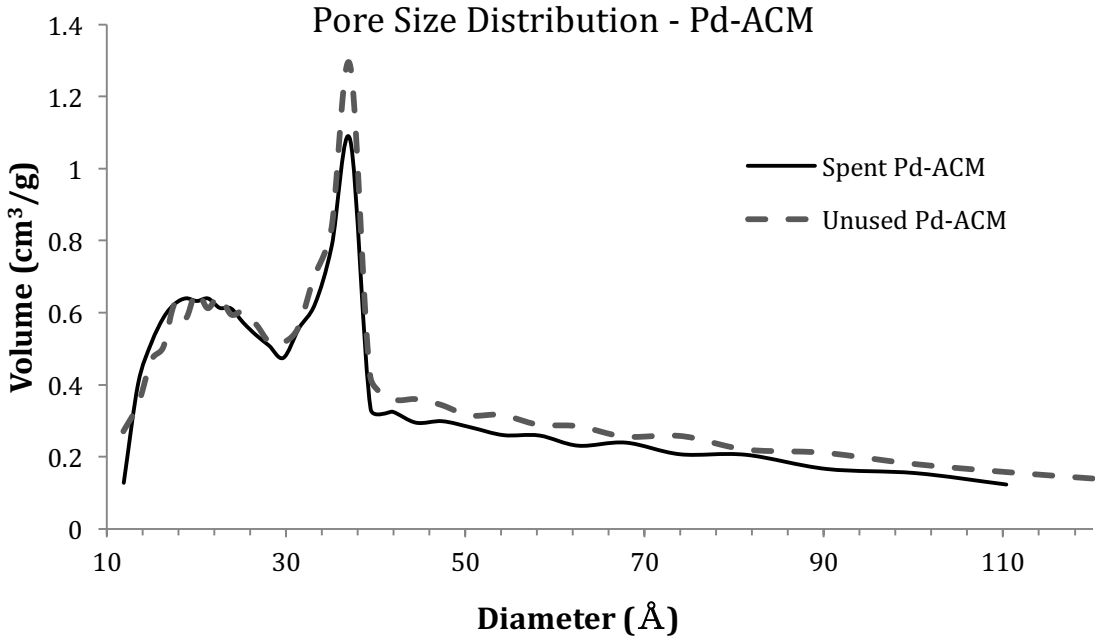

Figure 5.5 Pore Size Distribution of unused and spent Pd-ACM (0.8 wt%). Spent Pd-ACM was analyzed after approximately 40 continuous hydrogenation reactions over 5 months using acetone, 2-butanone, and cyclopentanones.

5.1.2 Temperature Programed Reduction (TPR)

Hydrogen temperature programmed reduction was used to determine the reducibility of the catalyst and estimate the valence state for iron oxides. The procedure used for TPR is outlined in section 4.2.4.5. TCD signal versus temperature plots indicate the amount of hydrogen consumed in the reduction of active metals at temperatures between 60-800 °C. This procedure did not involve standard curves for quantifying hydrogen consumption, and thus comparisons between TPR plots are purely qualitative.

Figure 5.6 shows TPR profiles for untreated red mud compared with red mud that was pre-reduced in H_2 at 400°C for 20 hours. A very small peak at 300 °C was observed for unreduced red mud, which represents hydrogen consumed in the reduction of hematite to magnetite. Reduction of red mud at 300 °C using the procedure outlined in section 4.2.1.6 was found to be very slow (taking longer than 8 hours). This explains why only a small peak was observed at 300 °C, which was acquired over only a few minutes. The large peak from 400-750 °C likely represents hydrogen consumed in the reduction of hematite and magnetite to zero valent iron. This peak was not observed for red mud pre-reduced at 400 °C, suggesting lower concentrations of hematite and magnetite. Figure 5.7 shows a hydrogen consumption peak around 500 °C for Fe-SiAl. No peaks were observed under 400 °C, which may indicate that higher temperatures are required for the reduction of hematite to magnetite due to interactions with silica alumina support. Evidence in the literature suggests that complete reduction to zero valent iron does not occur at temperatures below 900 °C, due to the formation of Fe_2SiO_2. Reduction of Fe-SiAl 400-500°C likely results a mixture of magnetite and wüstite (FeO), which has demonstrated hydrogenation activity at temperatures above 200°C

(Witsuthammakula & Sooknoi, 2015). Pd-ACM showed two co-eluting hydrogen consumption peaks centered at 220 and 280 °C (see Figure 5.8). These peaks likely represent complete reduction of Pd oxides to Pd metal, which has been shown to be possible at temperatures as low as 200 °C (Crozier et al., 1998). Pd-C granules showed two broad peaks centered around 350 °C and 560 °C (see Figure 5.9). This suggests that greater activation energy is required for complete reduction of Pd on traditional activated carbon support compared to monolithic support.

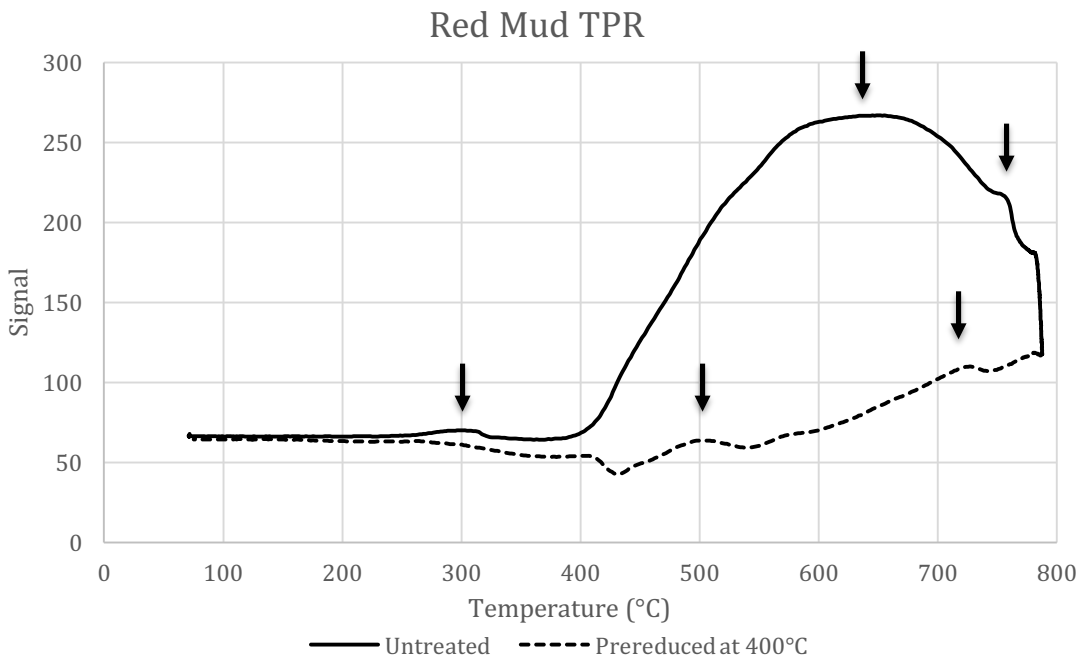

Figure 5.6 H_2 TPR for untreated red mud and red mud prereduced at 400°C. Arrows indicate H_2 reduction reactions.

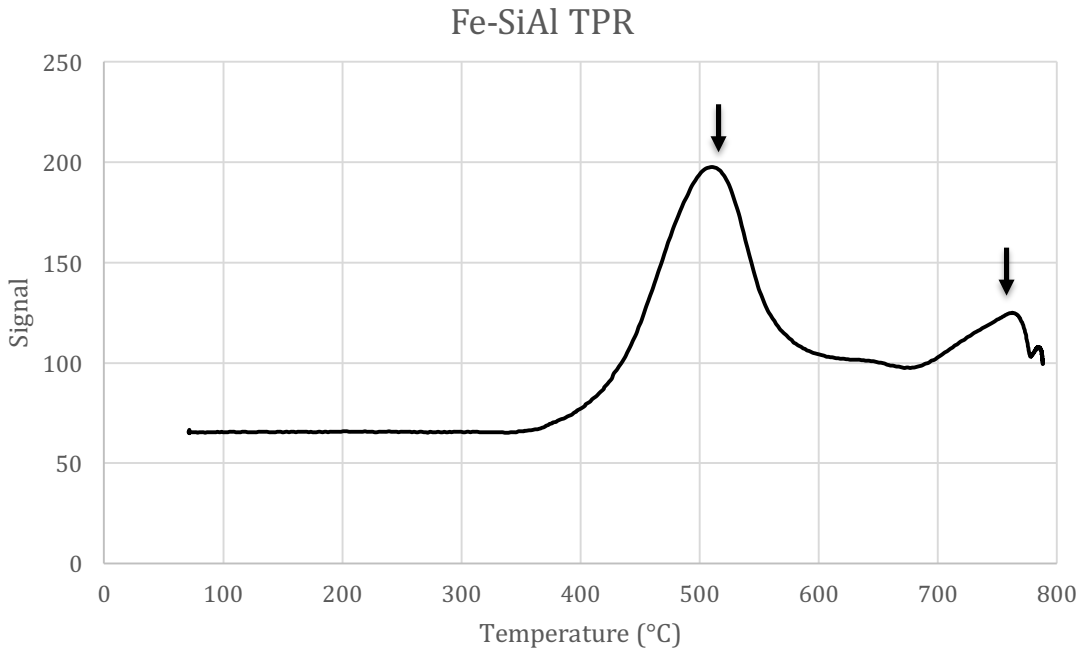

Figure 5.7 H_2 TPR for untreated Fe-SiAl. Arrows indicate H_2 reduction reactions.

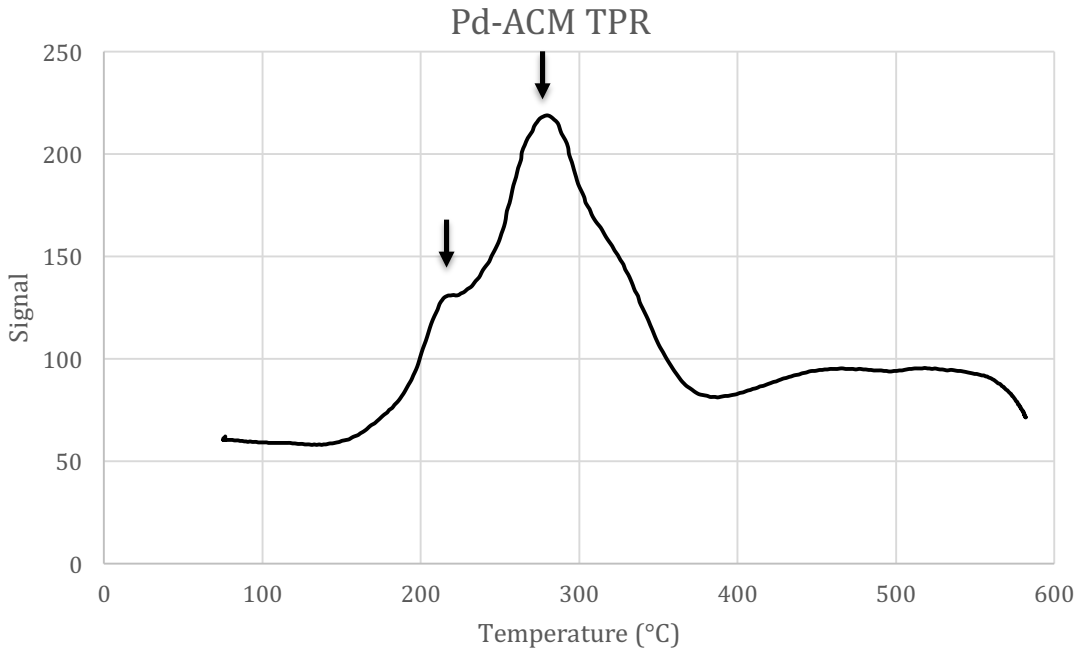

Figure 5.8 H_2 TPR for untreated Pd-ACM (0.8 wt%). Arrows indicate H_2 reduction reactions.

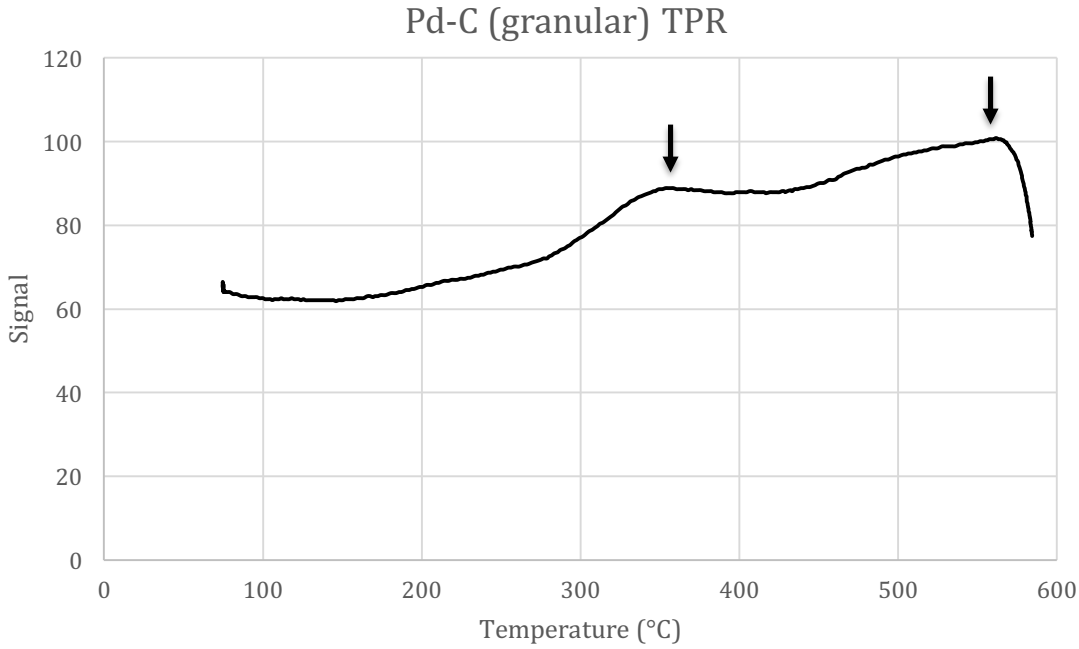

Figure 5.9 H_2 TPR for untreated Pd-C (granulated, 5 wt%). Arrows indicate H_2 reduction reactions.

5.1.3 Mössbauer Spectroscopy and Compositional Analysis of Red Mud

Compositional analysis was conducted on untreated and 300 °C-reduced red mud using methods described in section 4.2.4.4. Composition analysis indicated high levels of iron (22.6%), sodium (14.5%), and aluminum (14.4%) with lower levels of silicon, calcium and titanium (see Table 5.2). Red mud pre-reduced at 300, 400, and 500 °C were analyzed via Mössbauer spectroscopy to determine the composition of the iron phase (detailed in section 4.2.4.8). Figure 5.11 - Figure 5.14 show Mössbauer spectra for red mud catalysts. Mössbauer analysis shows that all of the iron in the unreduced red mud exists as hematite (see Figure 5.10). After reduction at 300 °C, all hematite was converted to magnetite. Increasing reduction temperature to 400 °C results in further reduction of a portion of the magnetite to zerovalent iron (24.9%). After reduction at 500 °C, a greater portion of the magnetite is reduced to zerovalent iron (46.8%).

Table 5.2 Compositional analysis of untreated red mud and RRM-300 (red mud reduced at 300°C for 20 hours)

Metal	**Red Mud, untreated**	**Red mud, reduced at 300°C**
	% wt (dry basis)	% wt (dry basis)
Fe	22.6	23.9
Na	14.5	15.9
Al	14.4	16.6
Si	8.6	9.3
Ca	4.4	5.2
Ti	4.4	4.8

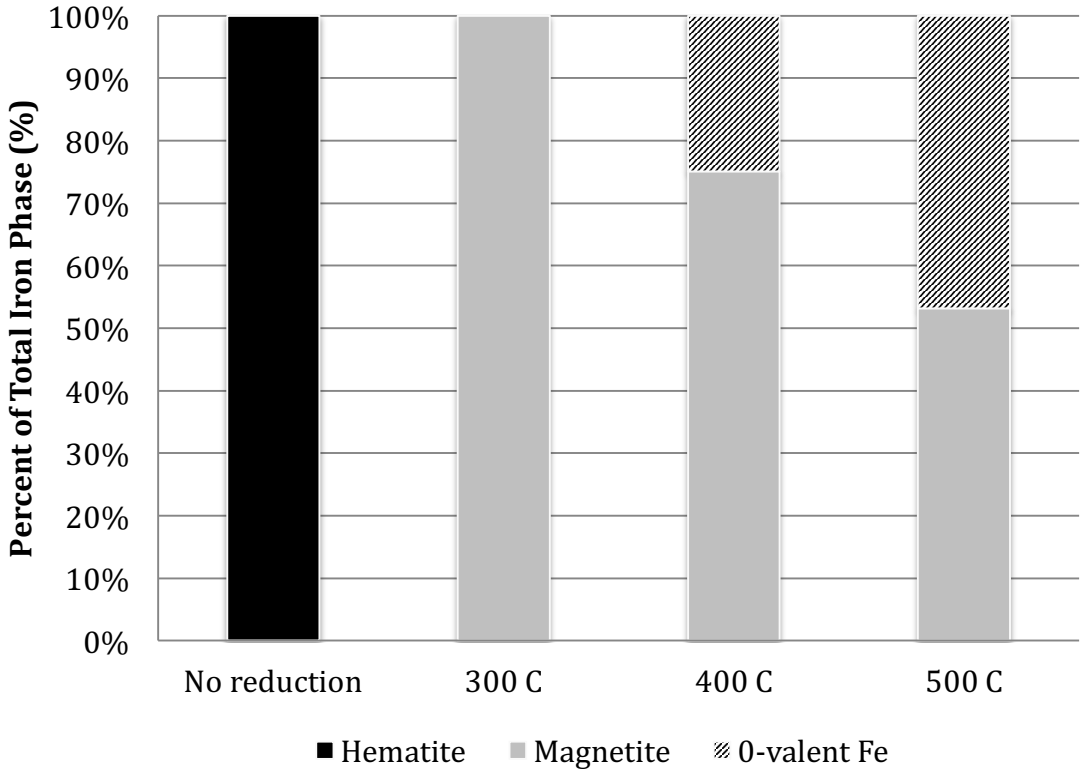

Figure 5.10 Iron redox state composition of RRM-300,400,500, and unreduced red mud. (RRM- indicates reduced red mud and the temperature it was reduced in H_2 for 20 hr)

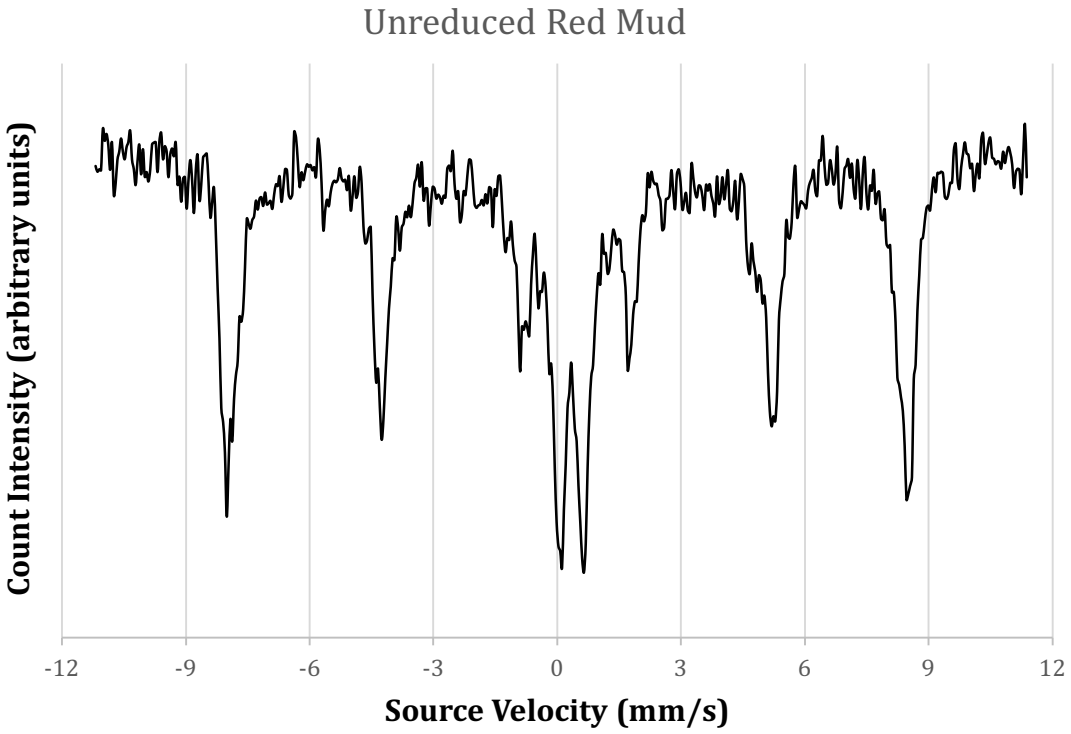

Figure 5.11 Mössbauer spectrum for unreduced red mud (collected at 295 K)

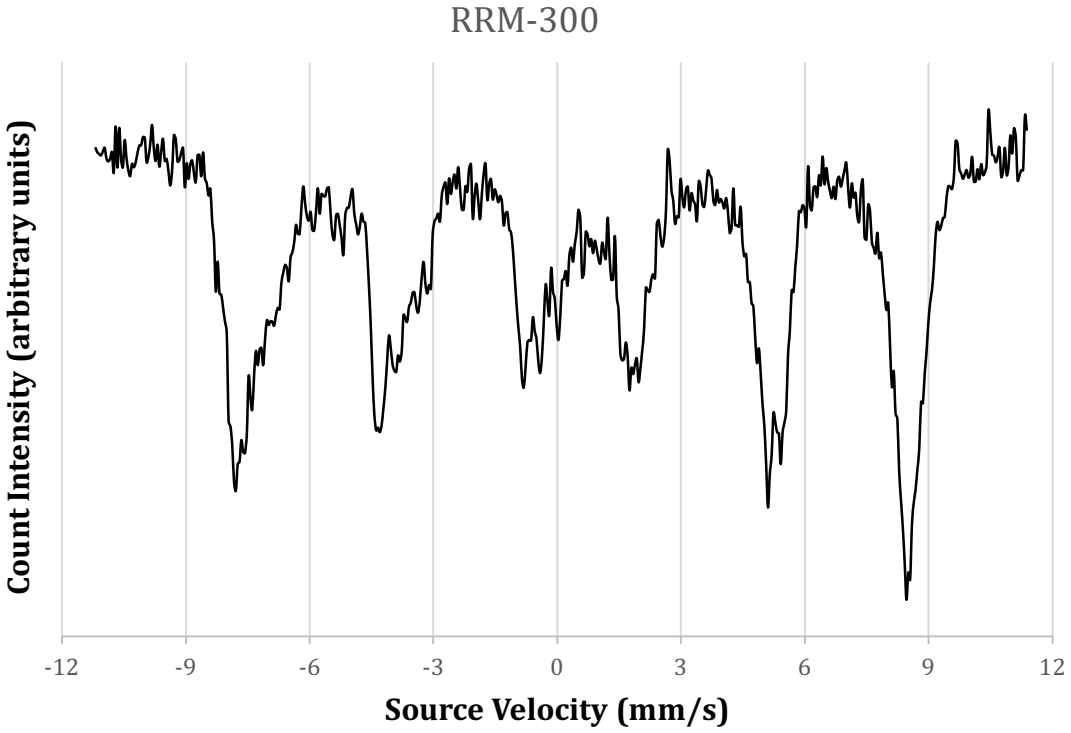

Figure 5.12 Mössbauer spectrum for RRM-300 (collected at 140 K)

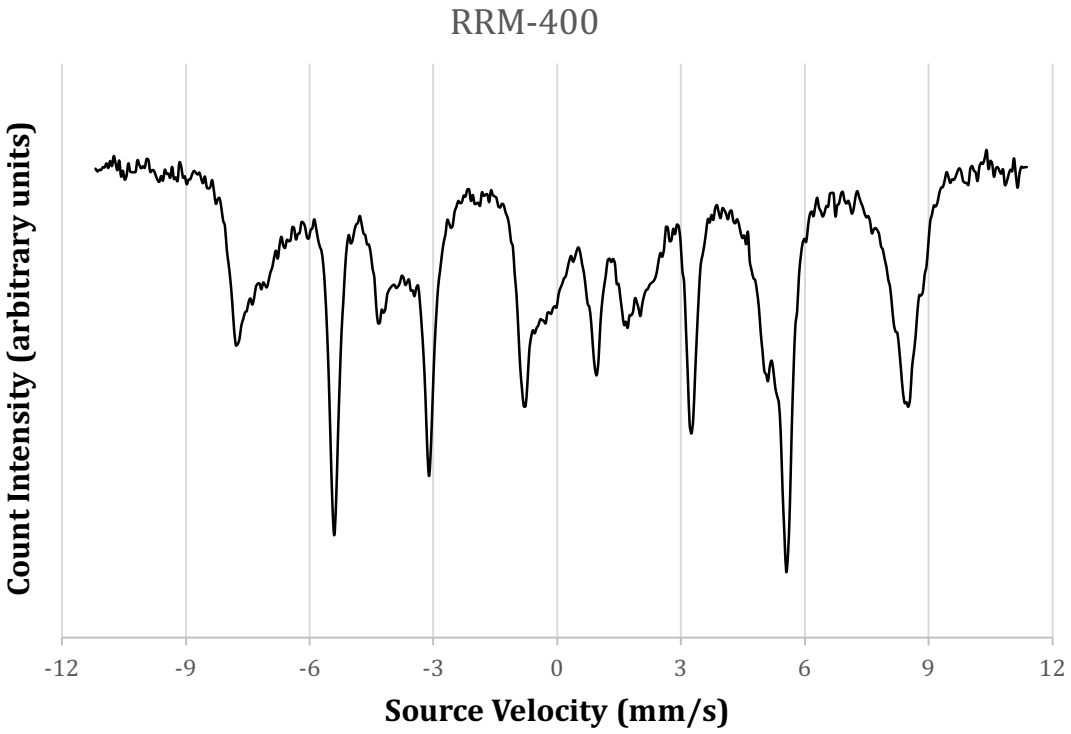

Figure 5.13 Mössbauer spectrum for RRM-400 (collected at 140 K)

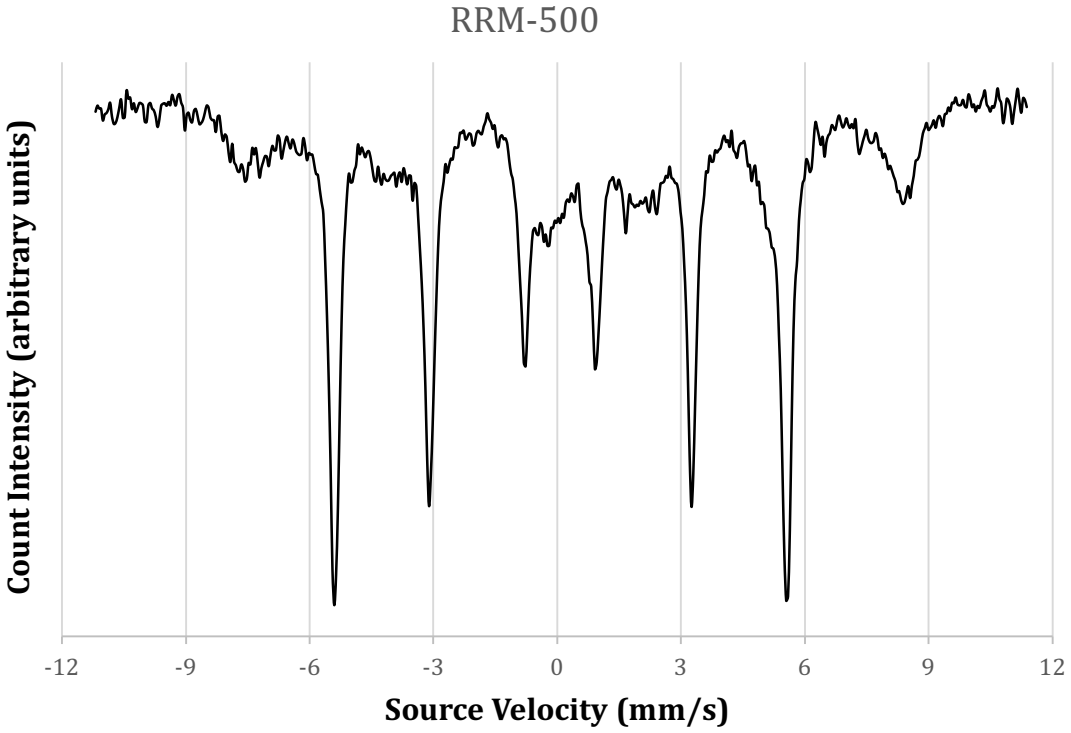

Figure 5.14 Mössbauer spectrum for RRM-500 (collected at 140 K)

5.1.4 Temperature Programmed Desorption Studies using Red Mud

NH_3- TPD was conducted on unreduced red mud and red mud pre-reduced at 300°C. Reduction treatment at 300°C increased the concentration of strong acid sites, indicated by the ammonia desorption peaks at 360, 400, and 525 °C (Figure 5.15). CO_2-TPD was conducted on red mud reduced at 300 and 400 °C in order to understand the effect of reduction treatment on basic sites. Figure 5.16 shows a comparison between red mud pre-reduced at 300 and 400 °C with a control that was performed using red mud without the addition of CO_2. The large peak centered at 500°C indicates the presence of strong basic sites on red mud pre-reduced at 300°C. Increasing reduction temperature leads to a significant reduction in strong base sites.

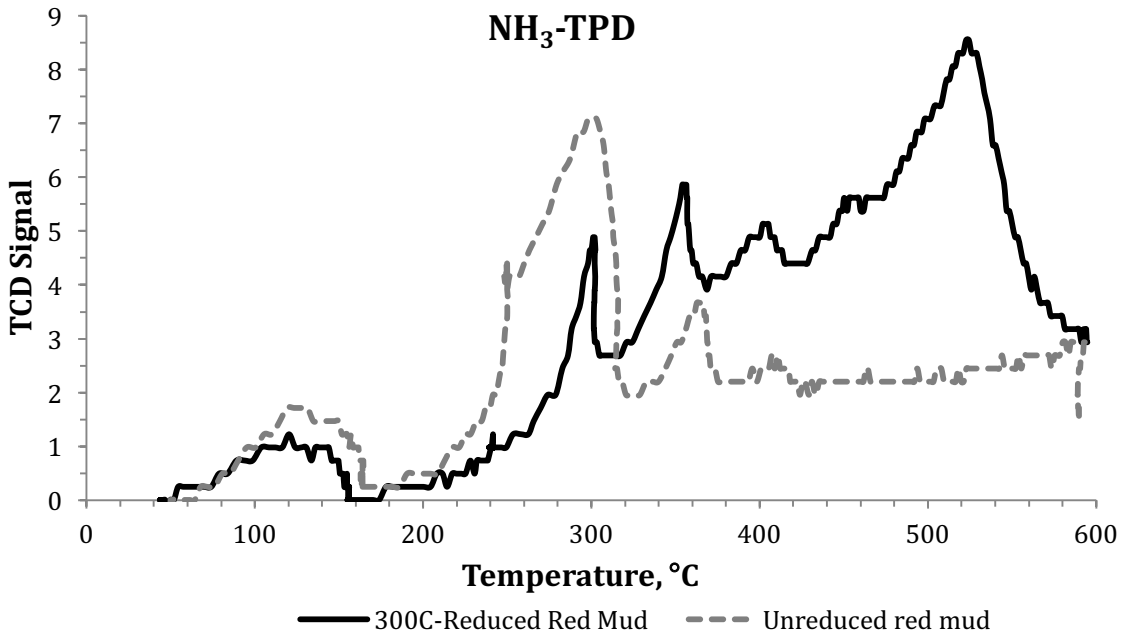

Figure 5.15 NH_3-TPD of red mud catalysts. 300°C indicates the reduction temperature (20 hours in H_2).

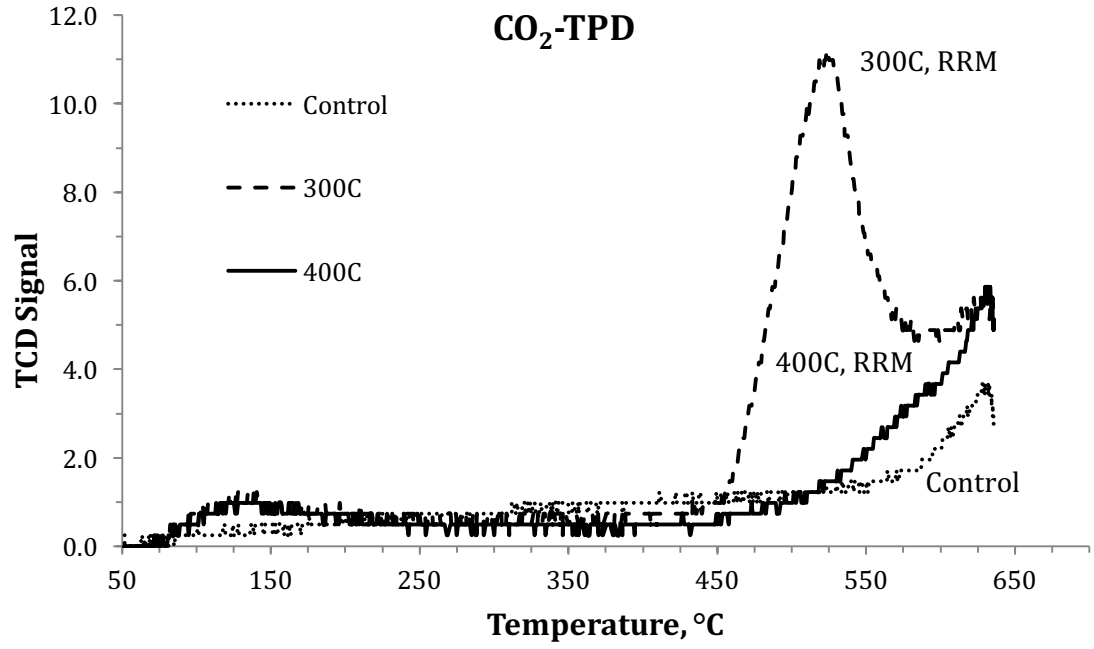

Figure 5.16 CO_2-TPD of red mud catalysts. 300°C and 400°C indicate the reduction temperature (20 hours in H_2)

5.1.5 Pulse Titration Studies using Red Mud, Fe-SiAl, and Pd-C

Hydrogen pulse titration studies were conducted in order to calculate the percent of total active metal available for hydrogen chemisorption (dispersion). H_2 pulse titration methods used are described in section 4.2.4.6, and dispersion calculations are described in section 7.4. Table 5.3 shows dispersion and specific hydrogen uptake for red mud, Fe-SiAl, Pd-ACM, and Pd-C granules. Red mud and Fe-SiAl catalysts were evaluated after reduction at 400°C and 500°C for 20 hours. Results indicated significantly lower dispersion and specific hydrogen uptake for Fe-SiAl compared to red mud at both reduction temperatures. Increasing reduction temperature from 400°C to 500°C led to increases in dispersion for both red mud (0.96-1.90%) and Fe-SiAl (0.13-0.50%). This may be explained by an increase in zero valent iron concentration, which is required for activation of hydrogen. Analyses indicated higher specific hydrogen uptake for granulated Pd-C compared to Pd-ACM on a catalyst mass basis (6923 vs. 1401 μL/g catalyst). However, when normalized based on mass of active metal, Pd-ACM had higher specific hydrogen uptake than granular Pd-C (175 vs. 138 mL/g active metal). Dispersion calculations for Pd-C granules and Pd-ACM indicated dispersion levels greater than 100%, which suggests that hydrogen adsorbed to other surface sites and not just active metal sites. In attempt to account for this, pulse titration was also conducted on a blank activated carbon monolith that did not contain any active metal, which adsorbed a small amount of hydrogen (145.2 μL/g). The specific hydrogen uptake of the blank activated carbon monolith did not account for all of the excess hydrogen adsorbed to the catalyst. This excess hydrogen adsorbed may be attributed to the hydrogen spillover effect, which has recently been described in the literature (C. H. Chen et al.,

2012). Metal sites activate H_2 causing dissociation into hydrogen atoms, which can then adsorb to activated carbon surrounding the metal sites. This phenomenon may explain why excess hydrogen adsorbed to Pd-C granules and Pd-ACM, but only small amounts of hydrogen adsorbed to the blank activated carbon monolith, which did not contain active metal sites to activate hydrogen.

Table 5.3 Dispersion and specific hydrogen uptake of RRM, Fe-SiAl, and Pd-C catalysts determined via H_2 pulse titration.

Catalyst	Reduction Temperature	Specific Hydrogen Uptake		Dispersion
	°C	μL/g catalyst	μL/g active metal	%
Fe-SiAl	400	25.99	259.9	0.13%
	500	99.50	995	0.50%
Red Mud	400	214.8	1918	0.96%
	500	427.9	3820	1.90%
Pd-C (5 wt%, granular)	500	6923	138,465	131.0%
Pd-ACM (0.8 wt%)	500	1401	175,169	157.7%
Blank ACM*	-	145.2	-	-

*Blank ACM indicates activated carbon monolith with no active metal.

5.2 Ketonization Studies

5.2.1 Kinetic Studies Using Reduced Red Mud

Reactions were conducted in a continuous packed bed reactor system with red mud catalyst (pre-reduced at 300°C) using a model compound mixture of acetic acid, formic acid, acetol, and levoglucosan (4% each in H_2O). The effect of temperature on catalytic ketonization of the model compound mixture was studied by varying the

reaction temperature from 350 °C to 425 °C. The effect of catalyst weight to flow ratio (W/F) was studied by varying the catalyst mass from 5 g to 20 g.

Figure 5.18 shows the conversion (A) and reaction rates (B) of these four compounds using 5 g of catalyst at 350°C, 1 atm, and a WHSV of 0.48 h^{-1}. The reaction rates achieved by RRM (~8 mmol/g-cat/hr) were similar to the reactions rates reported using $CeZrO_x$ (Hakim et al., 2013). Increasing the contact time with the catalyst (W/F) by increasing the mass of catalyst used and by decreasing the reactant feed rate increased conversion and selectivity with respect to ketone products (see Figure 5.19 and Figure 5.20). Acetone was the primary product from conversion of acetic acid. Acetone selectivity was 8-17%. Levoglucosan reaction rates were the lowest, but no reactor plugging was observed. Intermediate products formed from levoglucosan included acetic acid, formic acid, and acetol, which then formed ketones (diketones and cyclic ketones). Trace peaks of 2,3-butanedione, 2-butanedione, acetaldehyde, cyclopentanone, and methylated cyclopentanones were observed from levoglucosan. This study suggests similar ketonization pathways proposed by Hakim et al. (2013) using $CeZrO_X$. Acetol was converted via transfer hydrogenation to pyruvaldehyde and 1,2-propylene glycol. Pyruvaldehyde is then carbonylated to formaldehyde and acetic acid or acetaldehyde and formic acid. Pyruvaldehyde can condense with acetone and undergo hydrogenation to form a diketone. The decomposition of formic acid provides a source of H_2 for hydrogenation. Diketones can undergo base-catalyzed intermolecular cyclization, forming cyclic ketones. Figure 5.17 shows the reaction pathways for acetic acid, formic acid, levoglucosan, and acetol proposed in previous studies using individual model compound mixtures (Kastner et al., 2015)

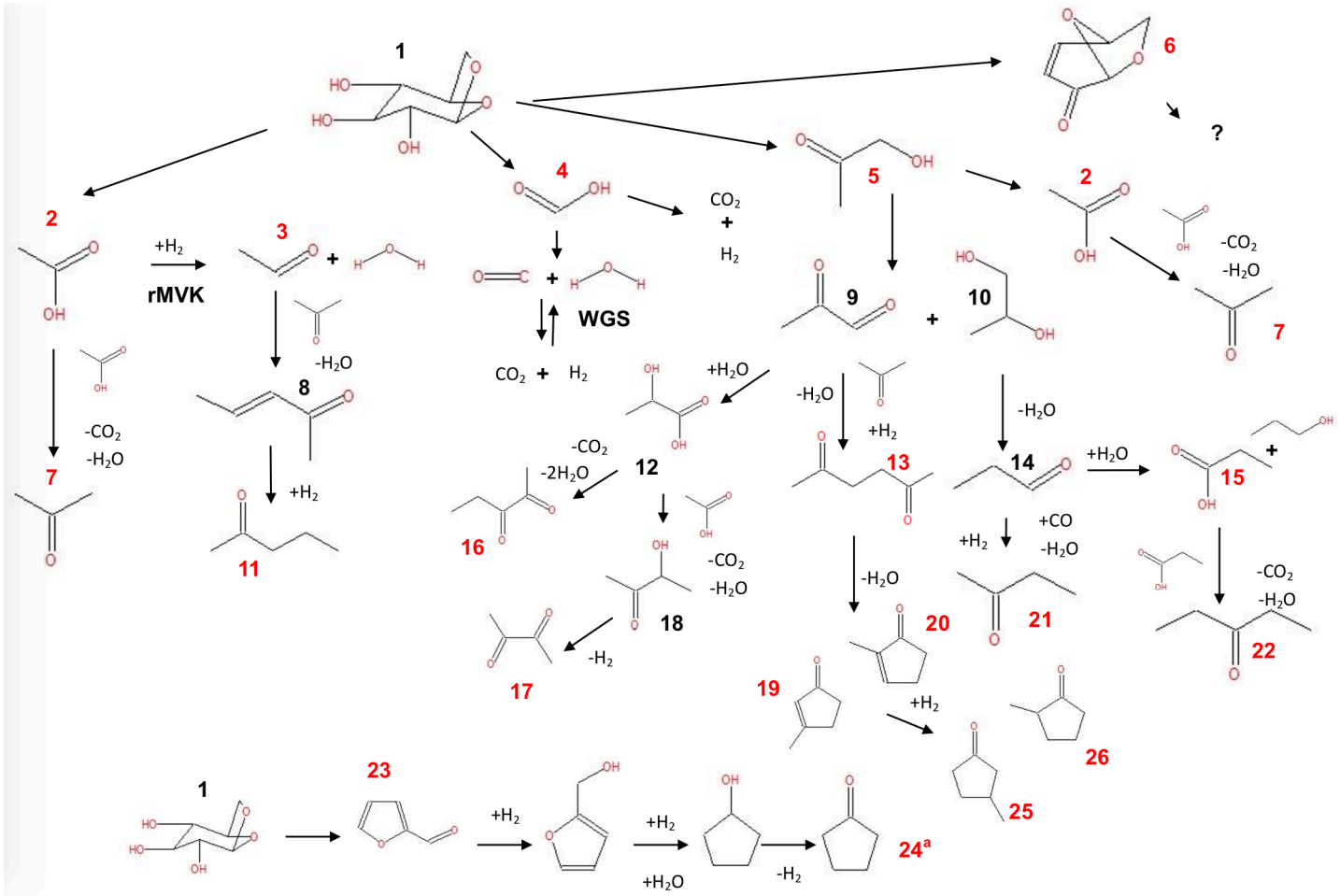

Figure 5.17 Proposed reaction pathways leading to products from levoglucosan (1), acetic acid (2), formic acid (4), and acetol (5). Products include levoglucosenone (6), acetaldehyde (3), pyruvaldehyde (9), propylene glycol (10), acetone (7), 3-penten-2-one (8), 2-pentanone (11), lactic acid (12), 2,5-hexanedione (13), propanal (14), propanoic acid (15), 2,3-pentanedione (16), 2,3-butanedione (17), 3-hydroxy-2-butanone (18), 3-methyl-2-cyclopenten-1-one (19), 2-methyl-2-cyclopenten-1-one (20), 2-butanone (21), 3-pentanone (22), furfural (23), cyclopentanone (24), 2-methylcyclopentanone (26), and 3-methylcyclopentanone (25). rMVK indicates reverse Mars van Krevelen mechanism, and WGS indicates water gas shift reaction. References: (Kastner et al., 2015); (Hakim et al., 2013)

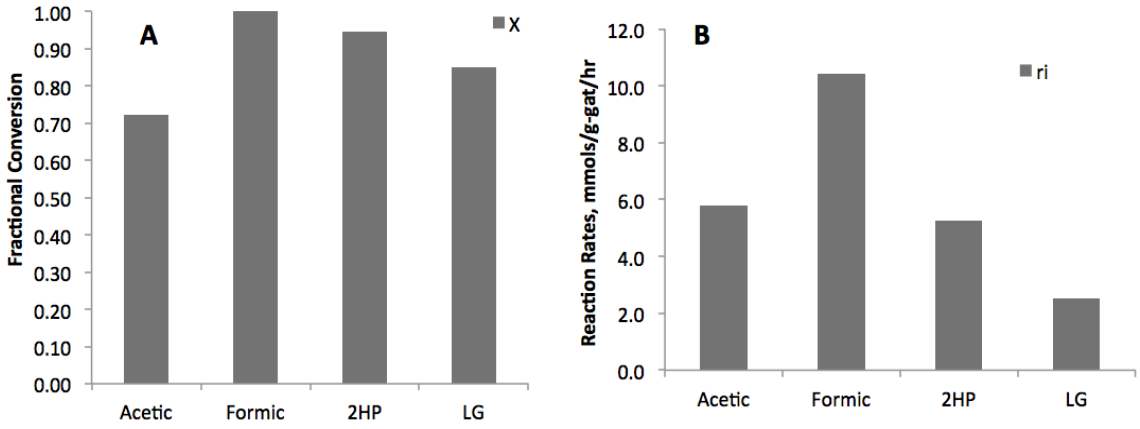

Figure 5.18 Conversion (A) and reaction rates (B) of model compounds using red mud at 350°C, 1 atm (N_2), and WHSV=0.48 h^{-1} (Kastner et al., 2015)

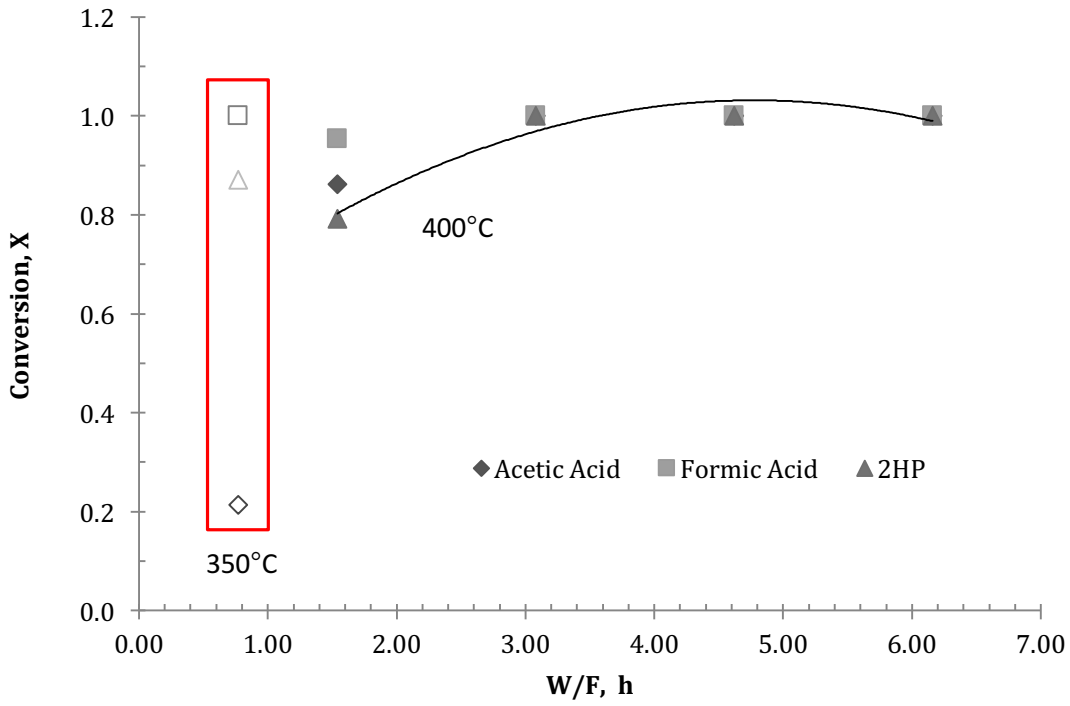

Figure 5.19 Conversion vs. W/F using red mud at 350°C and 400°C, 1 atm (N_2) (Kastner et al., 2015)

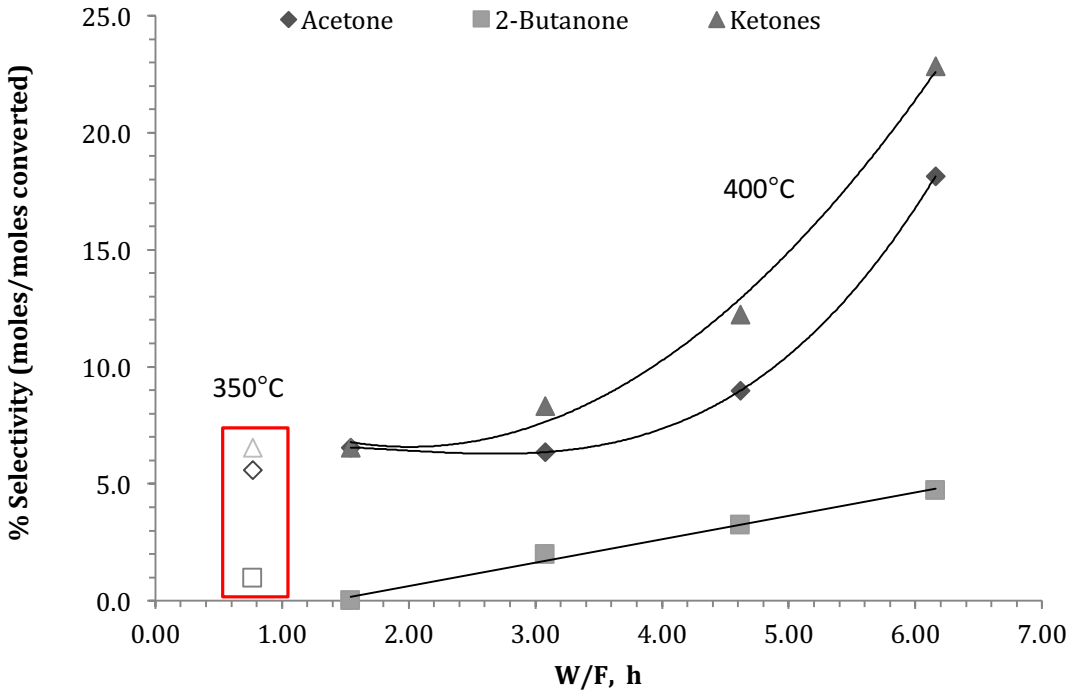

Figure 5.20 Selectivity vs. W/F using red mud at 350°C and 400°C, 1 atm (N_2) (Kastner et al., 2015)

5.2.2 Longevity Studies Using Reduced Red Mud

A catalyst longevity (time-on-stream) study was conducted using RRM-300 in a continuous reaction using the best conditions for ketonization determined in section 5.2.1 (T=400 °C, P= 1 atm (N_2), WHSV = 0.21 g/g-cat/hr, LHSV= 1.41 hr^{-1}). The reaction lasted approximately 400 minutes (6.67 hours) using 20 grams of RRM-300. Liquid and gas products were sampled every 100 minutes. Analysis of liquid products indicated that there was no measureable decline in conversion of acetol, formic, and levoglucosan, and only a 4% decline in acetic conversion (see Figure 5.22). In addition to high conversions, high levels of acetone (15-25 g/L), 2-butanone (~5 g/L), and cyclic ketones (9-13 g/L) were observed. Total ketone yields ranged from 16-27%, and space time yields ranged

from 40-70 g/L-cat/h (see Figure 5.21). Very little tar accumulation was observed (0.015 g tar/g catalyst). In addition, oxidative thermogravimetric analysis indicated little coke formation on the recovered catalyst (0.035 g-coke/g-cat). These results show that RRM-300 is resistant to deactivation, undergoes minimal leaching of active sites, and is capable of maintaining ketonization activity over long reaction times.

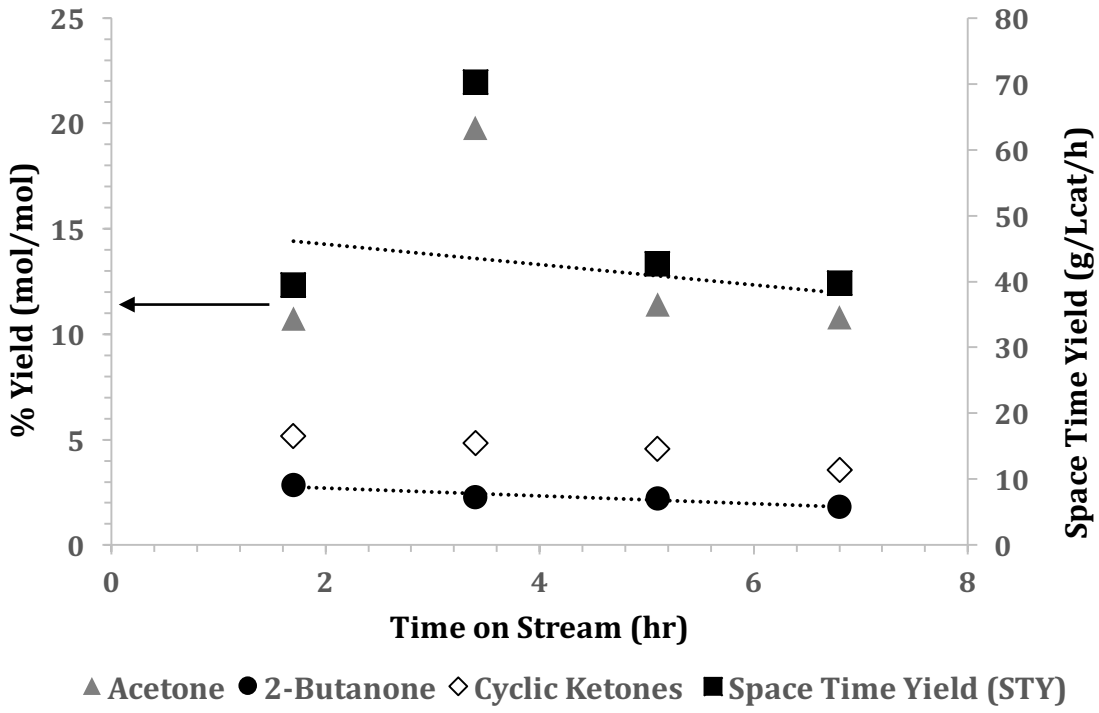

Figure 5.21 Product yields during time-on-stream study using RRM-300 (red mud reduced at 300°C): T= 400 °C, P=atm (N_2), WHSV = 0.21 g/g-cat/hr, LHSV= 1.41 hr^{-1}

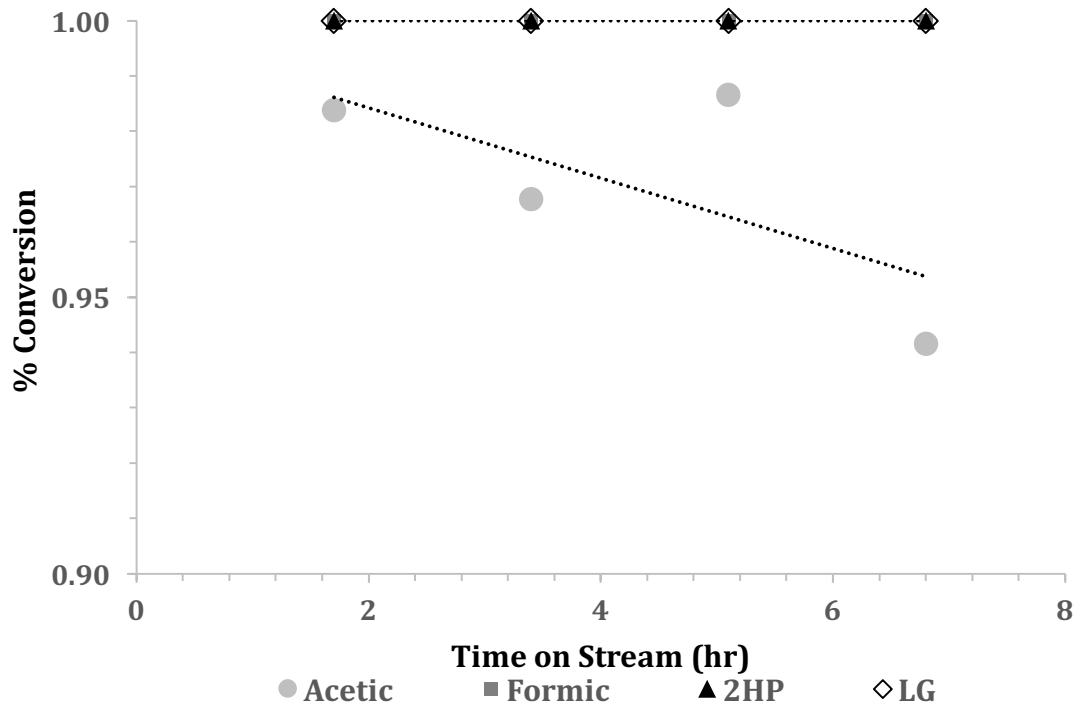

Figure 5.22 Conversion of reactants during time-on-stream study using RRM-300 (red mud reduced at 300°C): T= 400 °C, P=atm (N_2), WHSV = 0.21 g/g-cat/hr, LHSV= 1.41 hr^{-1}

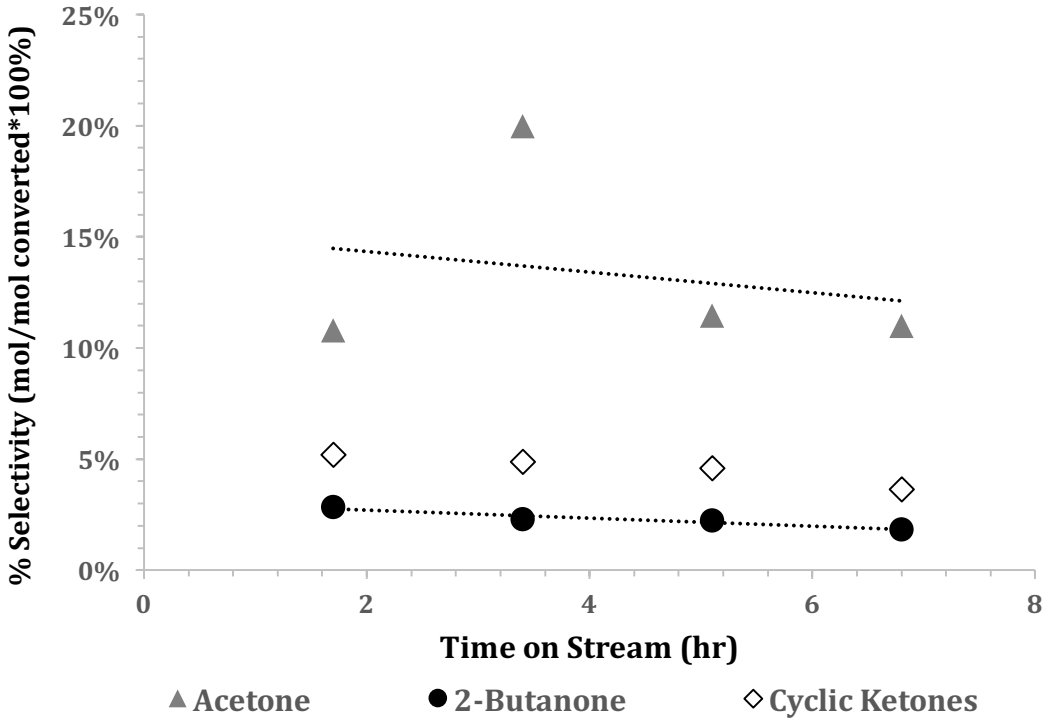

Figure 5.23 Product selectivity during time-on-stream study using RRM-300 (red mud reduced at 300°C): T= 400 °C, P=atm (N_2), WHSV = 0.21 g/g-cat/hr, LHSV= 1.41 hr^{-1}

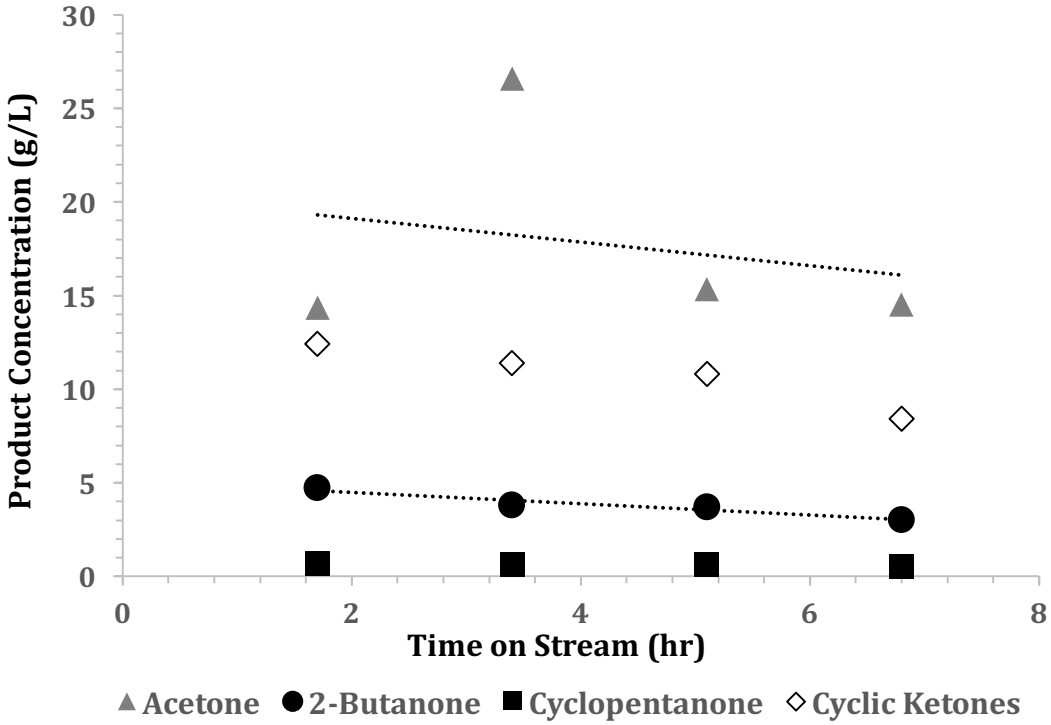

Figure 5.24 Product concentration during time-on-stream study using RRM-300 (red mud reduced at 300°C): T= 400 °C, P=atm (N_2), WHSV = 0.21 g/g-cat/hr, LHSV= 1.41 hr^{-1}

5.2.3 Effect of Reduction Treatment of Red Mud on Activity and Surface Properties

These studies investigated the effects of reduction treatment temperature on catalyst activity and surface properties of red mud. Reactions were conducted in a packed bed reactor system using the procedure described in 4.2.2 with the following conditions: T= 400 °C, P = atm (N_2), WHSV = 0.89 g/g-cat/hr, LHSV= 5.65 hr^{-1}. These reaction conditions were chosen based on the best results from the experimentation described in section 5.2.1. In addition to red mud reduced at three different temperatures, Fe_2O_3 on carbon nanoparticles and HCl-treated red mud were tested for comparison.

Figure 5.25 shows the space time yields with respect to primary products (acetone, 2-butanone, and cyclic ketones) for each catalyst used. The best results were seen in the reaction using RRM-300, which achieved acetone and 2-butanone space time yields of 66.97 and 15.08 g/L-cat/hr, respectively. The HCl-treated red mud achieved a higher space time yield with respect to cyclic ketones than RRM-400 and RRM-500, but showed low selectivity for acetone and 2-butanone. Low conversions of acetic acid seen using HCl-RRM may be due to the loss of promoting metals during the activation process (Alvarez et al., 1998). The lack of promoting metals may also explain the low activity of Fe_2O_3/C. Acetic acid was determined to be the rate limiting reactant. Figure 5.28 shows that the fractional conversion of acetic acid is lower than that of all other reactants across all catalysts. Figure 5.29 shows the carbon recovery in the liquid and gas phases for reactions using each catalyst. Carbon recovery in the liquid phase decreases with increasing catalyst reduction temperature. Figure 5.26 shows a clear decline in selectivity for ketone products with increasing reduction temperature of red mud. This can be attributed to the smaller amounts of magnetite present (seen in Figure 5.10), which is theorized to be the active metal for ketonization. Figure 5.30 shows an approximately linear relationship between the amount of magnetite present in the catalyst and the space time yields of ketone products achieved. Large acetaldehyde peaks were detected via GC-FID in products from reactions using RRM-400 and RRM-500. Increased conversion of acetic acid to acetaldehyde via the reverse Mars-van Krevelen mechanism may also explain the lower acetone yields in reactions using RRM-400 and RRM-500 (pathway shown in Figure 5.17).

Evidence in the literature suggests that the presence of zero valent iron in reduced red mud could promote hydrogenation activity (R. Pestman et al., 1998). In addition, previous studies indicate that decomposition of formic acid can provide an internal source of hydrogen needed for hydrogenation reactions to take place (Karimi et al., 2010). Thus, it was theorized that simultaneous ketonization and hydrogenation may be possible when using red mud reduced at higher temperatures. In this study, reduced red mud containing zero valent iron showed similar conversion of acetic acid, formic acid, acetol and levoglucosan, but showed lower selectivity for ketone products. This suggests that reactants or products were converted to coke. Although TGA analysis indicated little coke formation on all three red mud catalysts (Table 5.4), large chunks of coke were observed in reactions using RRM-400 and RRM-500. Higher reduction temperatures led to an increase in the total mass of solids collected after reactions (shown in Table 5.4). This suggests that coke formation increases with increasing reduction pretreatment temperature, but this coke does not seem to form uniformly on the surface of the catalysts. None of the expected hydrogenation products (isopropanol, 2-butanol, cyclopentanol, ethanol, methanol) were observed. Interestingly, hydrogen was detected in the gas products (3 mol%) using RRM-500 but not RRM-300 or RRM-400. It is theorized that this hydrogen was generated through the decomposition of formic acid. The presence of hydrogen may promote the hydrogenation of ketone products to alcohols and alkanes. However, it is unlikely that significant hydrogenation of ketone products could take place under the low hydrogen partial pressure conditions in these experiments.

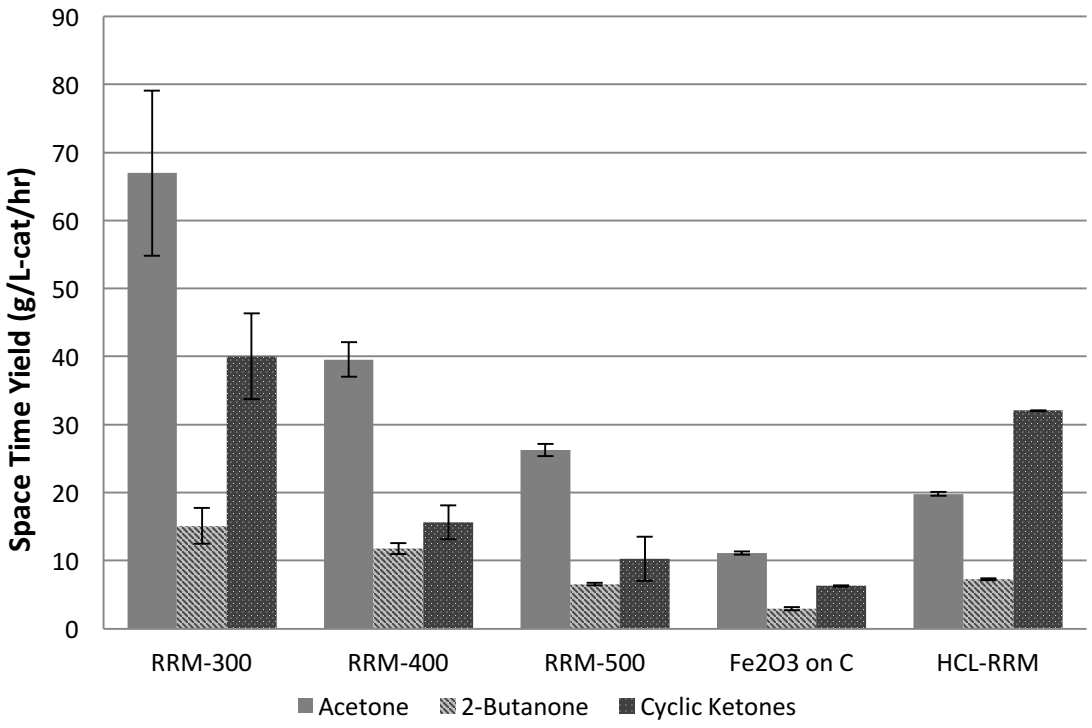

Figure 5.25 Space time yields of ketone products using RRM-300,400,500 (red mud reduced at 300, 400 and 500 °C): reaction temperature = 400°C, P = 1 atm (N_2), WHSV = 0.89 g/g-cat/hr, LHSV= 5.65 hr^{-1}

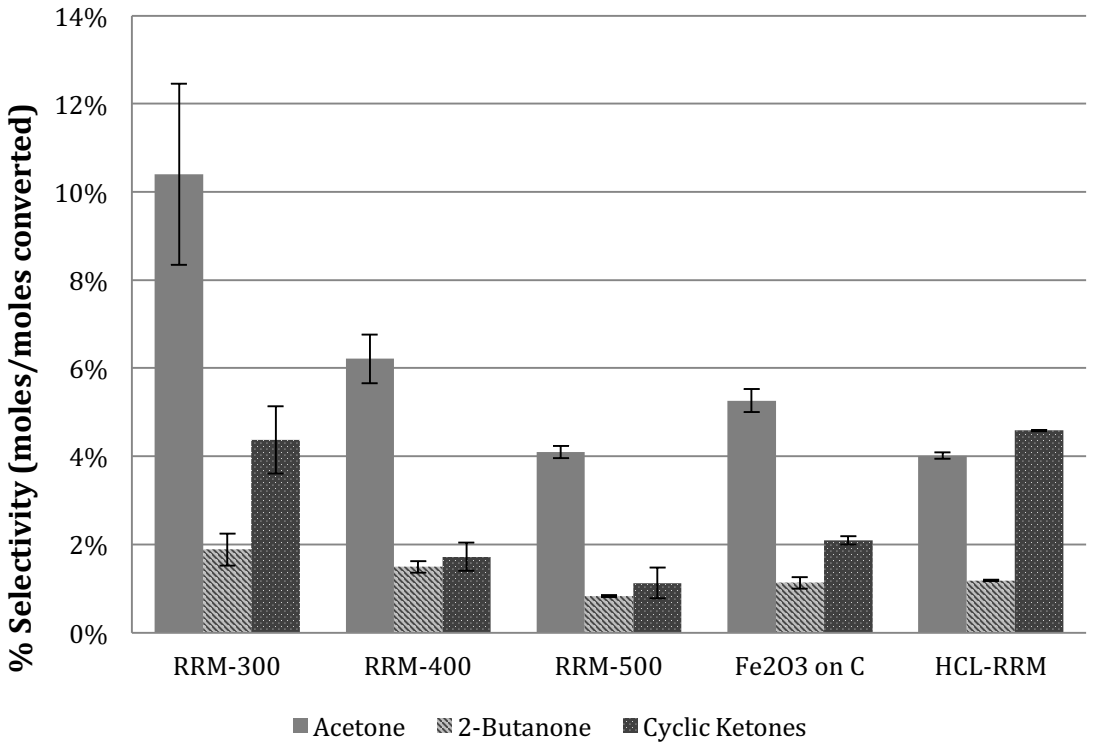

Figure 5.26 Selectivity with respect to ketone products using RRM-300,400,500 (red mud reduced at 300, 400 and 500 °C): reaction temperature = 400°C, P = 1 atm (N_2), WHSV = 0.89 g/g-cat/hr, LHSV= 5.65 hr^{-1}

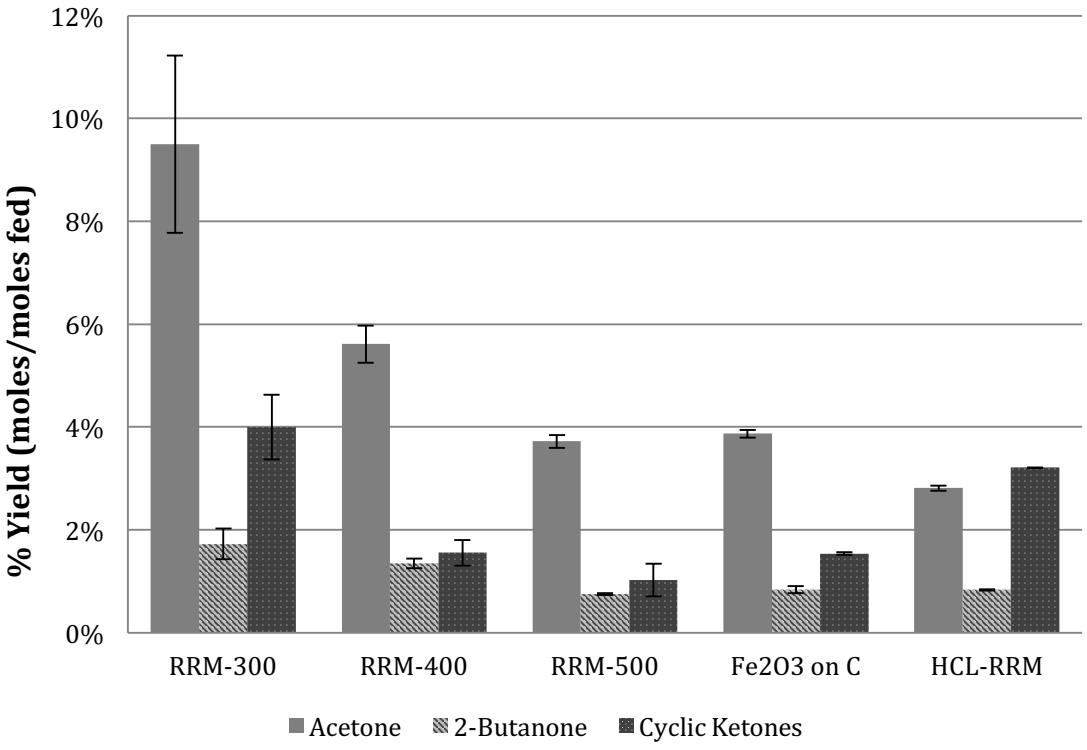

Figure 5.27 Ketone product yields using RRM-300,400,500 (red mud reduced at 300, 400 and 500 °C): reaction temperature = 400°C, P = 1 atm (N_2), WHSV = 0.89 g/g-cat/hr, LHSV= 5.65 hr^{-1}

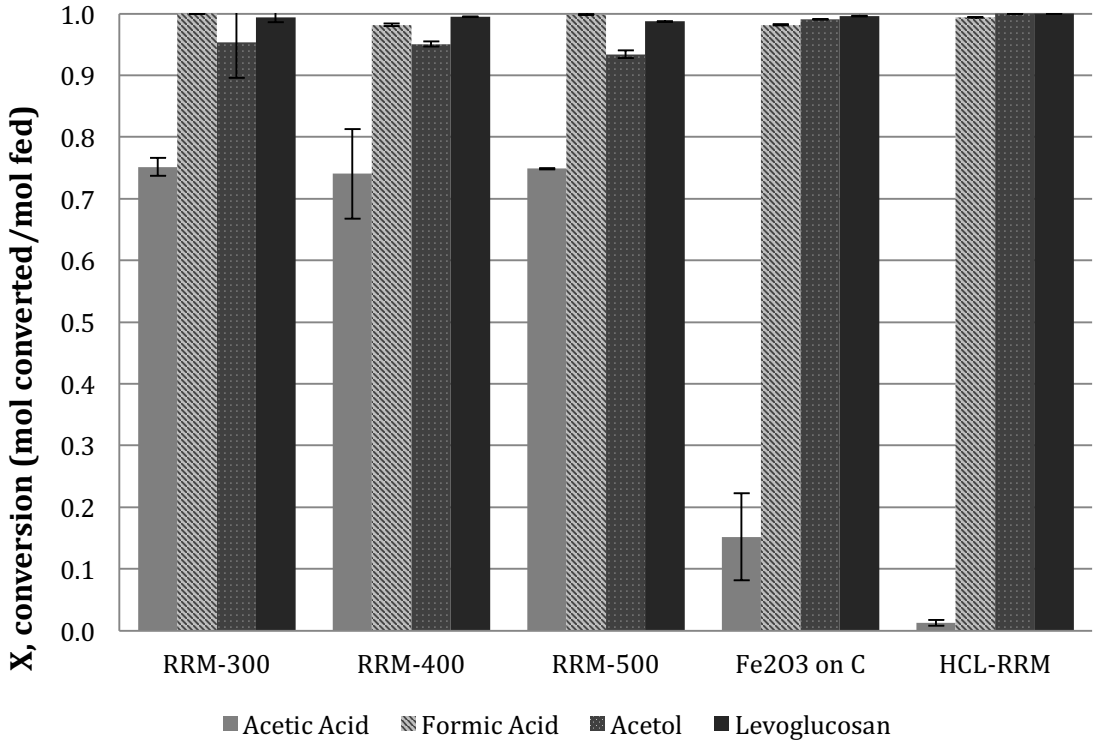

Figure 5.28 Conversion of reactants using RRM-300,400,500 (red mud reduced at 300, 400 and 500 °C): reaction temperature = 400°C, P = 1 atm (N_2), WHSV = 0.89 g/g-cat/hr, LHSV= 5.65 hr^{-1}

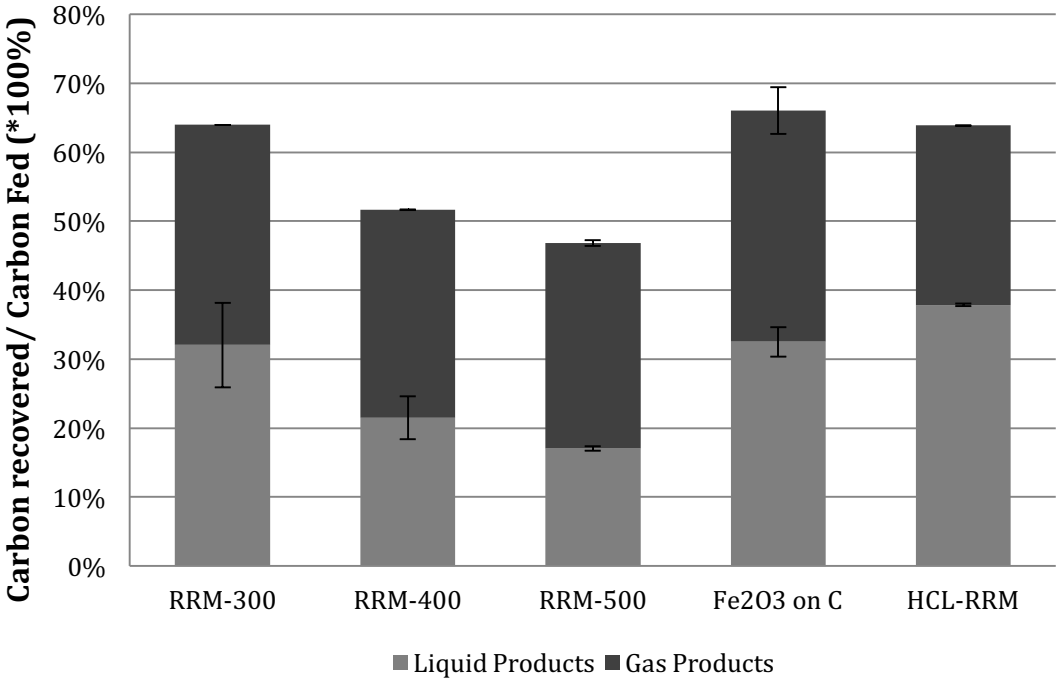

Figure 5.29 Carbon recovery using RRM-300,400,500 (red mud reduced at 300, 400 and 500 °C): reaction temperature = 400°C, P = 1 atm (N_2), WHSV = 0.89 g/g-cat/hr, LHSV= 5.65 hr^{-1}

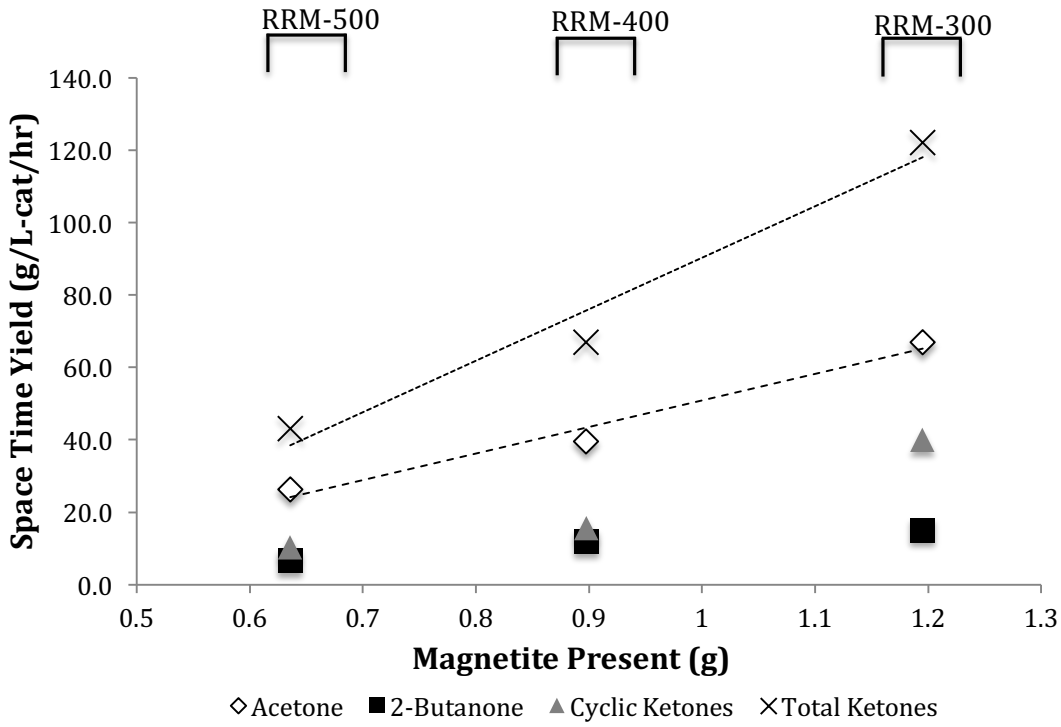

Figure 5.30 Space time yields vs magnetite present in RRM-300,400,500 (red mud reduced at 300, 400 and 500 °C): reaction temperature = 400°C, P = 1 atm (N_2), WHSV = 0.89 g/g-cat/hr, LHSV= 5.65 hr^{-1}. Magnetite quantified via Mössbauer spectroscopy.

Table 5.4 Coke formation and total solids collected after reactions using RRM-300,400 and 500.

Spent Catalyst	Percent Coke measured via TGA	Total Coke + Tar Collected from PBR
	% (w/w)	(g)
RRM-300	3.7%	0.0
RRM-400	2.4%	0.2
RRM-500	1.7%	0.7

Catalysts were analyzed via TGA after reactions at 400 °C, P=1 atm (N_2), WHSV = 0.89 g/g-cat/hr, LHSV= 5.65 hr^{-1}. RRM indicates reduced red mud and the corresponding temperature that it was reduced at prior to reactions. Total coke plus tar collected represents the total mass of solids that were collected from the packed bed after reactions minus the starting mass of catalyst loaded, and thus includes both tar accumulation and large chunks of coke.

5.2.4 Effect of Total Pressure On Ketonization of Carboxylic Acids using Red Mud

The presence of hydrogen measured in the gas phase products in reactions using RRM-500 supports the hypothesis that hydrogen is produced internally via decomposition of formic acid (proposed pathway shown in Figure 5.17). The very low hydrogen partial pressure observed (0.03 atm) is unlikely to lead to significant hydrogenation of ketone products. It was theorized that increasing hydrogen partial pressure may lead to simultaneous hydrogenation of ketone products to alcohols. In order to test this hypothesis, a series of experiments were conducted that tested the effect of total pressure on ketonization/hydrogenation of carboxylic acids using red mud. Continuous reaction studies were conducting using red mud (pre-reduced at 300 °C) under the following conditions: T= 400 °C, LHSV= 5.646 1/hr. Total reaction pressure was varied from atmospheric pressure to 600 psi using nitrogen. It was theorized that increasing total nitrogen pressure would increase the partial pressure of internally generated hydrogen, if present.

Figure 5.31 shows selectivity for primary ketone products versus total nitrogen pressure for RRM-300. Increasing total pressure from atmospheric pressure to 150 psi led to an increase in 2-butanone selectivity, but further increase in pressure shows no significant trend. Total conversion of reactants was not significantly affected by total pressure (see Figure 5.34). However, cyclic ketone selectivity decreases significantly when increasing total pressure above atmospheric pressure. Quantitative GC/MS analysis indicated increasing levels of linear pentanones (2-pentanone, 3-pentanone, and various methylated pentanones) (see Figure 5.31). It is theorized that increasing total pressure increases the availability of internally generated hydrogen, which leads to increased conversion of acetic acid to acetaldehyde via the reverse Mars-van Krevelen mechanism (shown in Figure 2.6). Acetaldehyde is then converted to 3-pentan-2-one via condensation with acetone and further hydrogenated to 2-pentanone. A shift in selectivity from acetol to propylene glycol rather than pyruvaldehyde may explain the decrease in cyclic ketones and increase in 3-pentanone and 2-butanone, although the exact mechanism is unclear. It is theorized that 3-pentanone is generated via hydrogenation of acetol to propylene glycol, followed by pinacol arrangement to propanal, followed by oxidation to propanoic acid and ketonization to form 3-pentanone (Chompoonut & Vithaya, 2005). The carbon balance (see Figure 5.35) shows that increasing total pressure leads to significantly reduced gas phase carbon generation (CO_2 and CO). The decrease in recovered carbon at higher pressures was attributed to increased coke formation. Similar to the findings in section 5.2.3, coke seemed to form into chunks near the top of the catalyst bed rather than on the surface of catalyst particles throughout the bed. The total mass of coke + tar collected after each reaction is depicted

in Table 5.5. Large plugs of coke were observed for reactions at 150 and 300 psi, but no plugging was observed at atmospheric pressure. No hydrogen was detected in the gas products, indicating that any hydrogen generated via formic acid decomposition was immediately consumed.

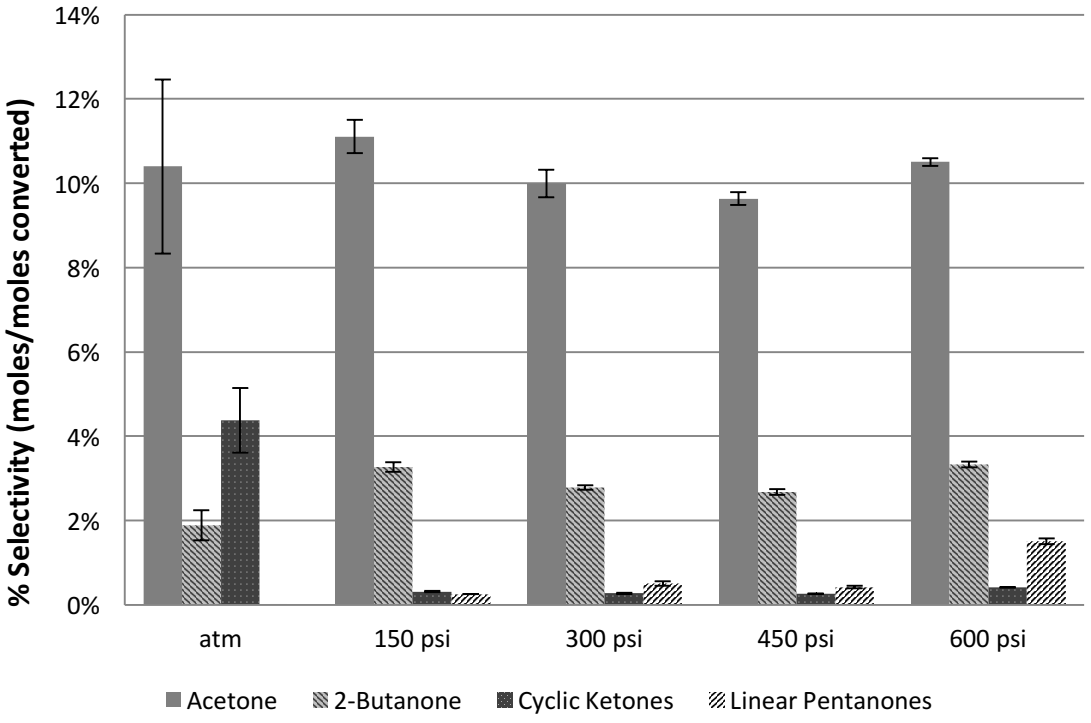

Figure 5.31 Ketone selectivity vs N_2 pressure using red mud reduced at 300 °C: reaction temperature = 400°C, WHSV = 0.89 g/g-cat/hr, LHSV= 5.65 hr^{-1}

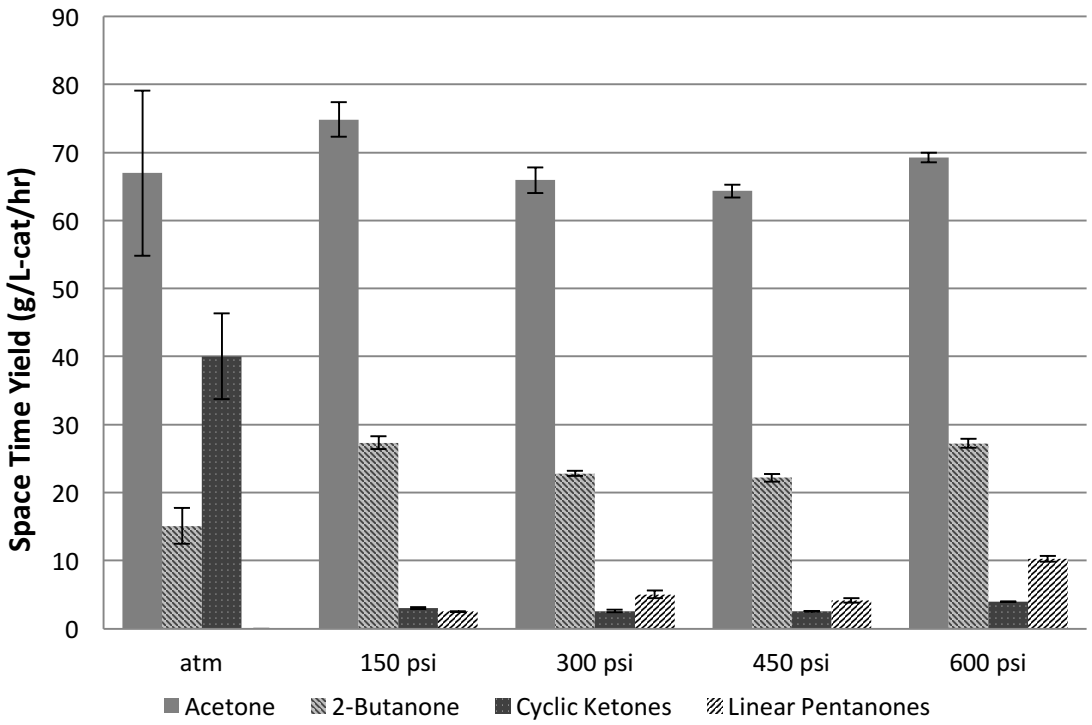

Figure 5.32 Space time yields vs N_2 pressure using red mud reduced at 300 °C: reaction temperature = 400°C, WHSV = 0.89 g/g-cat/hr, LHSV= 5.65 hr^{-1}

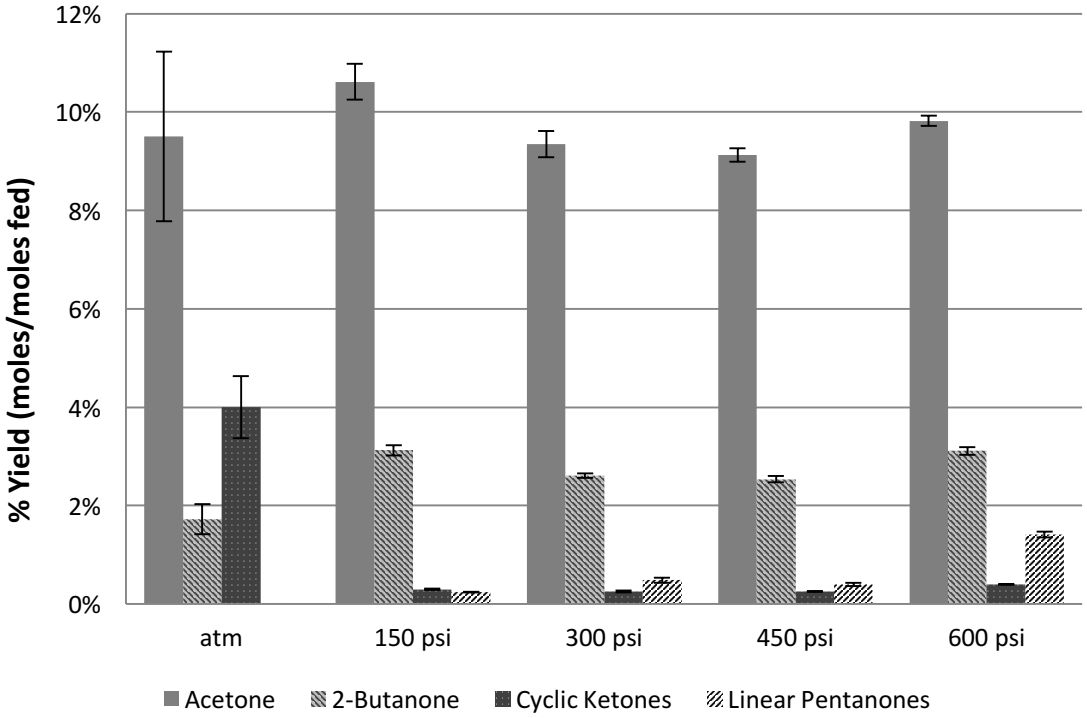

Figure 5.33 Ketone yield vs N_2 pressure using red mud reduced at 300 °C: reaction temperature = 400°C, WHSV = 0.89 g/g-cat/hr, LHSV= 5.65 hr^{-1}

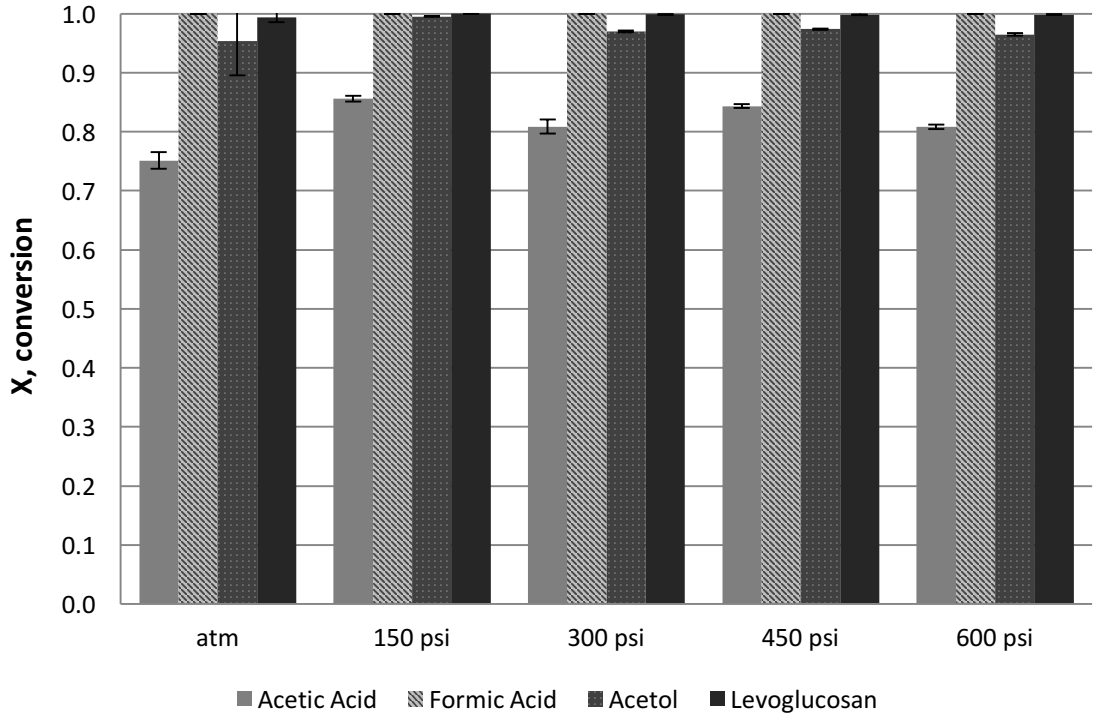

Figure 5.34 Conversion of reactants vs N_2 pressure using red mud reduced at 300 °C: reaction temperature = 400°C, WHSV = 0.89 g/g-cat/hr, LHSV= 5.65 hr^{-1}

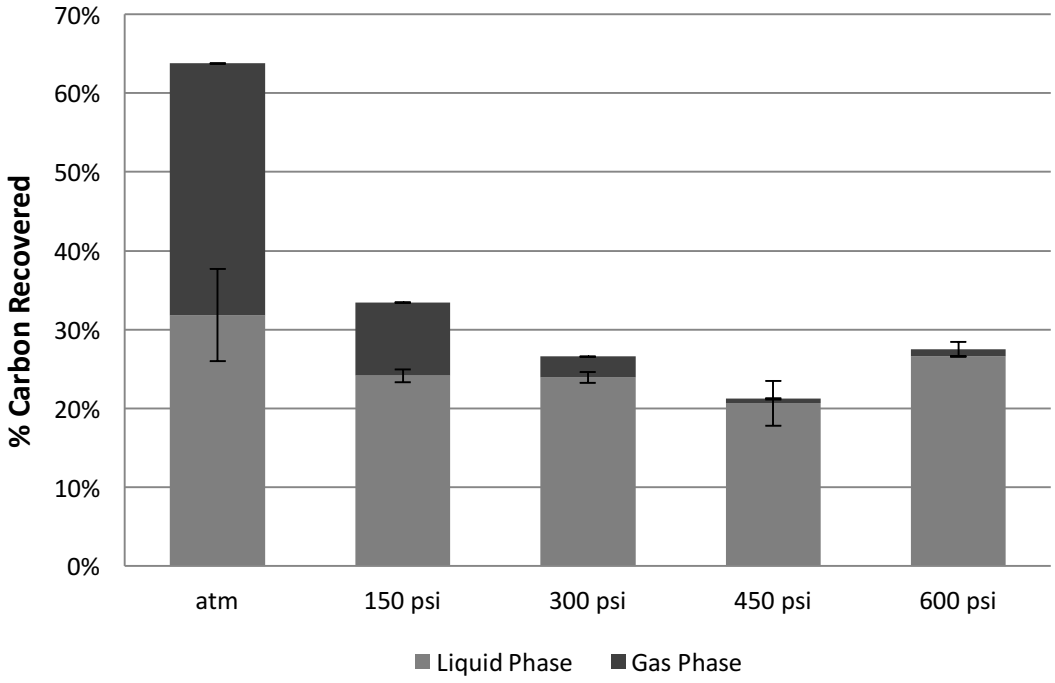

Figure 5.35 Carbon recovery vs N_2 pressure using red mud reduced at 300 °C: reaction temperature = 400°C, WHSV = 0.89 g/g-cat/hr, LHSV= 5.65 hr^{-1}

Table 5.5 Total weight of solids collected from the packed bed reactor vessel after reactions using RRM-300 at varing N_2 pressures.

Reaction Pressure	Total Coke+Tar Collected (g)
atm	0.0
150psi	0.5
300psi	0.4
450psi	0.2
600psi	0.0

Reaction conditions: T= 400 °C, WHSV = 0.89 g/g-cat/hr, LHSV= 5.65 hr^{-1}. Total coke plus tar collected represents the total mass of solids that were collected from the packed bed after reactions minus the starting mass of catalyst loaded, and thus includes both tar accumulation and large chunks of coke.

5.2.5 The Effect of Externally Added Hydrogen on Conversion of Carboxylic Acids using Red Mud

In the previous section, it was theorized that increasing the total pressure would increase the availability of internally generated hydrogen for hydrogenation of ketones to alcohols. However, none of the expected hydrogenation products from acetone, 2-butanone, or cyclopentanone were detected. In order to continue to explore the potential simultaneous ketonization/hydrogenation activity of red mud, hydrogen was added externally as a carrier gas. The proposed pathway depicted in Figure 5.17 indicates that hydrogen may have a role in the formation of several products including 2-butanone, 2-pentanone, and cyclopentanone. In order to further understand this, the best reaction conditions from the ketonization experiments with red mud were repeated using hydrogen instead of nitrogen as a carrier gas. The following reaction conditions were used: catalyst= RRM reduced at 300°C, reaction temperature= 400 °C, P= atm (H_2), WHSV = 0.89 g/g-cat/hr, LHSV= 5.65 hr^{-1}, feedstock= acetic acid, formic acid, levoglucosan, acetol (4% each).

Figure 5.36 and Figure 5.37 show a comparison between ketonization reactions using H_2 and N_2 as a carrier gas at atmospheric pressure. No significant differences between acetone or 2-butanone yields were observed. Significantly lower cyclic ketone yields were observed for reactions using externally added H_2. In addition, 2-pentanone and 3-pentanone peaks were observed via GCMS in reactions using H_2 (atm). The shift in selectivity from cyclic ketones to 2-pentanone and 3-pentanone was also observed in ketonization reactions at elevated nitrogen pressure (section 5.2.4), suggesting that increasing total pressure (N_2) or adding external hydrogen have a similar effect on

product selectivity. These observations support the original hypothesis described in section 5.2.4 that increasing total pressure shifts selectivity from cyclic ketones to linear pentanones by increasing the availability of internally generated hydrogen. The addition of hydrogen also resulted in larger acetaldehyde peaks (identified via GC/FID, but not quantified). This supports the hypothesis that H_2 increases selectivity for acetaldehyde from acetic acid via the reverse Mars van Krevelen mechanism.

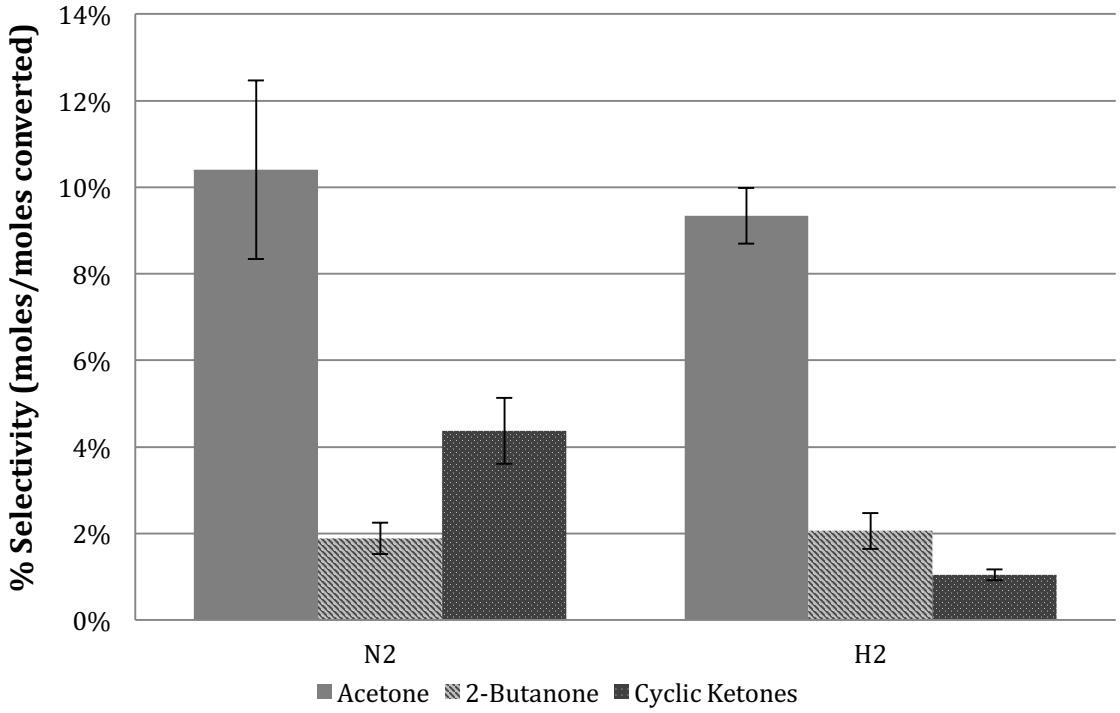

Figure 5.36 The effect of externally added hydrogen on ketone selectivity using RRM-300 (red mud reduced at 300 °C): reaction temperature= 400°C, P= 1 atm, WHSV = 0.89 g/g-cat/hr, LHSV= 5.65 hr^{-1}

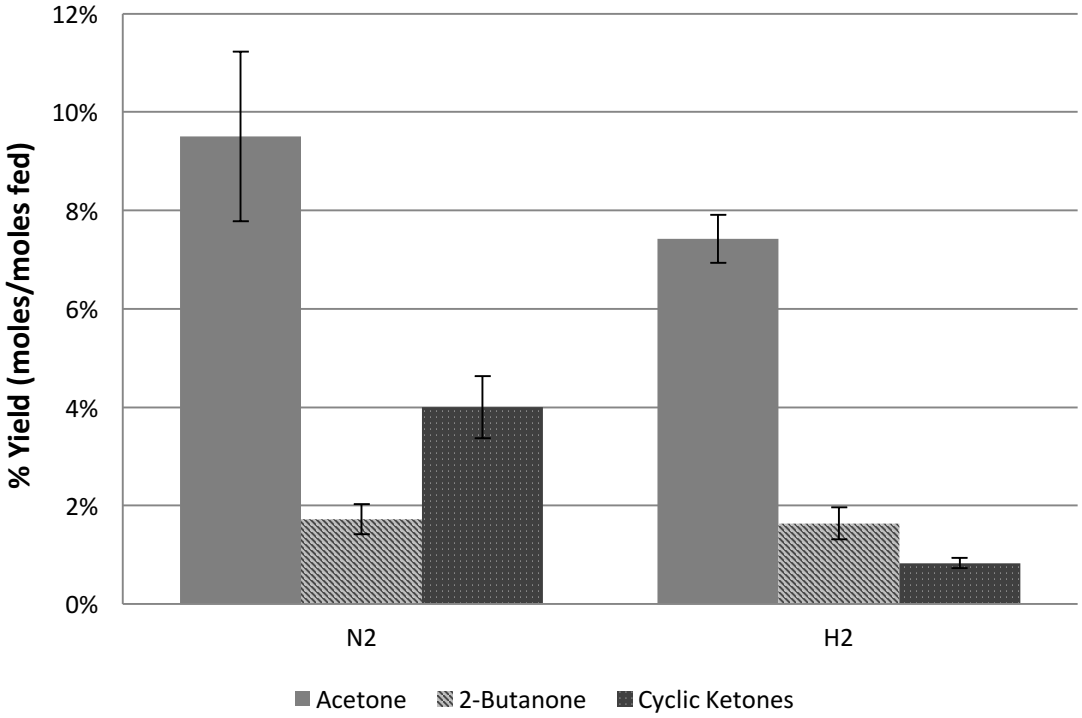

Figure 5.37 The effect of externally added hydrogen on ketone yield using RRM-300 (red mud reduced at 300 °C): reaction temperature= 400°C, P= 1 atm, WHSV = 0.89 g/g-cat/hr, LHSV= 5.65 hr^{-1}

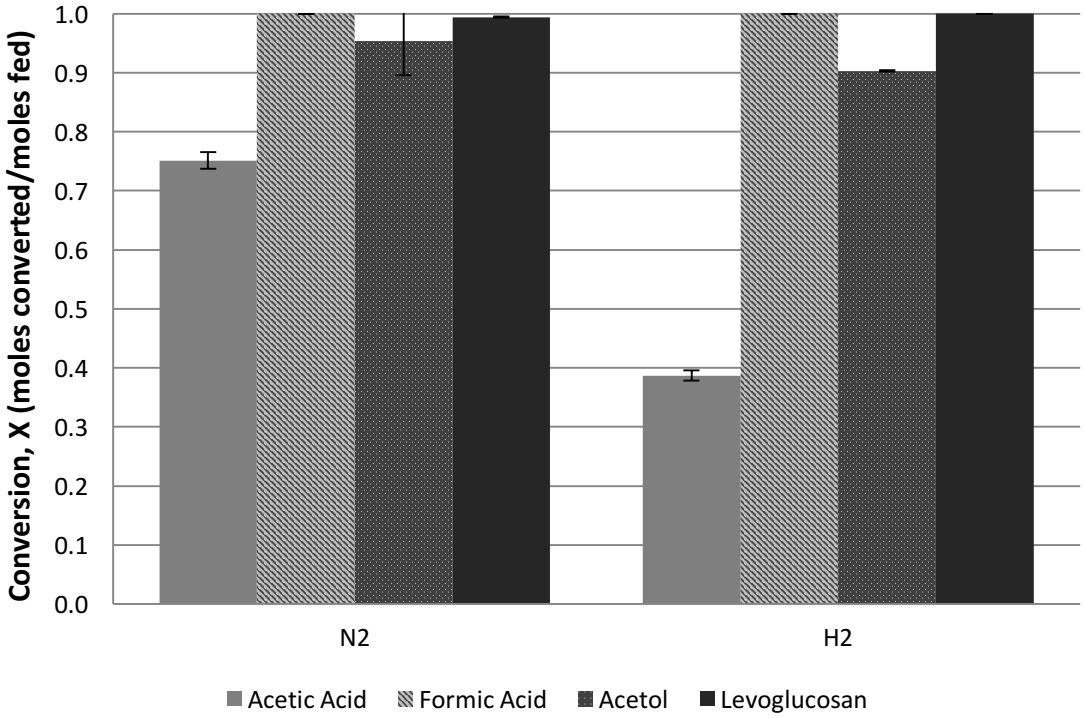

Figure 5.38 The effect of externally added hydrogen on reactant conversion using RRM-300 (red mud reduced at 300 °C): reaction temperature= 400°C, P= 1 atm, WHSV = 0.89 g/g-cat/hr, LHSV= 5.65 hr^{-1}

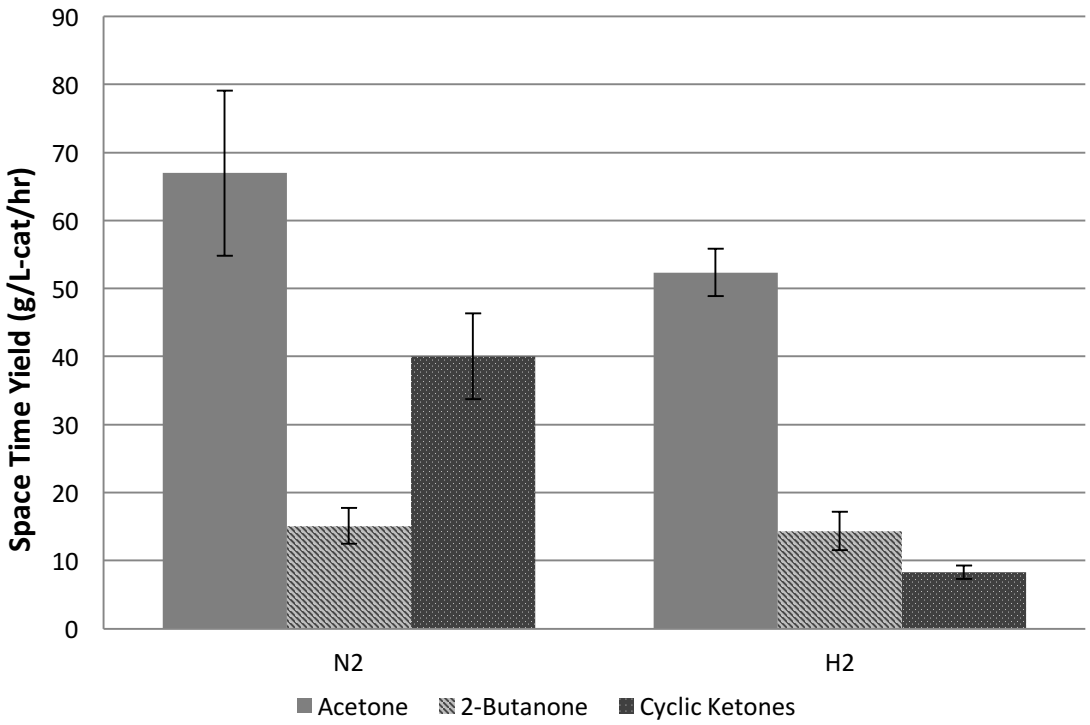

Figure 5.39 The effect of externally added hydrogen on space time yields using RRM-300 (red mud reduced at 300 °C): reaction temperature= 400°C, P= 1 atm, WHSV = 0.89 g/g-cat/hr, LHSV= 5.65 hr^{-1}

5.2.6 The Effect of Externally Added Hydrogen on Ketonization of Carboxylic Acids using Red Mud reduced at 400 °C and 500 °C

The purpose of this series of experiments is to test the effect of increasing hydrogen pressure on conversion of carboxylic acids using red mud reduced at 400°C and 500 °C. Due to the presence of zero valent iron in red mud reduced at these temperatures, it was hypothesized that ketone products (acetone, 2-butanone, and cyclic ketones) could be hydrogenated to alcohols. A series of experiments were conducted in a packed bed reactor system using RRM-400 and RRM-500 at atmospheric pressure, 150 psi, and 300 psi using the following conditions: reaction temperature= 400 °C, WHSV =

0.89 g/g-cat/hr, LHSV= 5.65 hr^{-1}. GC-FID analysis of the liquid products indicated that none of the expected hydrogenation products (isopropanol, 2-butanol, cyclopentanol) were formed in the reactions. Figure 5.40 shows that RRM-400 has higher selectivity for ketone products than RRM-500, which is consistent with the results of previous studies in N_2 at atmospheric pressure (section 5.2.3). In addition, lower cyclic ketone yields at elevated pressure were observed in agreement with the results described in section 5.2.4 and section 5.2.5. Interestingly, increasing pressure from 1 atmosphere to 150 psi resulted in a significant increase in acetone and 2-butanone space time yields using both RRM-400 and RRM-500. These observations are consistent with the results in section 5.2.4, where the effect of increasing nitrogen pressure was tested. It is apparent that increasing reaction pressure (regardless of carrier gas) from atmospheric pressure to 150 psi increases the conversion of acetic acid and acetol, which leads to higher acetone and 2-butanone space time yields (see Figure 5.43). Increasing pressure beyond 150 psi seems to have no significant effect on conversions of reactants or ketone product yields.

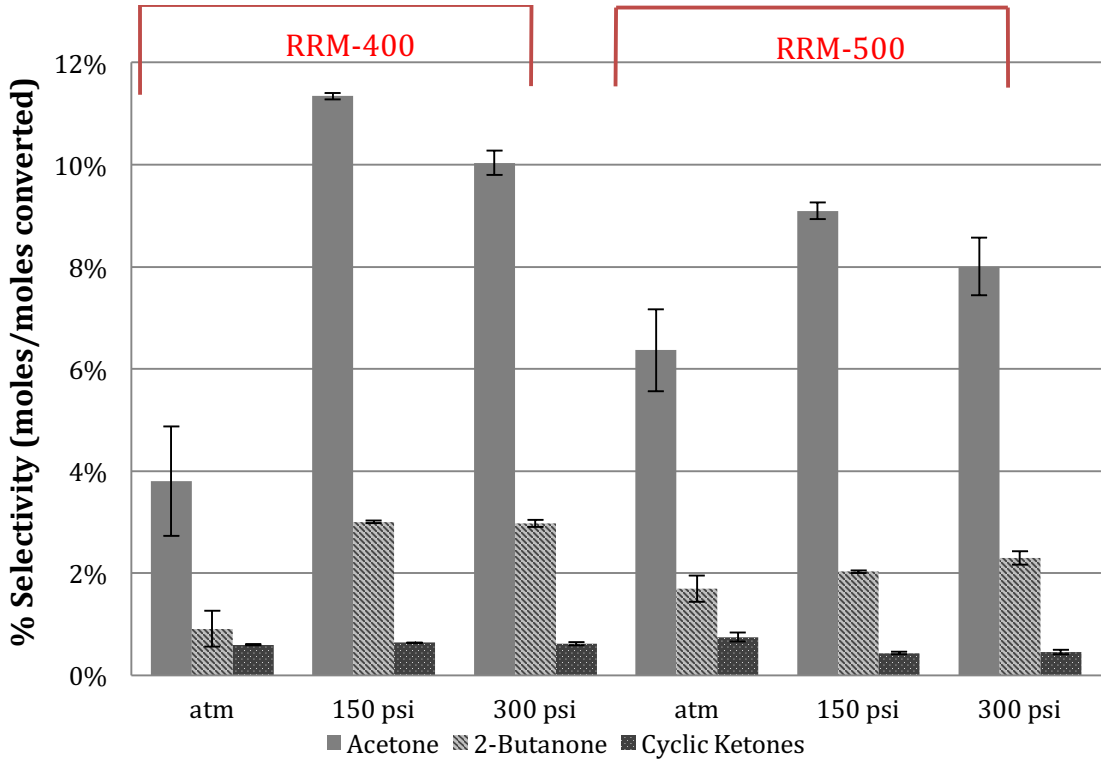

Figure 5.40 Selectivity vs. hydrogen pressure using RRM-400,500 (red mud reduced at 400 and 500 °C): reaction temperature= 400 °C, WHSV = 0.89 g/g-cat/hr, LHSV= 5.65 hr^{-1}

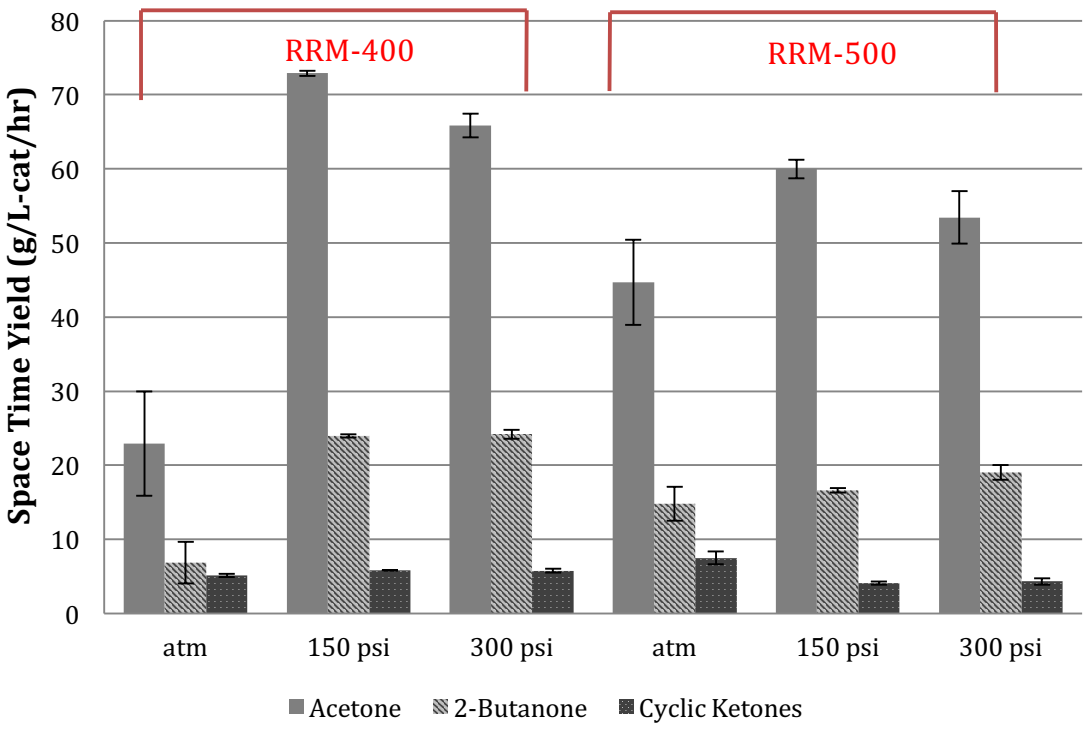

Figure 5.41 Space time yield vs. hydrogen pressure using RRM-400,500 (red mud reduced at 400 and 500 °C): reaction temperature= 400 °C, WHSV = 0.89 g/g-cat/hr, LHSV= 5.65 hr^{-1}

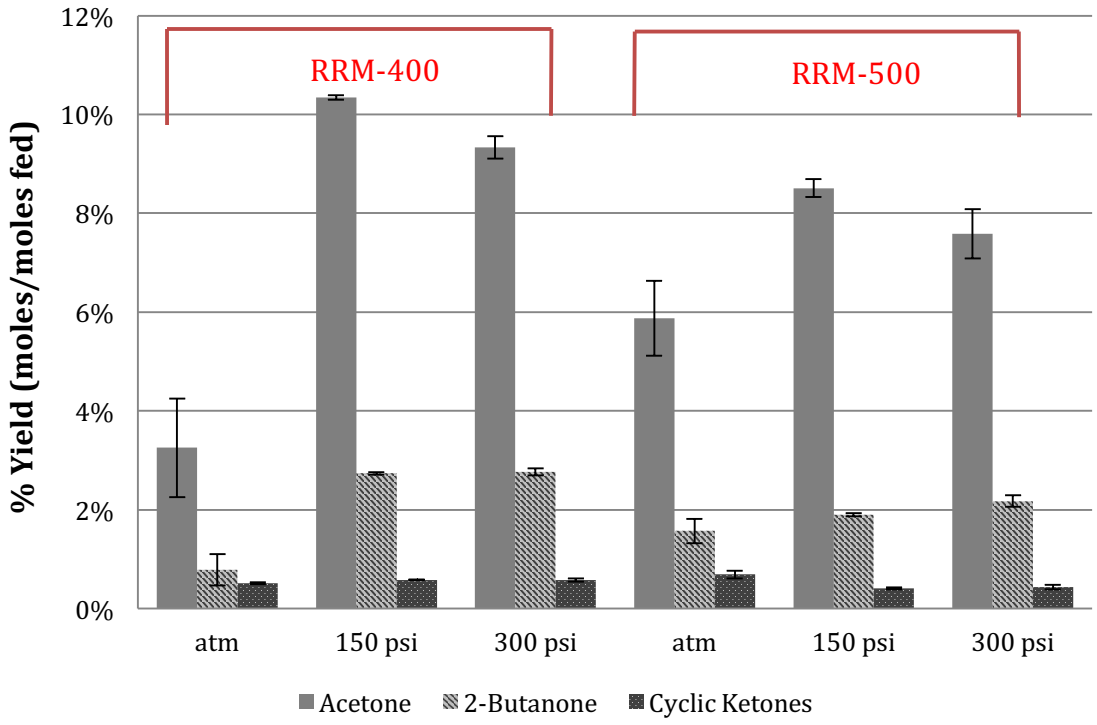

Figure 5.42 Ketone yields vs. hydrogen pressure using RRM-400,500 (red mud reduced at 400 and 500 °C): reaction temperature= 400 °C, WHSV = 0.89 g/g-cat/hr, LHSV= 5.65 hr^{-1}

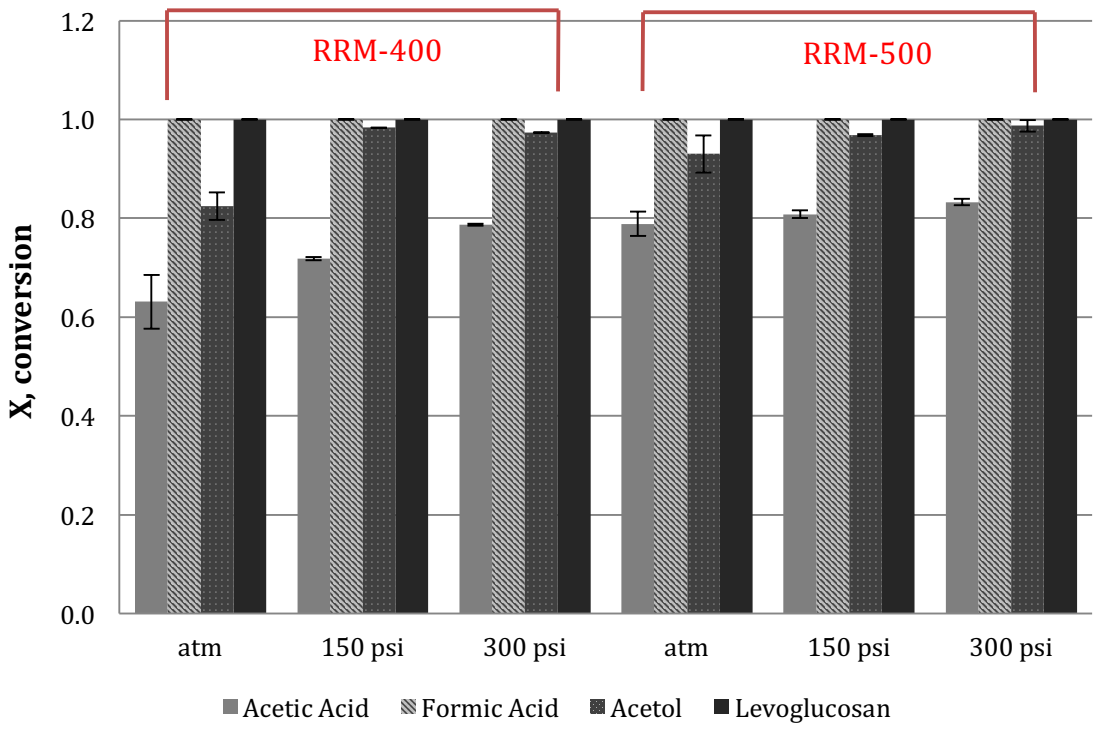

Figure 5.43 Reactant conversion vs. hydrogen pressure using RRM-400,500 (red mud reduced at 400 and 500 °C): reaction temperature= 400 °C, WHSV = 0.89 g/g-cat/hr, LHSV= 5.65 hr^{-1}

5.2.7 Ketonization of Carboxylic Acids using Fe-SiAl

Ketonization activity of Fe-SiAl was determined in a packed bed reactor system using the optimal reaction conditions determined in previous ketonization studies using red mud (section 5.2.1). The following reaction conditions were used: T= 400 °C, P = atm (N_2), WHSV= 5.646 1/hr. The Fe-SiAl catalyst was reduced at 300 °C in situ for 20 hours prior to reactions. A mixture of acetic acid, formic acid, 1-hydroxy, 2-propanone, and levoglucosan (4% each in H_2O) was fed into the reactor at a rate of 0.5 mL/min. Figure 5.44- Figure 5.48 compare the selectivity, space time yield and conversion of reactants of Fe-SiAl with that of reduced red mud at identical reaction conditions.

Analysis of liquid products indicated that Fe-SiAl forms the same major products as reduced mud in previous experiments. A comparison of the GC/MS chromatograms from red mud and Fe-SiAl at identical reaction conditions showed nearly identical products. This suggests that the ketonization pathway proposed for red mud (see Figure 5.17) is also valid for Fe-SiAl. However, Fe-SiAl showed significantly lower ketone yields than red mud (see Figure 5.45). Figure 5.47 shows that little to no acetic acid was converted by Fe-SiAl. However, acetol, levoglucosan, and formic acid were not detected in the liquid products and appear to be completely converted. The loss of carbon can be explained by the formation of coke. TGA analysis on spent Fe-SiAl indicated high levels of coke (0.094 g-coke/g-cat). An addition, a solid plug of coke (approximately 0.1g) was observed near the top of the Fe-SiAl catalyst bed that was not seen in experiments using red mud. This plug was likely the result of thermal polymerization of levoglucosan. The resistance to coke formation exhibited by red mud may be due to the presence of promoting metals (Na and K) (Dorner et al., 2009). In addition, higher levels of coke formation observed on Fe-SiAl may be caused by the higher number of strong acid sites, as described in the literature (Brillis & Manos, 2003). Coke formation that partially blocks active sites on Fe-SiAl is one explanation for the lower the ketonization activity observed. In addition, H_2 pulse titration of Fe-SiAl indicated much lower dispersion for Fe-SiAl compared to RRM (shown in Table 5.3). The low concentration of iron exposed on the surface of the Fe-SiAl catalyst provides another rationale for the low ketone yields and selectivity that were observed.

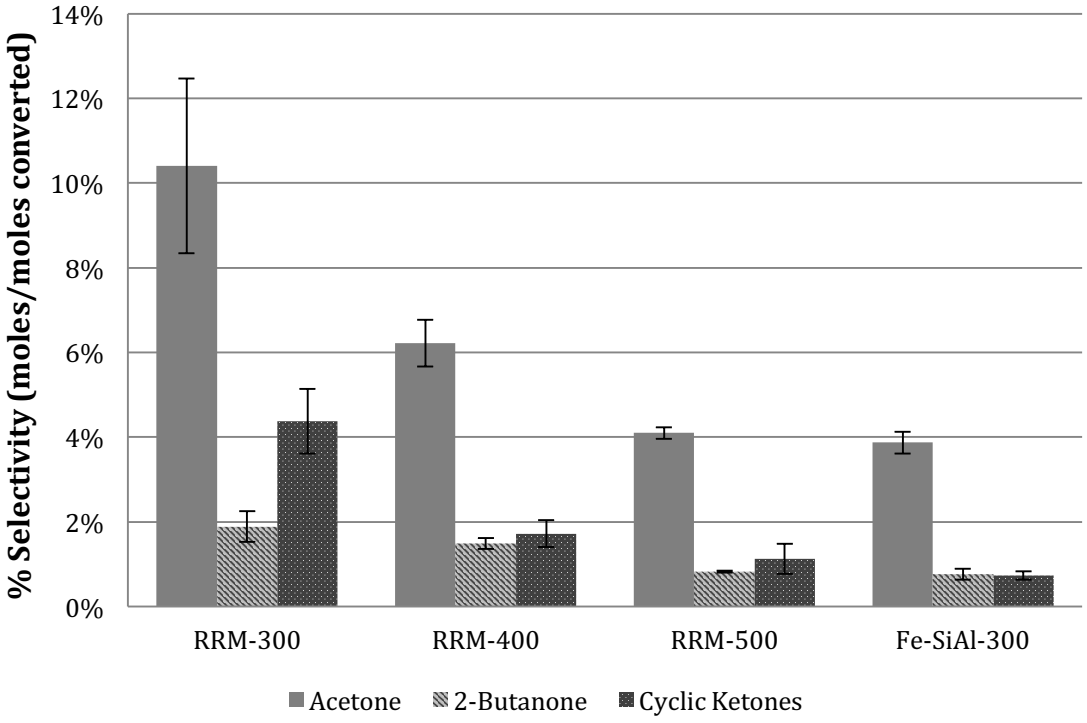

Figure 5.44 Ketone selectivity using RRM-300,400,500, and Fe-SiAl-300 (red mud reduced at 300, 400 and 500 °C and iron oxide on silica alumina support reduced at 300 °C): reaction temperature = 400°C, P = 1 atm (N_2), WHSV = 0.89 hr^{-1}

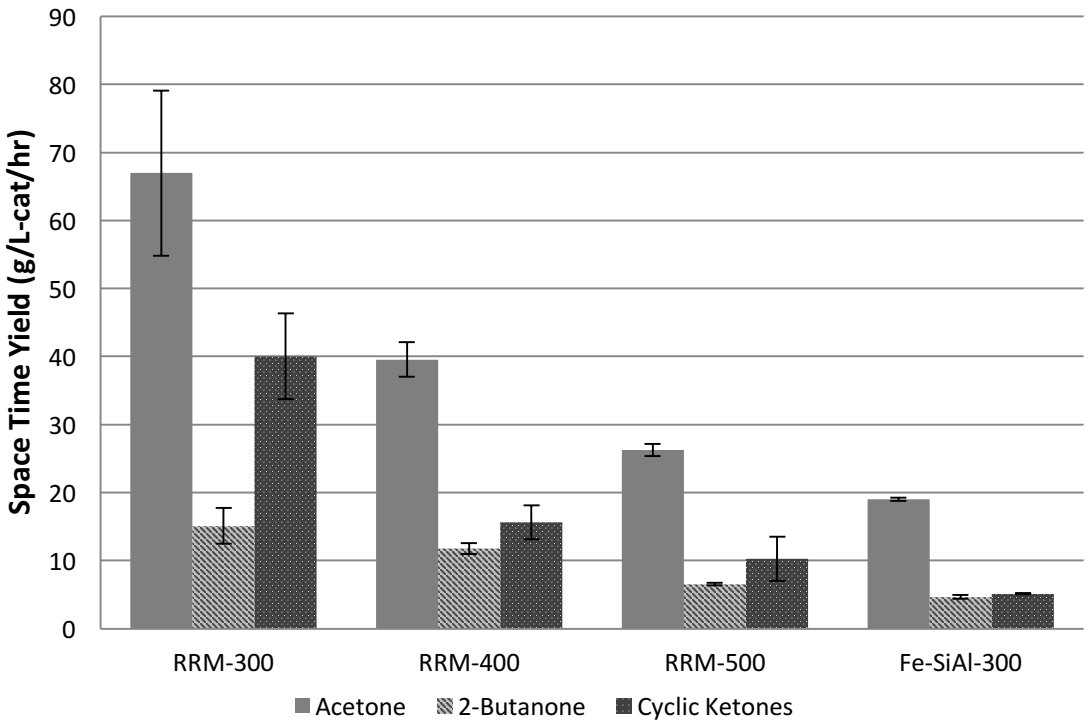

Figure 5.45 Space time yields using RRM-300,400,500, and Fe-SiAl-300 (red mud reduced at 300, 400 and 500 °C and iron oxide on silica alumina support reduced at 300 °C): reaction temperature = 400°C, P = 1 atm (N_2), WHSV = 0.89 hr^{-1}

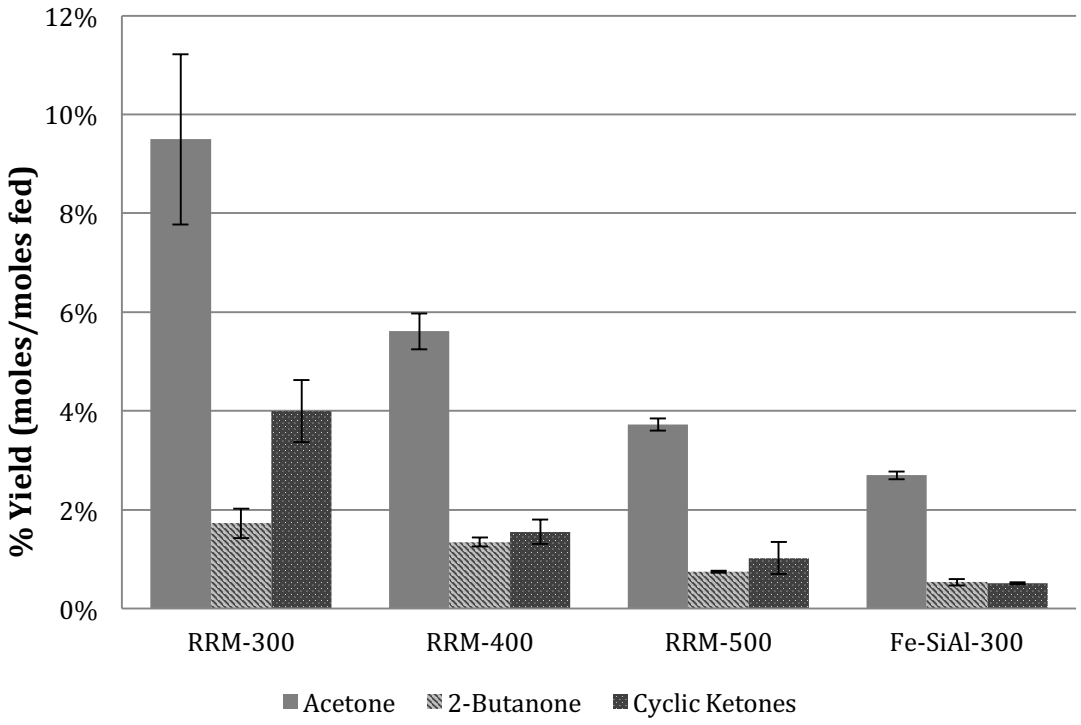

Figure 5.46 Ketone yields using RRM-300,400,500, and Fe-SiAl-300 (red mud reduced at 300, 400 and 500 °C and iron oxide on silica alumina support reduced at 300 °C): reaction temperature = 400°C, P = 1 atm (N_2), WHSV = 0.89 hr^{-1}

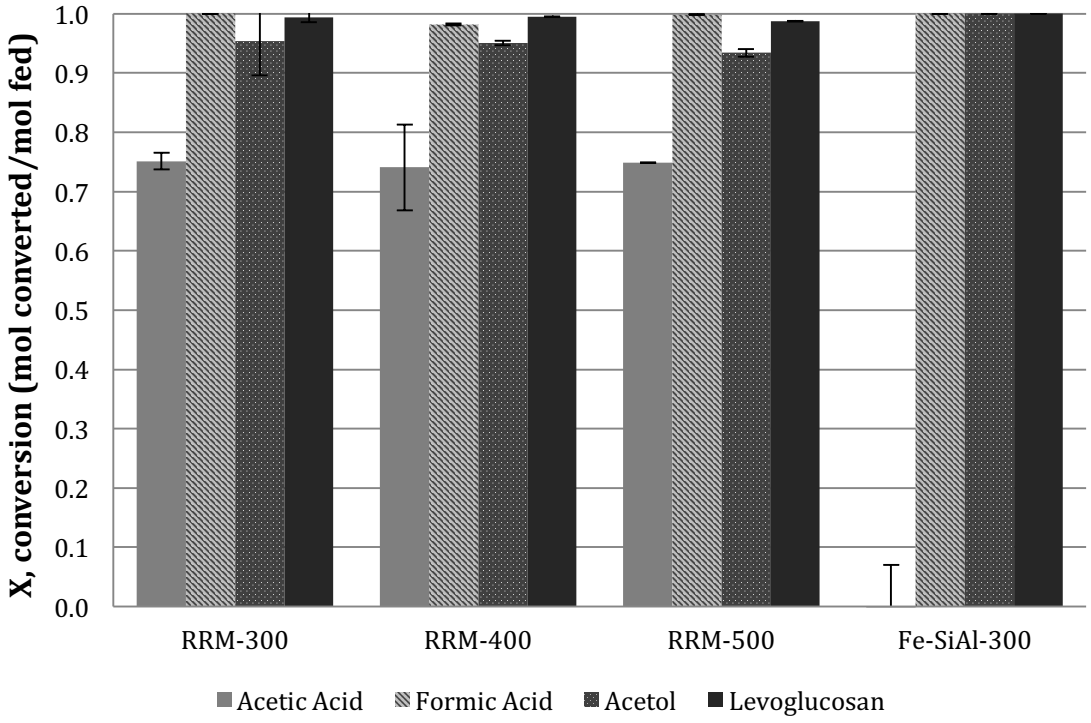

Figure 5.47 Conversion of reactants using RRM-300,400,500, and Fe-SiAl-300 (red mud reduced at 300, 400 and 500 °C and iron oxide on silica alumina support reduced at 300 °C): reaction temperature = 400°C, P = 1 atm (N_2), WHSV = 0.89 hr^{-1}

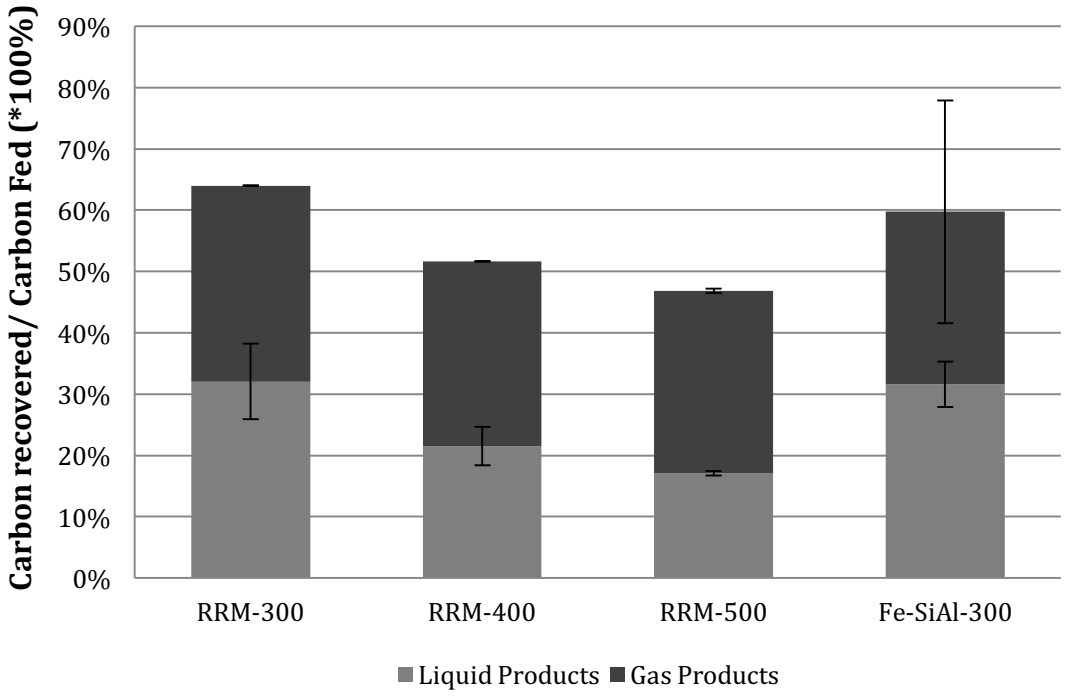

Figure 5.48 Carbon recovery using RRM-300,400,500, and Fe-SiAl-300 (red mud reduced at 300, 400 and 500 °C and iron oxide on silica alumina support reduced at 300 °C): reaction temperature = 400°C, P = 1 atm (N_2), WHSV = 0.89 hr^{-1}

Fe-SiAl was also compared with red mud for potential ketonization and simultaneous hydrogenation activity. In this series of experiments, Fe-SiAl and red mud were pre-reduced at 400°C for 20 hours. Reactions were then conducted in a packed bed reactor system with the following conditions: T= 400 °C, P = 300 psi (H_2), WHSV= 5.646 1/hr. Analysis of liquid products indicated significantly lower ketonization yields using Fe-SiAl, as seen in the previous experiment at atmospheric pressure in N_2 (see Figure 5.51). None of the expected hydrogenation products (isopropanol, 2-butanol, cyclopentanol) were observed using red mud or Fe-SiAl.

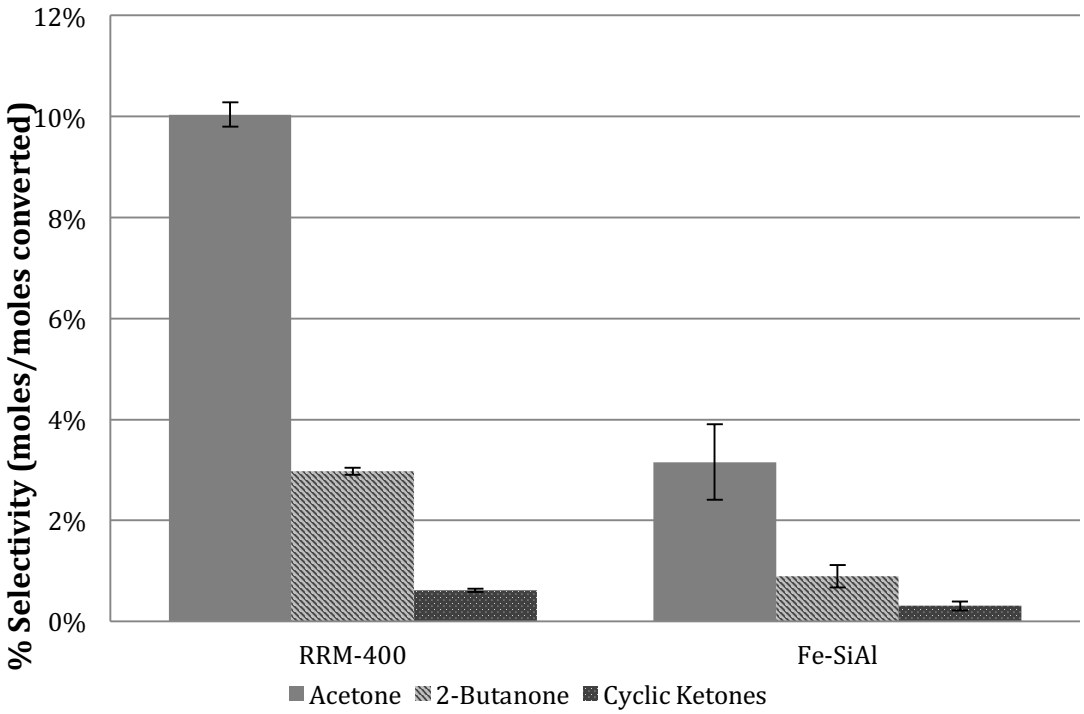

Figure 5.49 Ketone selectivity using RRM-400 and Fe-SiAl-400: catalysts prereduced at 400°C, reaction temperature= 400°C, P= 300 psi (H_2), WHSV=0.89 hr^{-1}

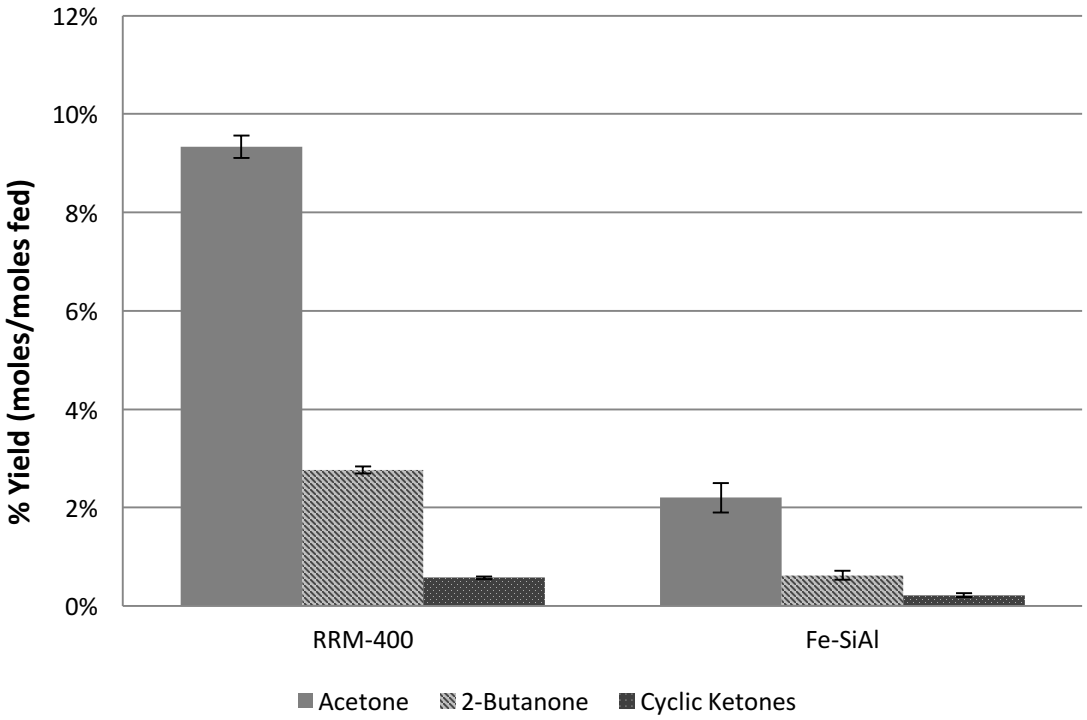

Figure 5.50 Ketone yield using RRM-400 and Fe-SiAl-400: catalysts prereduced at 400°C, reaction temperature= 400°C, P= 300 psi (H_2), WHSV=0.89 hr^{-1}

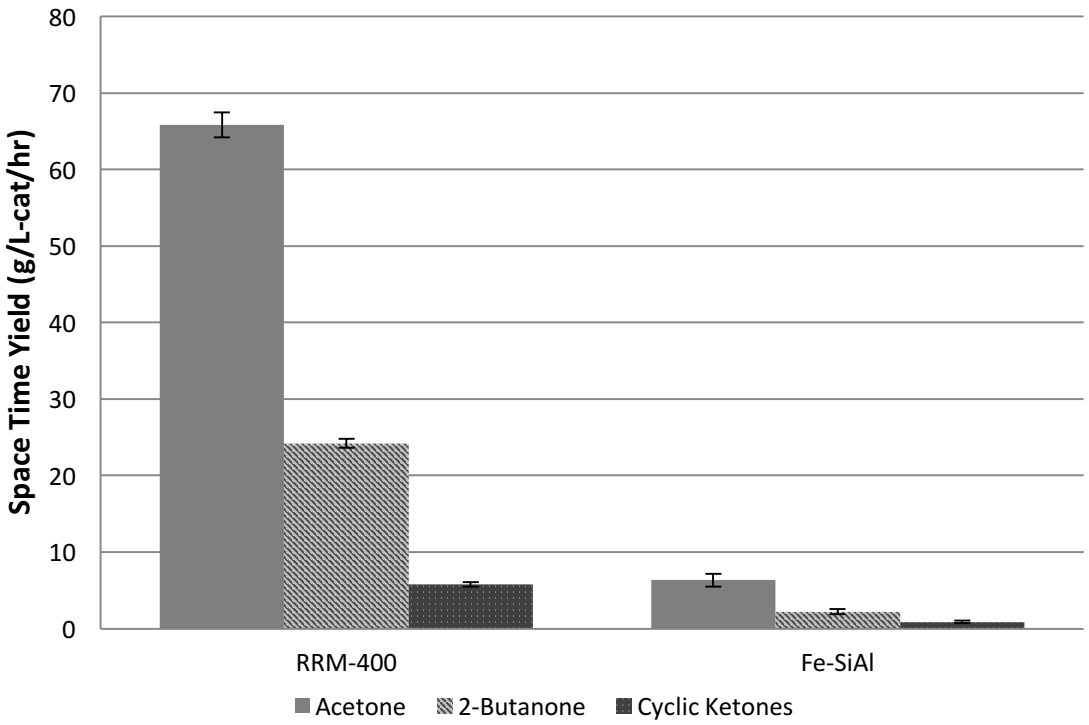

Figure 5.51 Space time yields using RRM-400 and Fe-SiAl-400: catalysts prereduced at 400°C, reaction temperature= 400°C, P= 300 psi (H_2), WHSV=0.89 hr^{-1}

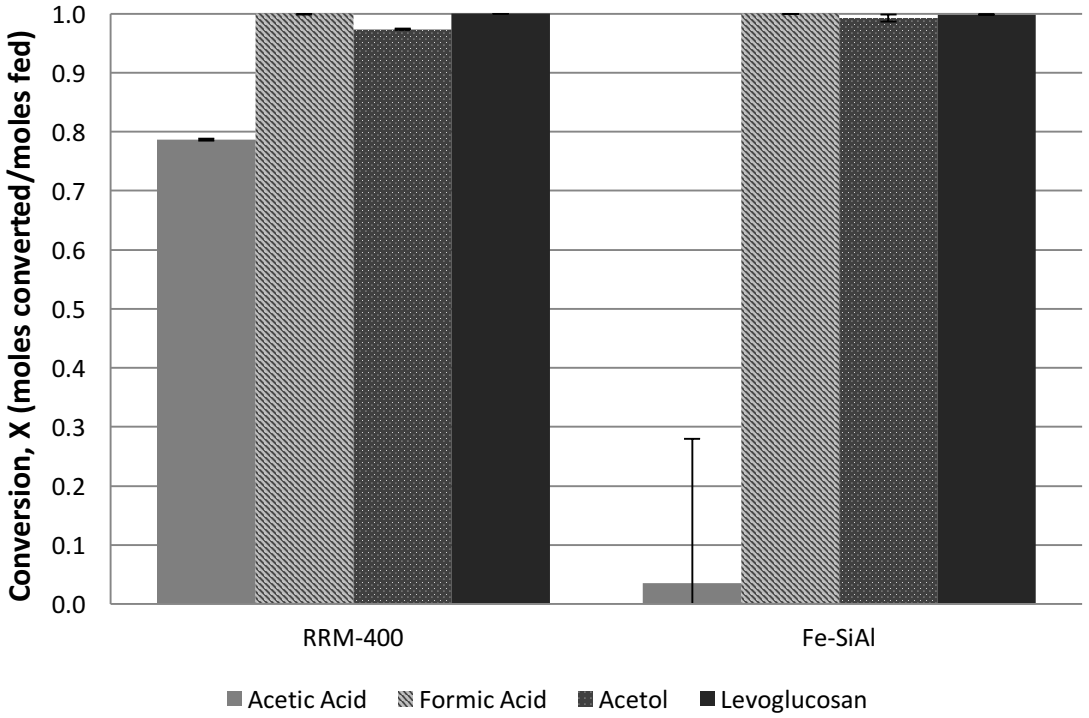

Figure 5.52 Reactant conversion using RRM-400 and Fe-SiAl-400: catalysts prereduced at 400°C, reaction temperature= 400°C, P= 300 psi (H_2), WHSV=0.89 hr^{-1}

5.3 Hydrogenation Studies

The studies described in sections 5.2.1- 5.2.3 demonstrate that mixed metal oxide catalysts prepared from red mud are capable of converting bio-oil oxygenates to a variety of ketone products including acetone, 2-butanone, and a variety of cyclic ketones. The following reactions were conducted to study the hydrogenation of these ketone products to alcohols and alkanes. Model compound mixtures representing the primary products from ketonization reactions were prepared. This mixture consists of acetone (2%), 2-butanone (0.5%), cyclopentanone (0.75%) and 2-cylcopenten-1-one (0.75%) in water, selected based on the typical product concentrations from the study described in section

5.2.1. In addition to studies using model compounds, hydrogenation studies using actual liquid products collected from ketonization reactions are described in section 5.4.

5.3.1 The effect of hydrogen pressure on Hydrogenation of Ketones Using Pd-C Monolith Catalysts

The effect of pressure on hydrogenation of ketones was studied in a series of reactions conducted in a packed bed reactor using Pd-ACM catalysts. Reactions were conducted using ketone model compound mixtures at the following conditions: reaction temperature= 180 °C, WHSV= 0.0538 hr^{-1}, LHSV 0.389 hr^{-1}. The effect of pressure was studied by conducting reactions at atmospheric pressure, 150 psi, and 300 psi (pure H_2). Figure 5.53 compares isopropanol, 2-butanol, and cyclopentanol selectivity at 1 atm, 150 psi, and 300 psi. Total selectivity was calculated by summing that of isopropanol, 2-butanol, and cyclopentanol. As expected, increasing hydrogen pressure lead to a general increase in reactant conversion and product yields. Conversion of acetone, 2-butanone, and cyclopentanone increased dramatically from atmospheric pressure to 150 psi, but only slightly from 150 psi to 300 psi (see Figure 5.55). The total alcohol space time yield was highest at 300 psi (7 g/L-cat/hr) and was chosen as the optimal pressure to be used in subsequent experiments. No cyclopenten-1-one was detected in the liquid products for any of the reaction conditions tested, which suggests that complete hydrogenation of cyclopenten-1-one to cyclopentanone occurs rapidly. For this reason, cyclopenten-1-one was not included in the feedstock for subsequent experiments. Approximately 75% of the carbon fed was recovered in the liquid products for all three reactions. No products were detected in the gas phase.

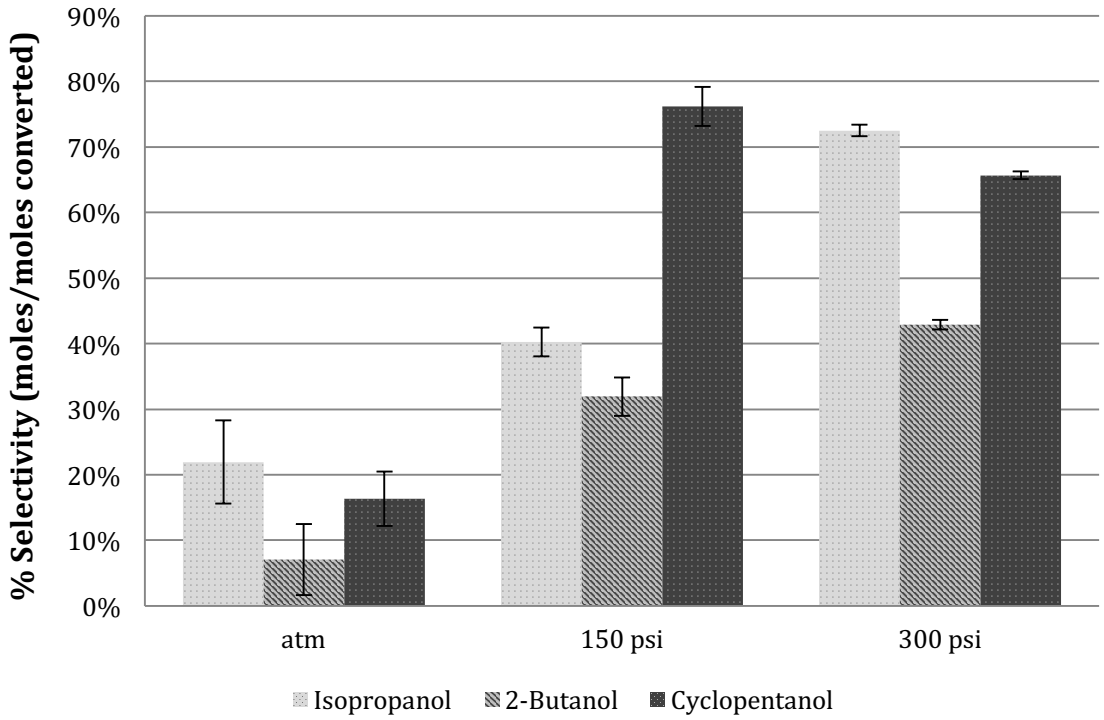

Figure 5.53 Alcohol selectivity versus H_2 pressure using Pd-ACM (0.8 wt%). Reaction conditions: T=180 °C, WHSV= 0.0538 hr^{-1}, LHSV 0.389 hr^{-1}

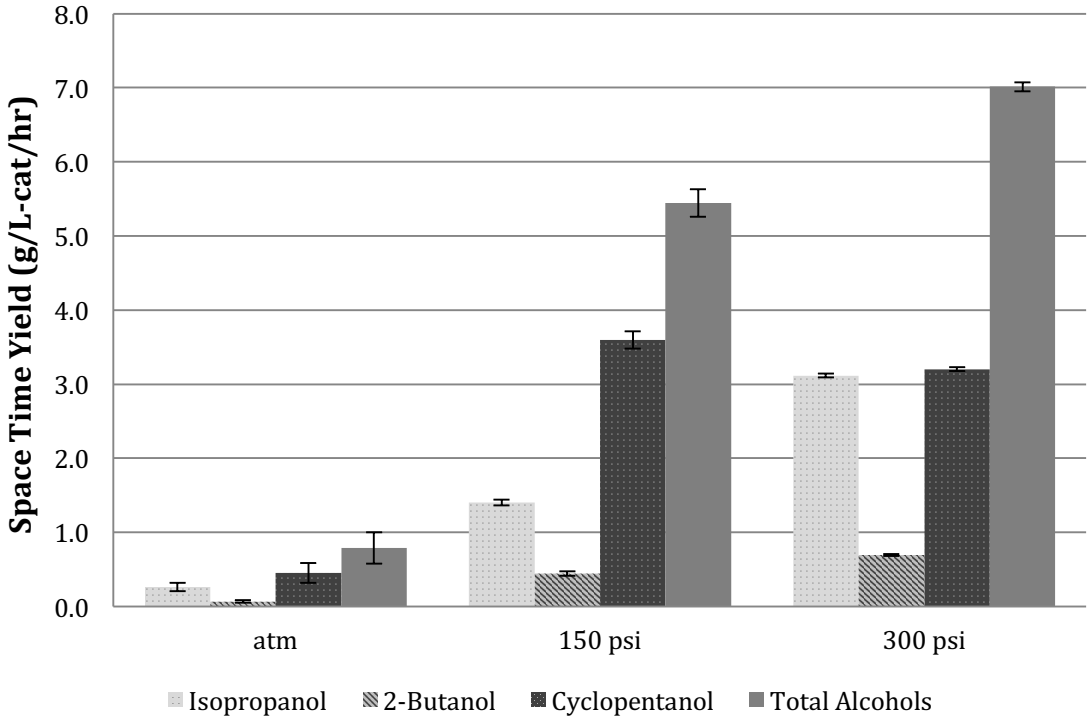

Figure 5.54 Space time yields versus H_2 pressure using Pd-ACM (0.8 wt%). Reaction conditions: T=180 °C, WHSV= 0.0538 hr^{-1}, LHSV 0.389 hr^{-1}

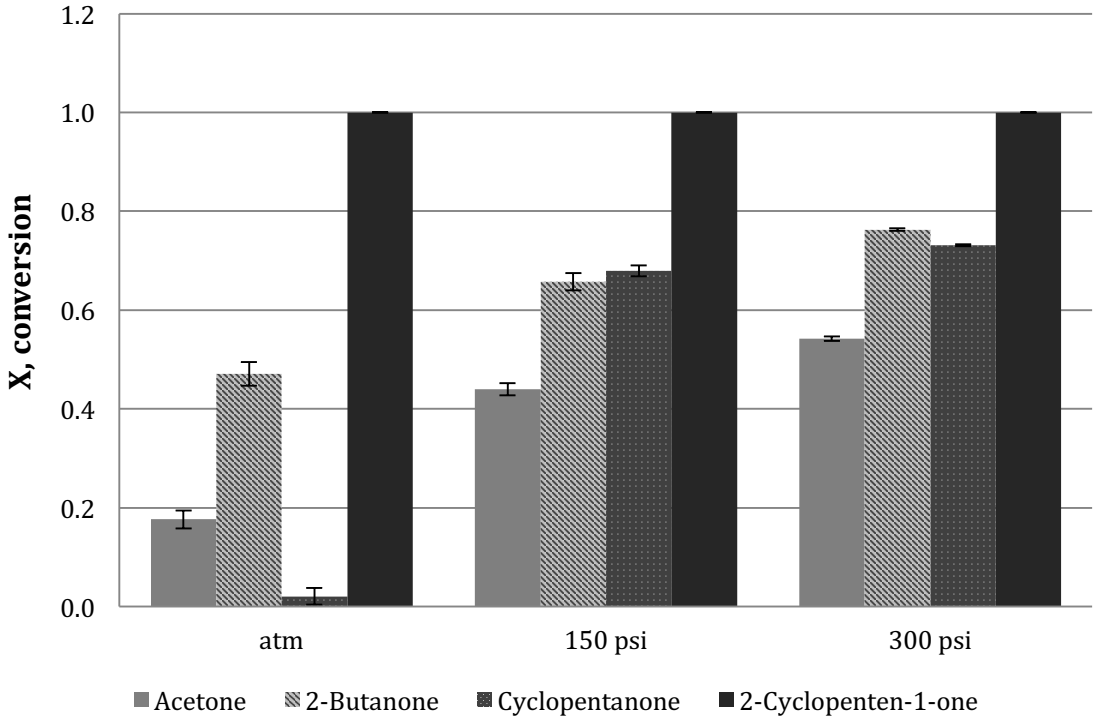

Figure 5.55 Conversion of ketones versus H_2 pressure using Pd-ACM (0.8 wt%). Reaction conditions: T=180 °C, WHSV= 0.0538 hr^{-1}, LHSV 0.389 hr^{-1}

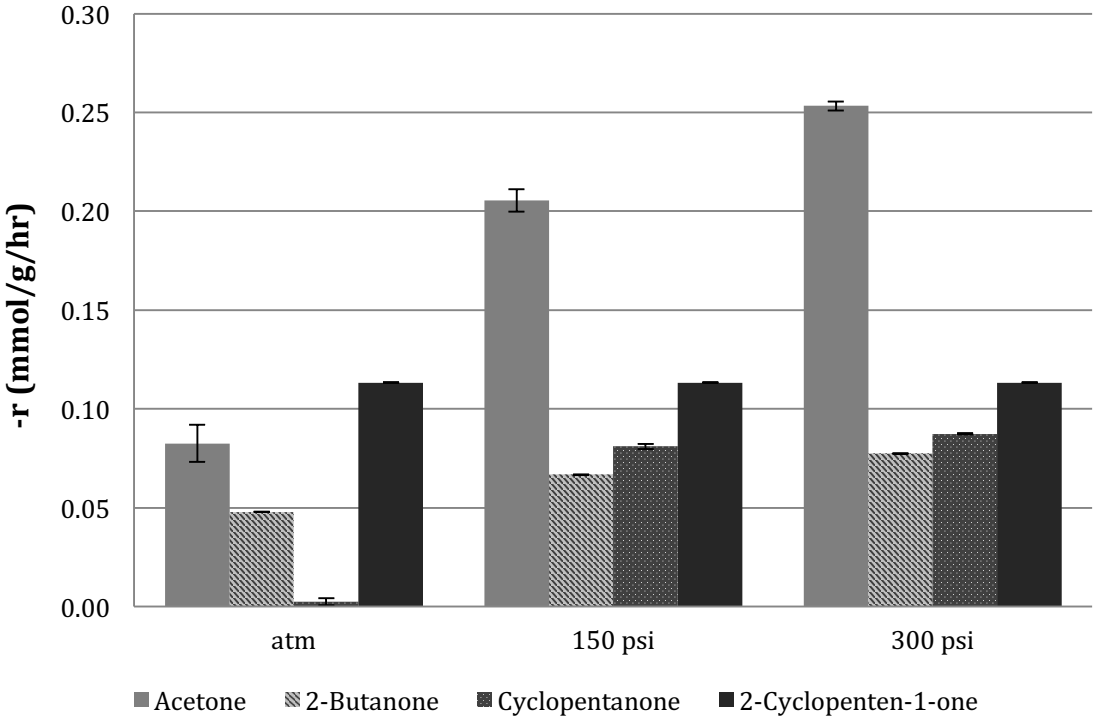

Figure 5.56 Observed reaction rates versus H_2 pressure using Pd-ACM (0.8 wt%). Reaction conditions: T=180 °C, WHSV= 0.0538 hr^{-1}, LHSV 0.389 hr^{-1}

5.3.2 The Effect of Temperature on Hydrogenation Activity Using Pd-C Monoliths

The effect of reaction temperature on hydrogenation of ketones to alcohols was using the optimal conditions determined in the previous section (P= 300 psi H_2, WHSV= 0.0538 hr^{-1}, LHSV 0.389 hr^{-1}). Reactions were run at three different temperatures (130, 150 and 180 °C) using the same 6 Pd-ACM cores tested in section 5.3.1 without replacement. Figure 5.57 indicates that increasing reaction temperature leads to higher selectivity with respect to isopropanol, 2-butanol, and cyclopentanol. Figure 5.58 shows that total alcohol space time yields were similar for reactions at 130°C and 150°C (≈ 2.5 g/L-cat/hr) and much higher for 180°C (≈ 7 g/L-cat/hr). Cyclopentanol yields appear to

be most affected by increasing temperature. Interestingly, conversion of acetone and 2-butanone decreases with increasing temperature (Figure 5.59). Figure 5.60 shows that carbon recovery in the liquid phase was significantly higher at 180°C than reactions at 130°C and 150°C (70% versus ≈ 35%). Based on the results of these experiments, 180°C was chosen as the optimal temperature for hydrogenation studies using Pd-C catalysts.

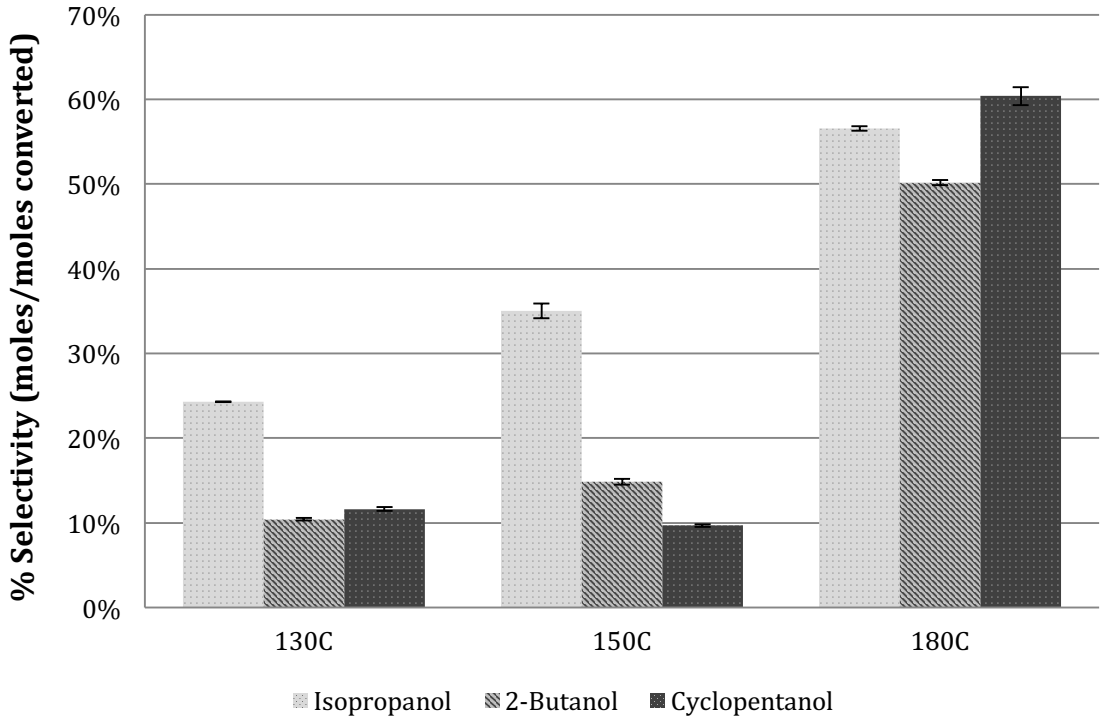

Figure 5.57 Alcohol selectivity versus temperature using Pd-ACM (0.8 wt%). Reaction conditions: P= 300 psi (H_2), WHSV= 0.0538 hr^{-1}, LHSV 0.389 hr^{-1}

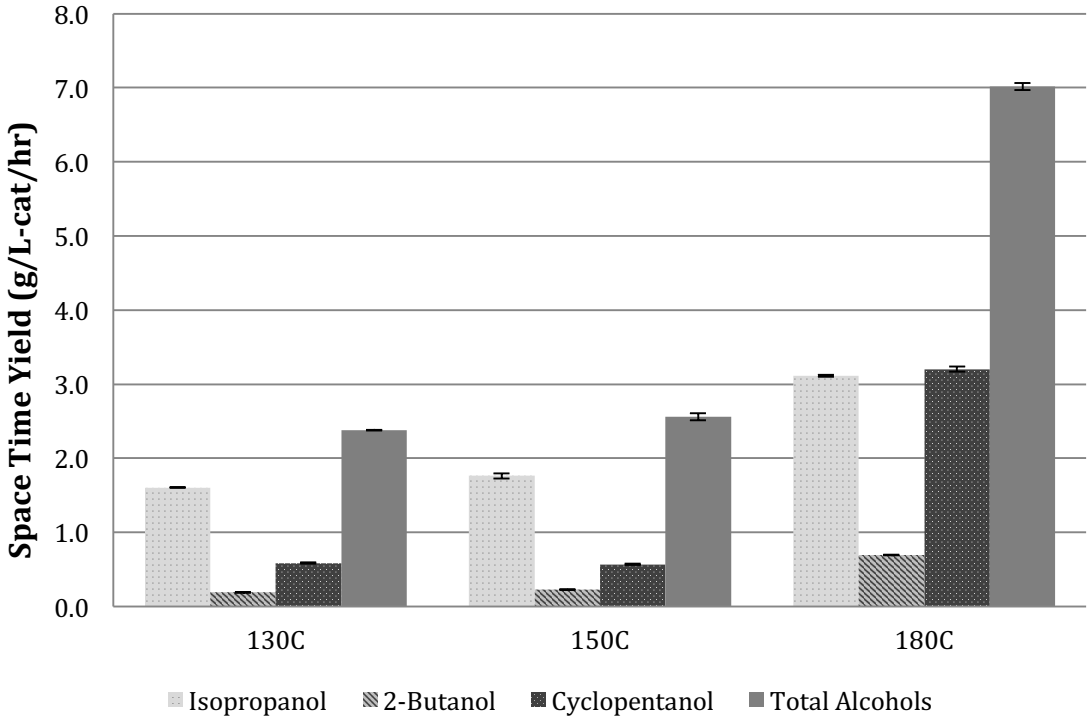

Figure 5.58 Space time yields versus temperature using Pd-ACM (0.8 wt%). Reaction conditions: P= 300 psi (H_2), WHSV= 0.0538 hr^{-1}, LHSV 0.389 hr^{-1}

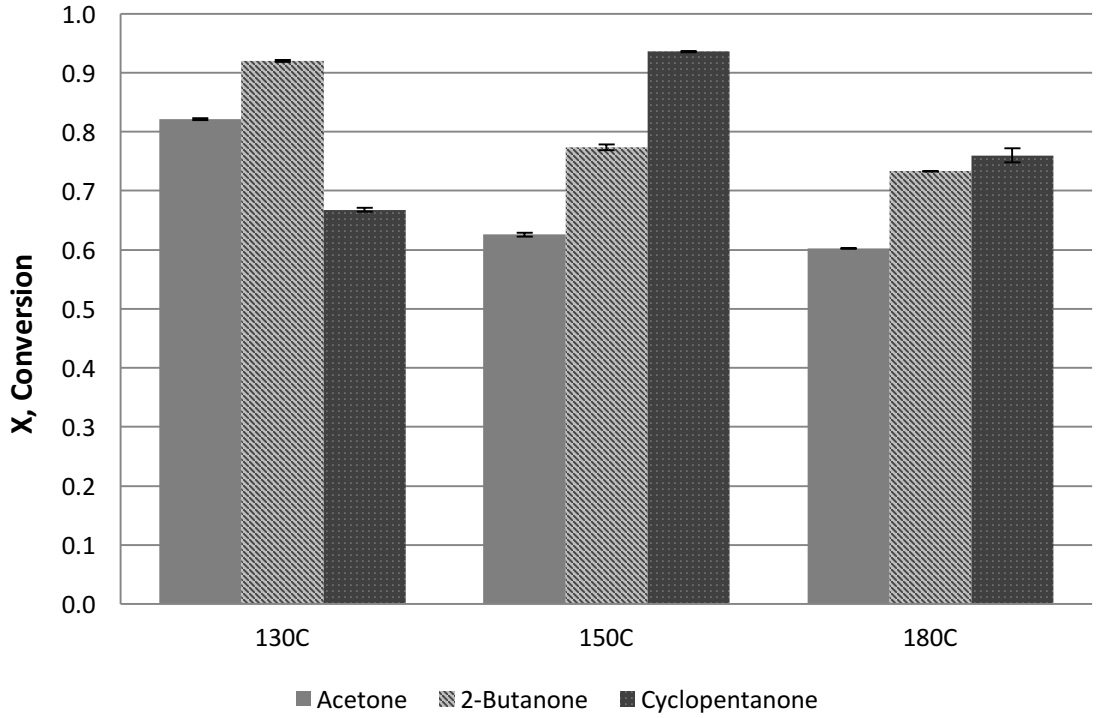

Figure 5.59 Ketone conversion versus temperature using Pd-ACM (0.8 wt%). Reaction conditions: P= 300 psi (H_2), WHSV= 0.0538 hr^{-1}, LHSV 0.389 hr^{-1}

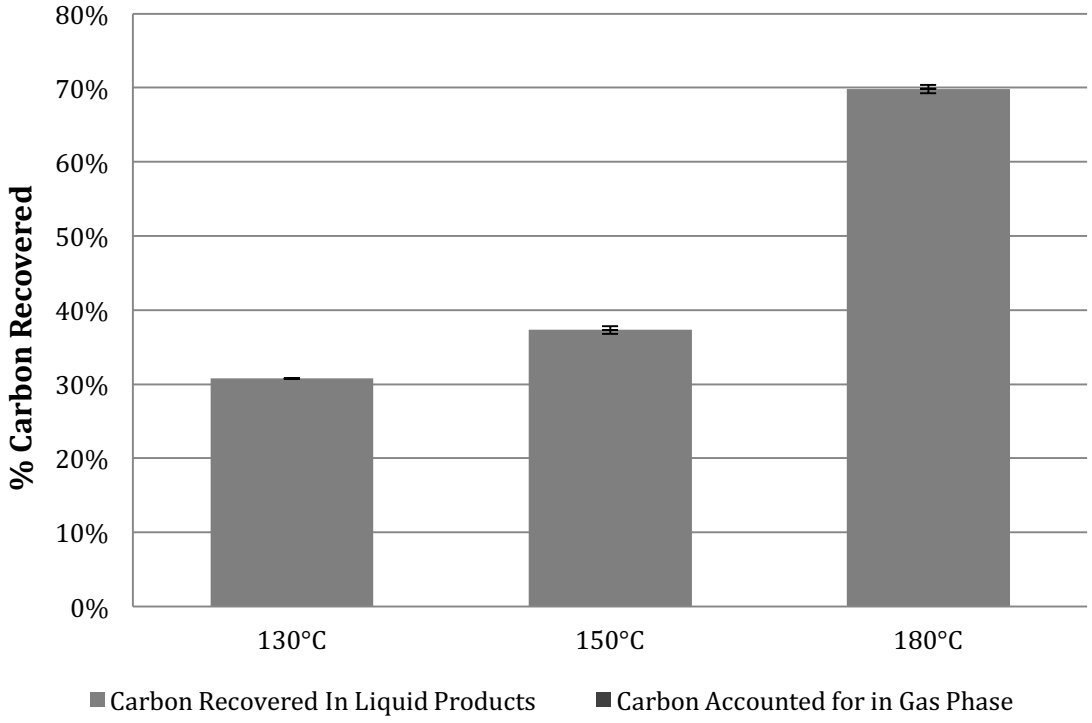

Figure 5.60 Carbon recovery versus temperature using Pd-ACM (0.8 wt%). Reaction conditions: P= 300 psi (H_2), WHSV= 0.0538 hr^{-1}, LHSV 0.389 hr^{-1}

5.3.3 Comparison of Pd-C Monoliths and Pd-C Granules for Hydrogenation of Ketones

This study aims to compare the hydrogenation activity of Pd-C monoliths (Pd-ACM) with that of granulated Pd-C. Reactions were conducted using the best reaction conditions determined in section 5.3.1 and section 5.3.2 (180 °C, 300 psi), using the ketone model compound mixture (acetone, 2-butanone, cyclopentanone). Liquid hourly space velocity was varied by varying the reactant feed rate from 0.5 mL/min to 8.0 mL/min. Figure 5.61- Figure 5.63 compare space time yields with respect to isopropanol, 2-butanol, and cyclopentanol for Pd-C granules and Pd-ACM. Reactions using Pd-ACM achieved higher space time yields with respect to all three alcohol products. For

reactions using Pd-ACM at the higher LHSV tested, isopropanol space time yield exceeded 35 g/L-cat/hr, 2-butanol space time yield exceeded 9 g/L-cat/hr, and cyclopentanol space time yield approached 50 g/L-cat/hr. Space time yields for both catalysts increased linearly with increasing LHSV and did not appear to approach a maximum. Figure 5.64 and Figure 5.65 show higher observed reactions with respect to acetone for Pd-ACM comparted to Pd-C granules. In addition, Figure 5.64 and Figure 5.65 show that observed reaction rates increase linearly with increasing reactant feed rate. This suggests that the observed reaction rates are limited by the feed rate of reactants rather than reaction kinetics for the conditions tested. Figure 5.66 and Figure 5.67 show reactant conversion versus LHSV for Pd-C and Pd-ACM, respectively. Pd-ACM achieved higher conversions of reactants than Pd-C granules. There were no noticeable trends between conversion and LHSV for either catalyst. No products other than isopropanol, 2-butanol, and cyclopentanol were observed in any of the reactions conducted. The results of this study indicate that Pd-ACM catalysts achieved higher conversion and space time yields than Pd-C for all conditions tested despite lower palladium loading (0.8% versus 5%for granular Pd-C). These results demonstrate the advantages of using monolith catalysts over traditional granular catalysts.

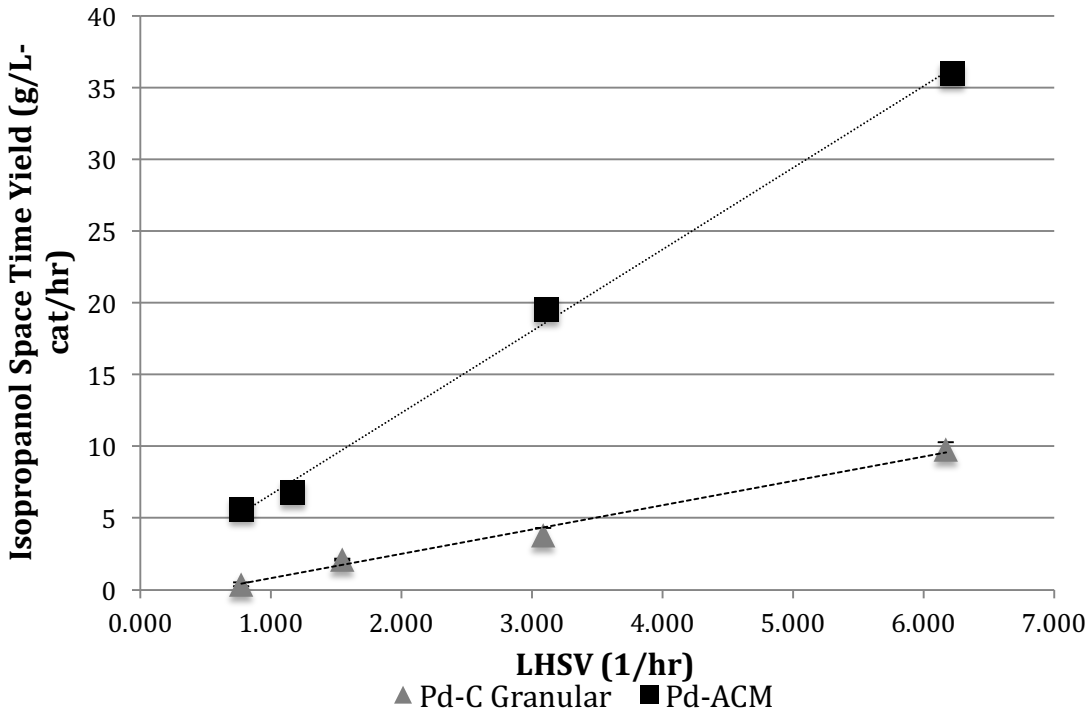

Figure 5.61 Isopropanol space time yield using Pd-ACM and Pd-C granules. Reaction conditions: P= 300 psi (H_2), T=180°C.

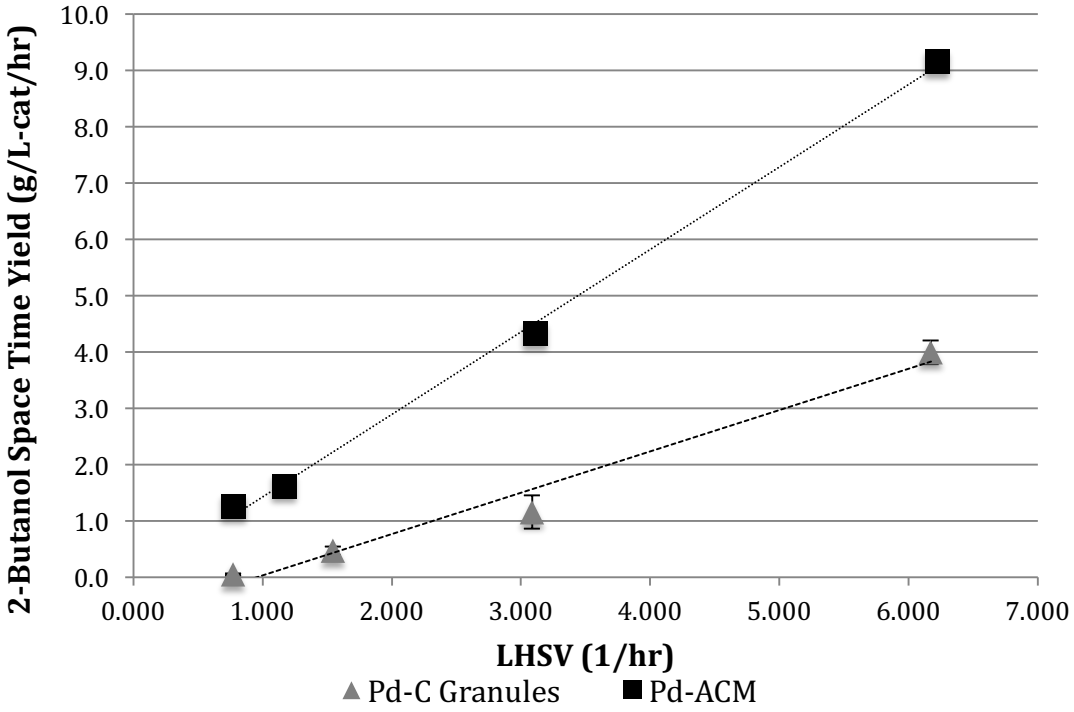

Figure 5.62 2-Butanol space time yield using Pd-ACM and Pd-C granules. Reaction conditions: P= 300 psi (H_2), T=180°C

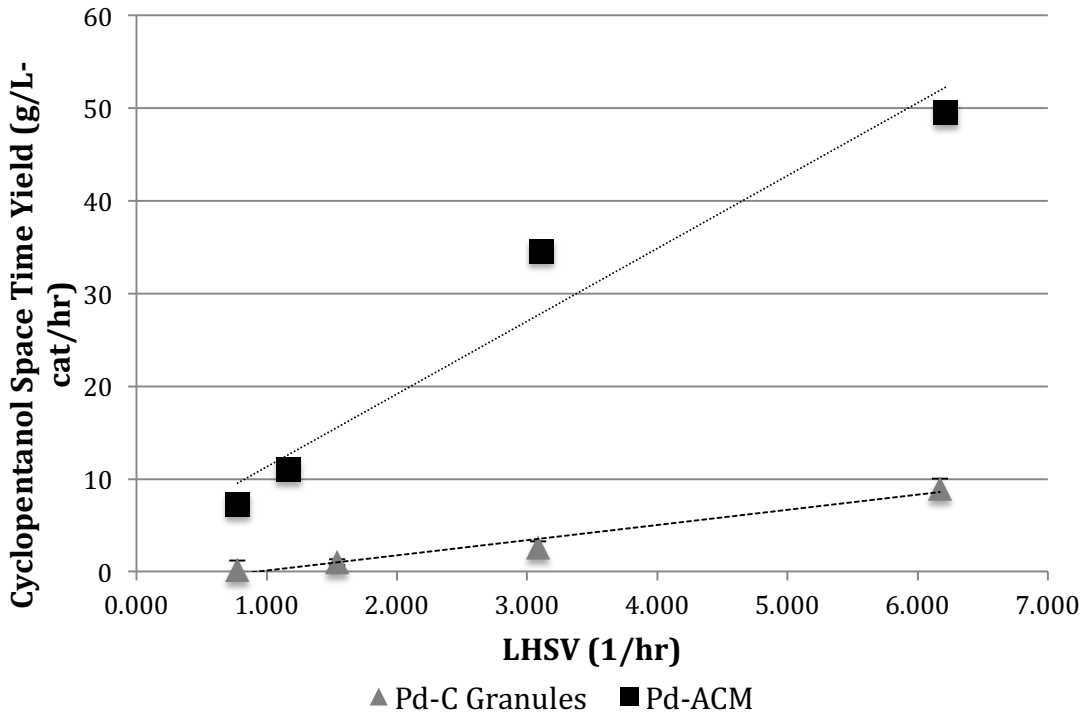

Figure 5.63 Cyclopentanol space time yield using Pd-ACM and Pd-C granules. Reaction conditions: P= 300 psi (H_2), T=180°C

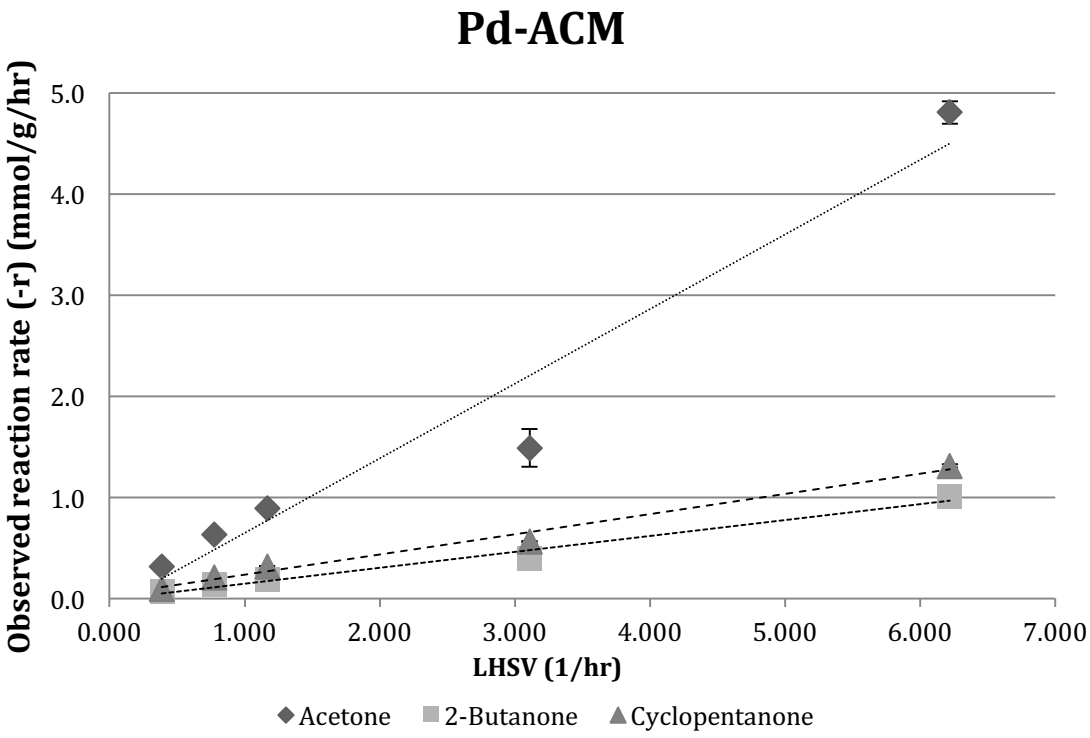

Figure 5.64 Observed reation rates versus LHSV using Pd-ACM. P= 300 psi (H_2), T=180°C

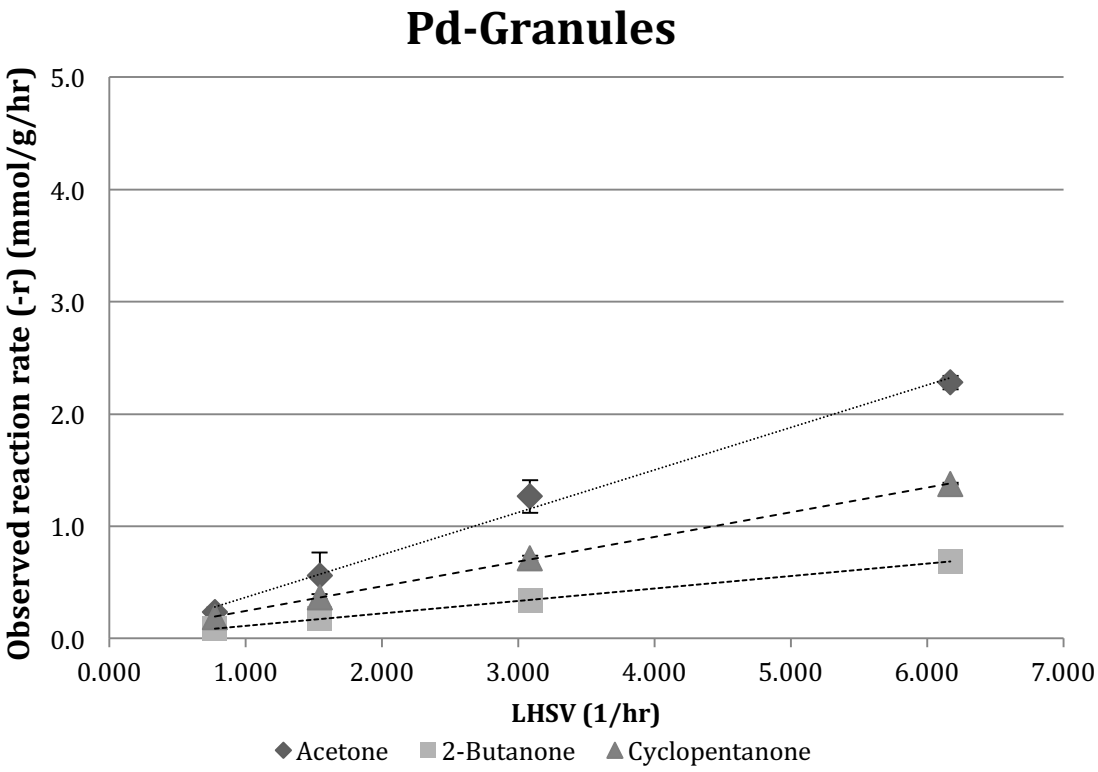

Figure 5.65 Observed reation rates versus LHSV using Pd-C granules. P= 300 psi (H_2), T=180°C

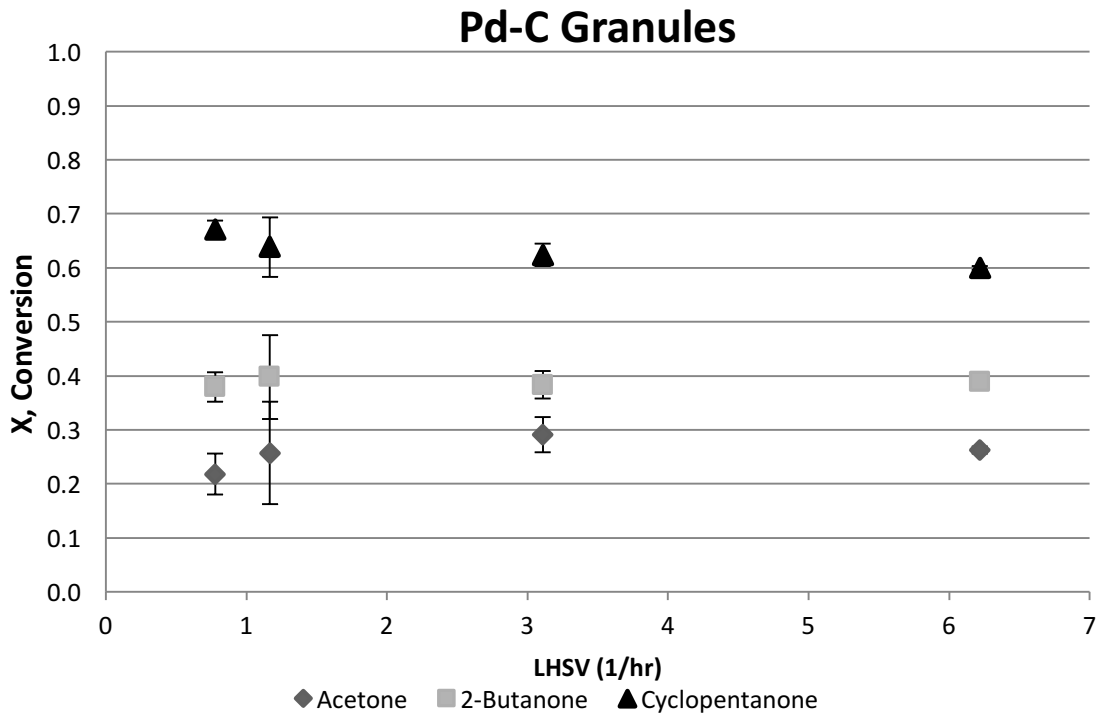

Figure 5.66 Conversion of reactants versus LHSV using Pd-C granules. P= 300 psi (H_2), T=180°C

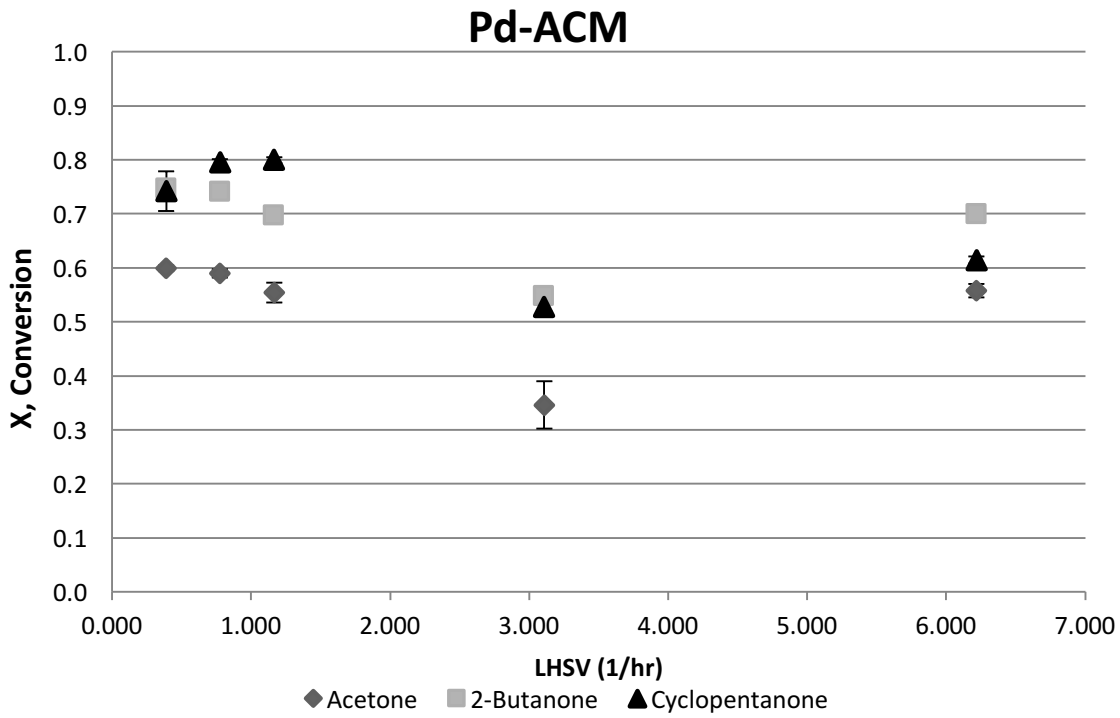

Figure 5.67 Conversion of reactants versus LHSV using Pd-ACM (monlith). P= 300 psi (H_2), T=180°C

5.3.4 Hydrogenation of Ketones Using Red Mud and Fe-SiAl

Previous studies in sections 5.2.5 and 5.2.6 explored reduced red mud and Fe-SiAl for simultaneous ketonization and hydrogenation activity. When using reduced red mud and Fe-SiAl to convert a mixture of carboxylic acids to ketones in the presence of hydrogen, ketonization activity was observed, but none of the hydrogenation products from ketones were detected. In order to further study the hydrogenation activity of reduced red mud and Fe-SiAl, hydrogenation reactions were conducted using model compound mixtures of ketones (acetone, 2-butanone, and cyclopentanone). Figure 5.68 - Figure 5.71 show alcohol selectivity, space time yield, and conversion of ketones using

red mud and Fe-SiAl pre-reduced at 400°C and 500°C using the following reaction conditions in a packed bed reactor: P= 300 psi (H_2), reaction temperature= 400 °C, WHSV= 0.1262 hr^{-1}. Interestingly, reactions using Fe-SiAl lead to 60-80% conversion of ketones, although none of the expected hydrogenation products (isopropanol, 2-butanol, or cyclopentanol) were detected in the liquid products. In addition, acetic acid (≈ 2 g/L) was detected in the liquid products for Fe-SiAl-400 and Fe-SiAl-500, but the mechanism of acetic acid formation is unclear. Total alcohol space time yields for RRM-400 and RRM-500 approached 2.5 g/L-cat/hr and 4.5 g/L-cat/hr, respectively. Red mud reduced at 500°C showed higher selectivity for alcohols, but achieved lower conversion of acetone. The results of these experiments indicate that red mud does exhibit activity for hydrogenation of ketones to alcohols, and increasing reduction pretreatment temperature for 400°C to 500°C increases selectivity for alcohol products, most likely due to the increased concentration of zero valent iron. However, red mud reduced at 500°C showed much lower hydrogenation activity compared to that of Pd-ACM in section 5.3.3. Conversions of acetone, 2-butanone, and cyclopentanone ranged from 10- 27% using RRM-500 (compared to 60-80% achieved using Pd-ACM). Total alcohol space time yield using red mud was also significantly lower (4.4 g/L-cat/hr compared to 7 g/L-cat/hr achieved using Pd-ACM at similar conditions).

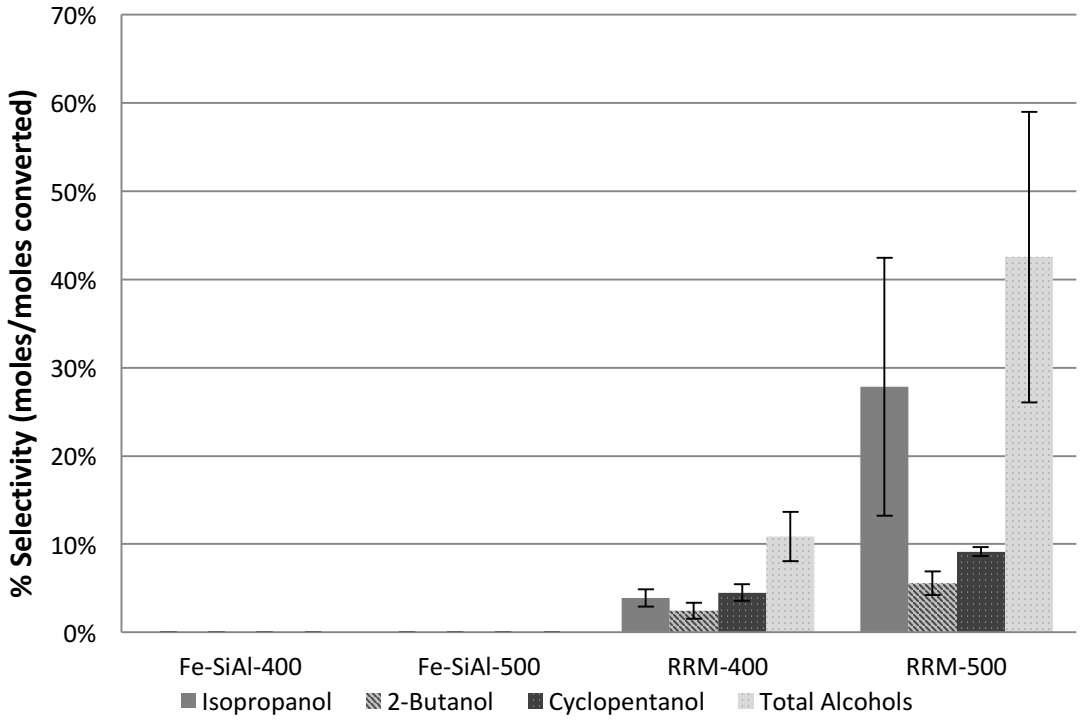

Figure 5.68 Alcohol selectivity using red mud (RRM) and Fe-SiAl reduced at 400°C and 500°C. Reaction conditions: P= 300 psi (H_2), T= 400 °C, WHSV= 0.1262 hr^{-1}

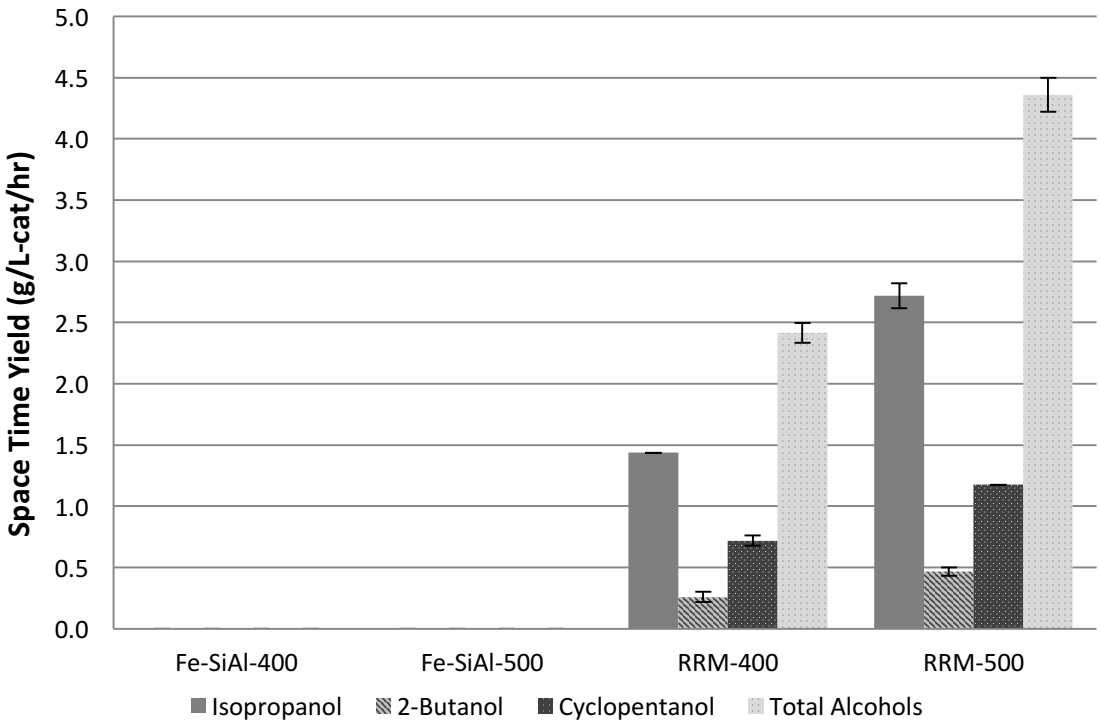

Figure 5.69 Space time yields using red mud (RRM) and Fe-SiAl reduced at 400°C and 500°C. Reaction conditions: P= 300 psi (H_2), T= 400 °C, WHSV= 0.1262 hr^{-1}

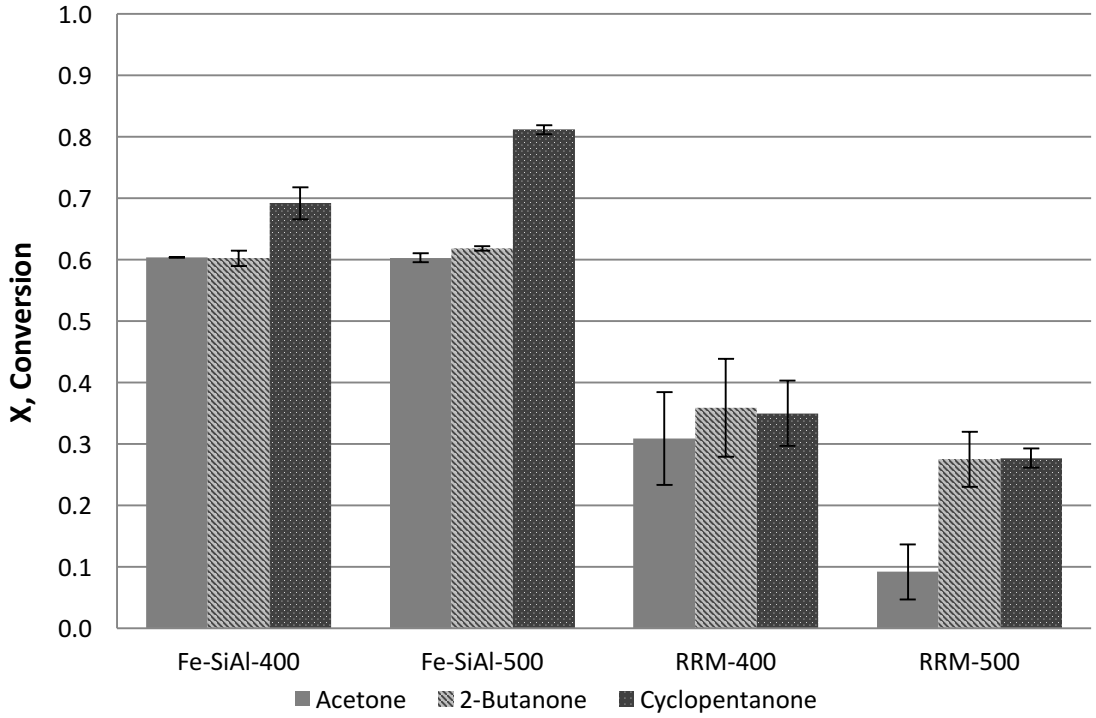

Figure 5.70 Conversion of ketones using red mud (RRM) and Fe-SiAl reduced at 400°C and 500°C. Reaction conditions: P= 300 psi (H_2), T= 400 °C, WHSV= 0.1262 hr^{-1}

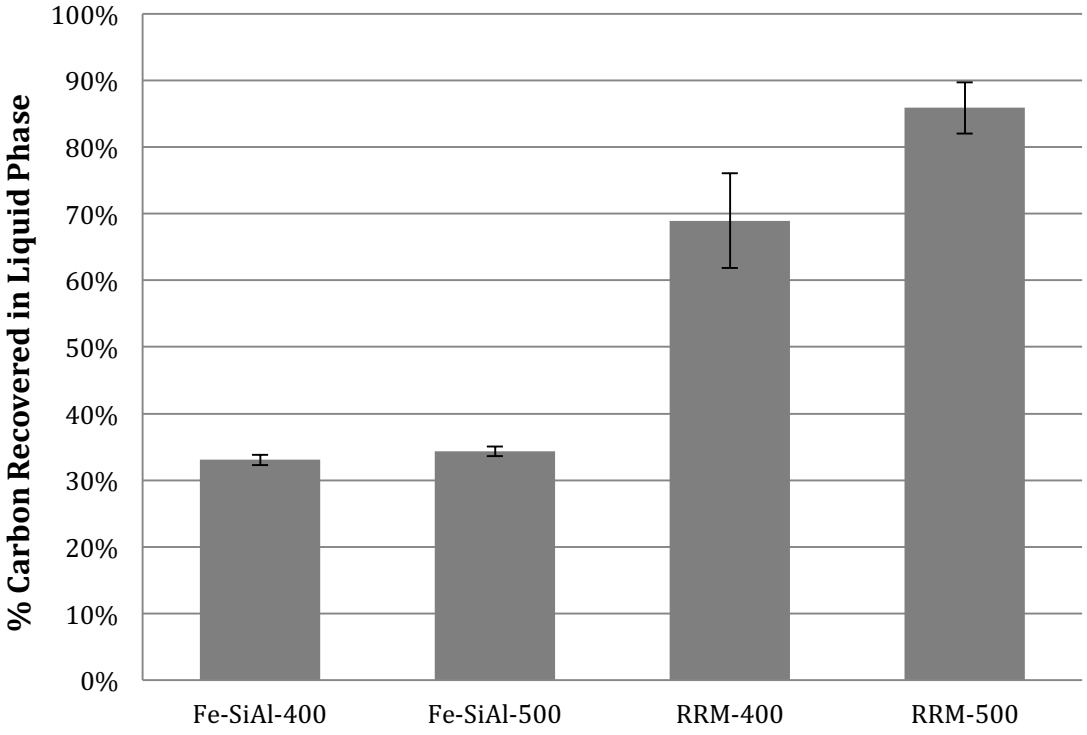

Figure 5.71 Carbon recovery using red mud (RRM) and Fe-SiAl reduced at 400°C and 500°C. Reaction conditions: P= 300 psi (H_2), T= 400 °C, WHSV= 0.1262 hr^{-1}. No carbon was detected in the gas phase.

5.4 2-Stage Ketonization/Hydrogenation Studies

Previous hydrogenation experiments used aqueous model compound mixtures of acetone, 2-butanone, and cyclopentanones. In the following 2-stage experiments, the liquid products generated in ketonization reactions were used as a feedstock for hydrogenation studies in a continuous reactor system. The best reaction conditions determined from ketonization studies in sections 5.2.1 and 5.2.2 were used for stage 1 (RRM-300, T= 400°C, P= atm (N_2), WHSV = 0.21 g/g-cat/hr, LHSV= 1.41 hr^{-1}). Products from stage 1 were then fed into 2nd stage hydrogenation reactions using Pd-C

and Pd-ACM at the best reaction conditions determined in sections 5.3.2 and 5.3.3 (T= 180 °C, P= 300 psi (H_2), LHSV= 0.78 hr^{-1}). Figure 5.72 and Figure 5.73 show alcohol selectivity and space time yields achieved in the 2nd stage hydrogenation reactions using Pd-C granules and Pd-ACM. Selectivity and space time yields achieved in hydrogenation reactions with model compounds under similar conditions (section 5.3.2) are included for comparison. Pd-ACM showed selectivity for isopropanol, 2-butanol, and cyclopentanol, whereas no 2-butanol or cyclopentanol was detected using Pd-C granules. Pd-ACM achieved significantly higher isopropanol space time yield compared to Pd-C granules (4.2 vs 0.7 g/L-cat/hr). Space time yields for all products were lower in 2-stage experiments compared to 1-stage hydrogenation reactions that used aqueous model compound mixtures (acetone, 2-butanone, and cyclopentanones). Interestingly, ethanol (≈ 3 g/L) was formed in the 2nd stage hydrogenation reaction using Pd-ACM, but not using Pd-C granules. Ethanol was likely formed via hydrogenation of acetic acid, which was not completely converted in stage 1 (≈ 12 g/L was left over). HDO catalysts typically have very low activity for hydrodeoxygenation of carboxylic acids, which are more difficult to convert than aldehydes, ketones, or esters (Nakagawa et al., 2015). These results suggest that Pd-ACM catalysts exhibit “deeper” hydrogenation activity than traditional Pd-C catalysts.

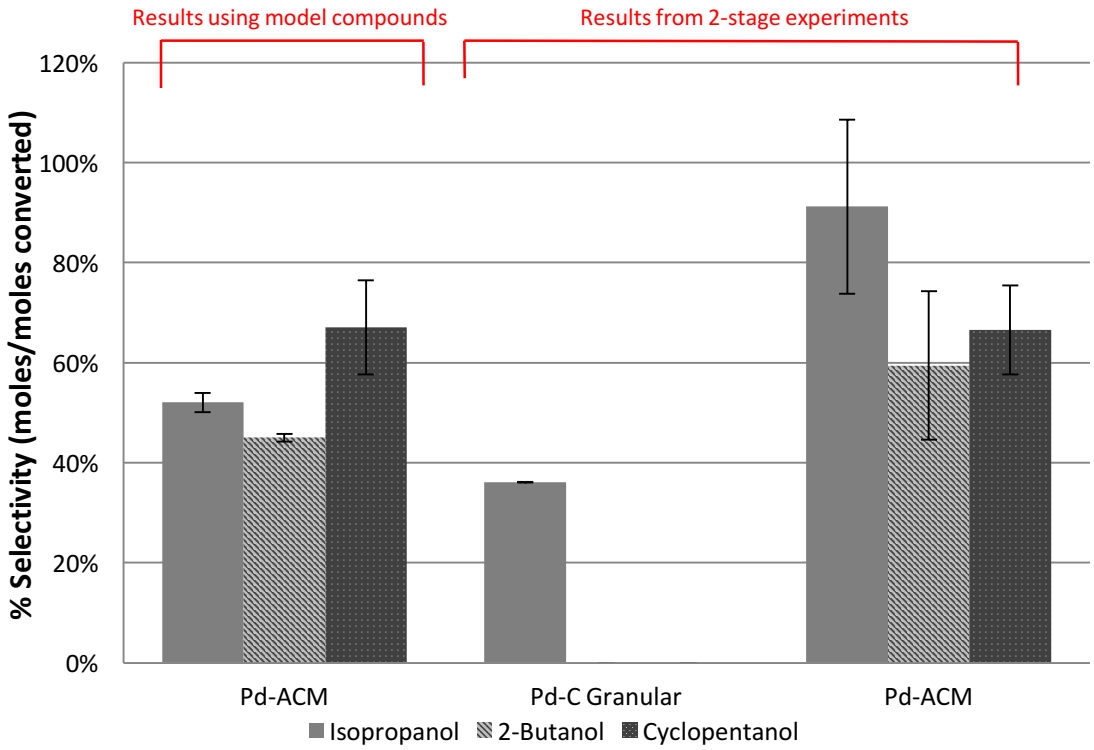

Figure 5.72 Comparison of alcohol selectivity for granulated Pd-C (5 wt% Pd) and Pd-ACM (activated carbon monolith, 0.8 wt% Pd) in 2nd stage hydrogenation reaction using liquid products from ketonization as feedstocks. Reaction temperature= 180°C, P= 300 psi (H_2), LHSV= 0.78 hr^{-1}. Data from previous hydrogenation experiments using Pd-ACM with model compounds (1 stage hydrogenation only) is shown for comparison. Granular Pd-C

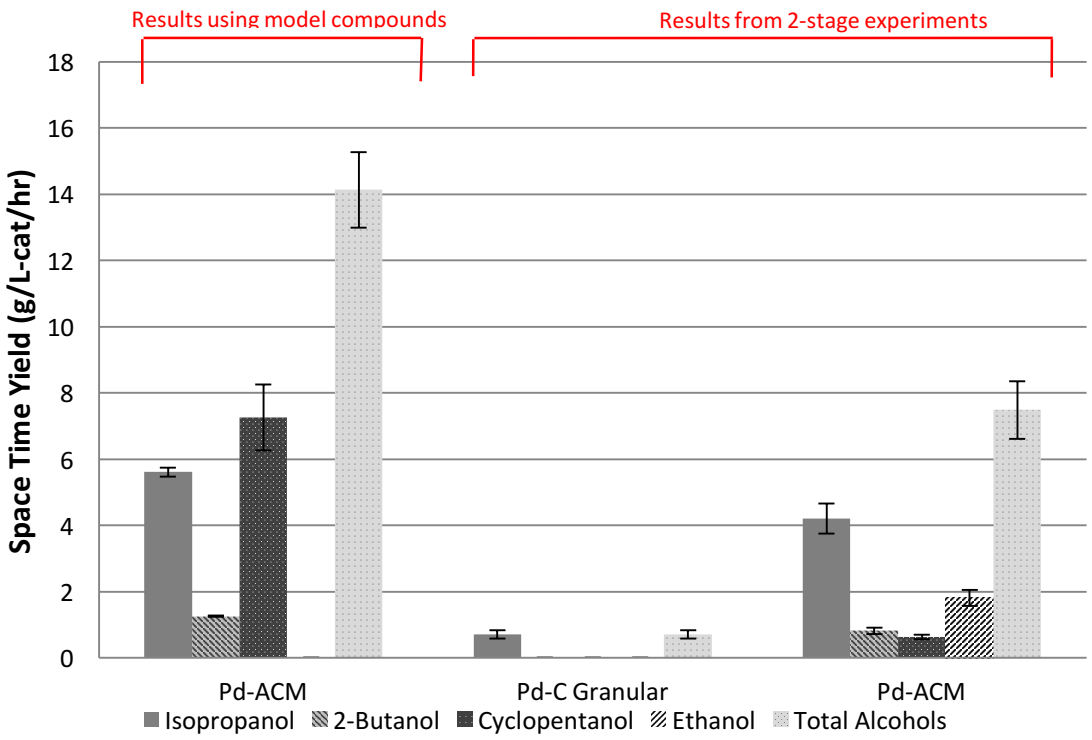

Figure 5.73 Comparison of alcohol space time yields for granulated Pd-C (5 wt% Pd) and Pd-ACM (activated carbon monolith, 0.8 wt% Pd) in 2nd stage hydrogenation reaction using liquid products from ketonization as feedstocks. Reaction temperature= 180°C, P= 300 psi (H_2), LHSV= 0.78 hr^{-1}. Data from previous hydrogenation experiments using Pd-ACM with model compounds (1 stage hydrogenation only) is shown for comparison.

Chapter 6 Conclusions and Recommendations

6.1 Ketonization studies

The results indicate that conversion of oxygenates in aqueous extracted bio-oil to higher value compounds with greater energy density and stability is possible in a continuous process using red mud as a catalyst. Reaction rates were similar to those reported using $CeZrO_x$, but no significant reactor plugging was observed (Hakim et al., 2013). RRM-300 was highly stable in a 6.6-hour study, showing only a 4% decline in conversion of acetic acid, and little coke formation was observed (0.035 g/g-cat). Increasing reduction pre-treatment temperature led to lower ketone selectivity and yield, likely due to lower surface area and lower concentration of magnetite and strong basic sites. It was theorized that RRM-400 could ketonize carboxylic acids and simultaneously hydrogenate ketone products to form alcohols, but simultaneous ketonization/hydrogenation was not observed, even when hydrogen was added externally. However, increasing reduction temperature did lead to an increase in hydrogenation activity in separate hydrogenation studies using a model compound mixture of acetone, 2-butanone, and cyclopentanone. This suggests that a 2-stage process using red mud for both ketonization and hydrogenation of aqueous extracted bio-oil may be possible. Further studies using red mud in two separate packed beds with separate reaction conditions are recommended.

It was demonstrated that pressures above 1 atmosphere inhibit the formation of cyclic ketones and favor formation of linear pentanones. This effect was also observed

when hydrogen was added externally. A shift in the reaction pathway due to increased hydrogen availability was proposed. Further ketonization studies using individual compounds (acetol, acetic acid, and levoglucosan) are recommended in order to verify this theory.

Ketonization studies using Fe-SiAl showed the formation of the same products as seen in studies with red mud, which suggests that the ketonization pathway theorized for red mud (Figure 5.17) is also valid for Fe-SiAl. Despite much higher surface area (400 m^2/g vs 30 m^2/g for RRM-300), Fe-SiAl showed lower activity for ketonization reactions compared to RRM-300. This was attributed to lower dispersion and deactivation due to coke formation. Additional studies that expand upon this work using iron oxide catalysts doped with promoting metals (Na and K) are recommended.

6.2 Hydrogenation Studies

The results of hydrogenation studies demonstrate the usefulness of Pd monolith catalysts in upgrading aqueous-extracted bio-oil oxygenates, and the advantages of monolith catalysts over granulated catalysts. In studies using a model compound mixture of ketones, conversion of reactants and product space time yields were significantly higher using Pd-ACM compared to Pd-C for all residence times ($LHSV^{-1}$) tested. Pd-ACM showed higher activity despite significantly lower Pd loading than granulated Pd-C. The manufacture of catalysts requiring less rare-earth materials is important in order to bring down processing costs of biofuel refining.

In addition to model compound studies, 2-stage ketonization/hydrogenation of bio-oil oxygenates was demonstrated in two separate continuous reactions. Ketonization

using RRM-300 followed by hydrogenation using Pd-ACM showed the best results. Space time yield of total alcohols approached 8 g/L-cat/hr in 2nd stage hydrogenation reactions using Pd-ACM. Pd-ACM was able to hydrogenate acetic acid directly to ethanol, which was not observed using Pd-C granules. The ability to catalyze "deep" hydrogenation of carboxylic acids makes Pd monoliths attractive for future studies involving hydrogenation of bio-oil oxygenates. Future studies that investigate catalyst longevity in 2-stage ketonization/hydrogenation reactions using actual bio-oil rather than model compounds are highly recommended.

Chapter 7 Calculations

7.1 List of Parameters used in Kinetic Studies

Several important parameters involved in reaction kinetics include conversion of reactants, product yield/selectivity, space time yield, and reaction rates. These variables were calculated for each reaction using parameters that are directly measured, such as reactant and product concentrations (measured via GC/FID). Table 7.1 lists important parameters that were used in kinetic calculations and their respective units. Reaction kinetic parameters were calculated using Equation 1- Equation 11. These parameters were used to evaluate the effectiveness of each catalyst.

Table 7.1 Parameters and units for calculations

Symbol	Description	Units	
MW_A	Molecular weight of species A	g/mol	Defined
C^{out}	Outlet concentration	mol/L	Measured
C^{in}	Inlet concentration	mol/L	Measured
F^{out}	Outlet molar flow rate	mol/hr	Calculated
F^{in}	Inlet molar flow rate	mol/hr	Calculated
F_T	Total molar flow rate	mol/hr	Calculated
Q^{out}	Outlet volumetric flow rate	mL/min	Calculated
Q^{in}	Inlet volumetric flow rate	mL/min	Measured
Q_{gas}	Carrier gas flow rate	mL/min	Measured
M_{feed}	Mass of product fed	g	Measured
M_{prod}	Mass of product recovered	g	Measured
t	Reaction time	minutes	Calculated
ρ_{cat}	Catalyst density	g/mL	Measured
ρ_{feed}	Feedstock density	g/mL	Measured
W	Catalyst Mass	g	Measured

χ	Fractional Conversion	unit less	Calculated
y	Yield	mol produced/total mol fed	Calculated
s	Selectivity	mol prod/total mol conv	Calculated
r	Reaction rate	mmol/g-cat/hr	Calculated
WHSV	Weight hourly space velocity	gA/g-cat/hr	Calculated
LHSV	Liquid hourly space velocity	1/hr	Calculated
GHSV	Gas hourly space velocity	1/hr	Calculated

7.2 List of Equations used in Kinetic Studies

Equation 1 Reaction time

$$t = \frac{M_{feed}}{\rho * Q^{in}}$$

Equation 2 Outlet volumetric flow rate

$$Q^{out} = \frac{M_{prod}}{t}$$

Equation 3 Outlet molar flow rate

$$F_A^{out} = C_A^{out} * Q^{out} * \frac{60}{1000}$$

Equation 4 Total molar flow rate

$$F_T = \sum_{species} F^A$$

Equation 5 Fraction conversion

$$\chi_A = 1 - \frac{F_A^{out}}{F_A^{in}}$$

Equation 6 Yield

$$y_A = \frac{F_A^{out}}{F_T^{in}}$$

Equation 7 Selectivity

$$s_a = \frac{F_A^{out}}{F_T^{in} - F_T^{out}}$$

Equation 8 Reation Rate

$$r_A = \frac{F_A^{out} - F_A^{in}}{W} * 1000$$

Equation 9 Weight hourly space velocity

$$WHSV = \frac{MW^A * F_A^{in}}{W}$$

Equation 10 Liquid hourly space velocity

$$LHSV = \frac{Q^{in} * \rho_{cat}}{W * 60}$$

Equation 11 Gas hourly space velocity

$$GHSV = \frac{Q_{gas} * \rho_{cat}}{W} * 60$$

7.3 Brunauer-Emmet-Teller and Barret-Joyner-Halenda Calculations

Surface area was calculated by BET analysis, based on the principal that a gas near its boiling point will physically adsorb to the surface of a solid at pressures below its saturation pressure (Kershenbaum, 1982). The amount of gas adsorbed (V, cc-STP) on solid catalysts as a function of relative pressure (P/P_o) was measured using a Quantachrome Austosorb-1C (section 4.2.4.3). The monolayer coverage volume (V_m, cc-STP) can be calculated using Equation 12 by plotting $\frac{P}{V(P_o-P)}$ vs $\frac{P}{P_o}$. Surface area is then

calculated using the cross sectional area of the adsorbing molecule. Equation 13 is used for N_2 at 195.6 °C.

Equation 12 Linearized BET Equation

$$\frac{P}{V(P_o - P)} = \frac{1}{V_m C} + \frac{C-1}{V_m C}\frac{P}{P_o}$$

Equation 13 Surface area using N_2 at -195.6°C

$$S.A. = \frac{4.28\, V_m}{wt.}$$

S.A.= surface area (m^2/g), wt.= weight of catalyst (g)

Pore volume distribution was calculated using the nitrogen desorption (BJH) method. This is based on the principle that low temperature nitrogen adsorption at higher pressures results in multilayer adsorption that eventually bridges pores. Continued nitrogen uptake takes place via capillary condensation, which occurs first for smaller pores and then for larger pores (Kershenbaum, 1982). After collecting adsorption and desorption curves at P/P_o values from 0 to 1, the modified Kelvin equation (Equation 14) can be used to calculate pore radius, r. For N_2 at 78 K, Equation 14 can be simplified to Equation 15.

Equation 14 Modified Kelvin Equation

$$\ln\left(\frac{P_o}{P}\right) = \frac{2\sigma V_o cos\theta}{(r-t)RT}$$

$$\text{where film thickness } \; t = 7.34\left(ln\frac{P_o}{P}\right)^{-\frac{1}{3}}$$

V_0= pore volume when completely filled; σ= surface tension of fluid;

Equation 15 Modified Kelvin Equation simplified for N_2 at 78 K

$$r = t + 8.83 \left(ln \frac{P_o}{P} \right)^{-1}$$

where r and t have units of Å

7.4 Dispersion Calculations

Dispersion was calculated using H_2 pulse titration (described in section 4.2.4.6). The fraction of active atoms that are available on the surface (dispersion) can be calculated based on the fact that certain gases selectively chemisorb only active metals. Knowing the total active metal loading, specific hydrogen uptake, and the following stoichiometry, dispersion can be calculated using Equation 16.

$$Pd_{surface} + 2H \rightarrow Pd_{surface}\text{-}H$$

Equation 16 Dispersion

$$D = \frac{Pd_{surface}}{Pd_{total}}$$

7.5 Statistics

Error bars that were calculated for reaction rates, product yields, selectivity, conversion, and several other parameters represent 95% confident intervals. These statistics are based on duplicate analysis of liquid and gas products collected from each reaction. All quantitative analyses including GC-FID, HPLC, and GC-TCD were

conducted in duplicate. Data collected in the first replicate was used to calculate each parameter (yield, selectivity, conversion, etc.). The same calculations were then performed using data from the second replicate. Standard deviations were estimated based on the sample range of the two values calculated from each of the two replicates. This estimation method is based on the fact that for a random sample of size *n* from a normal population, the sampling distribution of the sample range *R* has a mean equal to $d_2\sigma$ (Miller & Freund, 1985). Thus, the standard deviation of a sample of size 2 can be estimated using Equation 17.

Equation 17 Estimation of standard deviation for small sample size (Miller & Freund, 1985)

$$\sigma \cong \frac{R}{d_2}$$

where R = range of sample; d_2 = 1.128 for n = 2

Although *t* tests were not conducted for all the parameters discussed in Chapter Chapter 5, Equation 18 provides an example of how a two-sample *t* test can be conducted using the data presented:

Equation 18 *t* statistic for comparing two means from small samples

$$t = \frac{(\tilde{x}_1 - \tilde{x}_2)}{\sqrt{(n_1 - 1)s_1^2 + (n_2 - 1)s_2^2}} \sqrt{\frac{n_1 n_2 (n_1 + n_2 - 2)}{n_1 + n_2}}$$

where x_a = mean of sample a; n_a = sample size of a; s_a^2 = sample variance of a

The *t* statistic calculated in Equation 18 is then compared with values of t_α for a significance level of 0.05 (from *t* table). The null hypothesis states that there is no statistical difference between the means of the two samples. The null hypothesis is rejected if $t < - t_\alpha$.

It is important to note that the statistics reported in this study only account for variance from analytical measurements and not variance from reactions in the packed bed reactor system. Variance from reactions could be accounted for by performing multiple replicates of each reaction in future studies. However, this was not feasible for this study, given the number of reactions that were conducted.

Chapter 8 Works Cited

Albrecht, K. O., Dagle, R. A., & Howe, D. T. (Producer). (2015). Characterization and Valorization of Aqueous Phases Derived from Liquefaction and Upgrading of Bio-oils. *DOE Bioenergy Technologies Office (BETO) 2015 Project Peer Review*. [Presentation]

Alvarez, J., Rosal, R., Sastre, H., & Diez, F. (1998). Characterization and deactivation studies of an activated sulfided red mud used as hydrogenation catalyst. *Applied Catalysis A: General, 167*(2), 215-223.

Boe, R. (Producer). (2012). Luftbilder von der Nordseeküste. [Photograph]

Bridgwater, A. V. (2011). Review of fast pyrolysis of biomass and product upgrading. *Biomass and Bioenergy, 2011*, 1-27.

Brillis, A. A., & Manos, G. (2003). Coke Formation during Catalytic Cracking of C8 Aliphatic Hydrocarbons over Ultrastable Y Zeolite. *Industrial & Engineering Chemistry Research, 42*, 2292-2298.

Bryden, K., & Habib, E. T. (2013). *Flexible Pilot Plant Technology for Evaluation of Unconventional Feedstocks and Processes*. Paper presented at the AFPM Annual Meeting, San Antonio, TX.

Chen, C. H., Yu, M. S., Tsao, C. S., Chuang, H. Y., Tseng, H. H., & Chung, T. Y. (2012). Characterization of hydrogen adsorption in platinum-doped microporous carbon with varied catalytic properties. *Microporous and Mesoporous Materials, 152*, 157–162.

Chen, K. D., Fan, Y. N., & Yan, Q. J. (1997). Metal–Support Interactions in Fe/ZrO2 Catalysts for Hydrogenation of CO. *Journal of Catalysis, 167*, 573–575.

Chompoonut, R., & Vithaya, R. (2005). A Density Functional Study of Propylene Glycol Conversion to Propanal and Propanone of Various Acid-Catalyzed Reaction Models: A Water-Addition Effect. *Journal Of Computational Chemistry, 26*(15), 1592-1599.

Crozier, P. A., Sharma, R., & Datye, A. K. (1998). Oxidation and Reduction of Small Palladium Particles on Silica. *Microscopy And Microanalysis, 4*(3), 278-285.

Dorner, R. W., Hardy, D. R., Williams, F. W., & Willauer, H. D. (2009). K and Mn doped iron-based CO2 hydrogenation catalysts: Detection of KAlH4 as part of the catalyst's active phase. *Applied Catalysis A: General*(373 (2010)), 112-121.

Elliott, D. C., Hart, T. R., Neuenschwander, G. G., Rotness, L. J., Olarte, M. V., Zacher, A. H., & Solantausta, Y. (2012). Catalytic Hydroprocessing of Fast Pyrolysis Bio-oil from Pine Sawdust. *Energy and Fuels, 26*(6), 3891-3896.

Hakim, S. H., Shanks, B. H., & Dumesic, J. A. (2013). Catalytic upgrading of the light fraction of a simulated bio-oil over CeZrOx catalyst. *Applied Catalysis B: Environmental, 142-143 (2013)*, 368-376.

Hargus, C., Michalsky, R., & Peterson, A. (2014). Looped-oxide catalysis: a solar thermal approach to bio-oil deoxygenation. *Energy & Environmental Science, 7*(10), 3122-3134.

Hossain, A. K., & Davies, P. A. (2013). Pyrolysis liquids and gases as alternative fuels in internal combustion engines – A review. *Renewable and Sustainable Energy Reviews, 21*, 165–189.

Jollet, V., Gissane, C., & Schlaf, M. (2014). Optimization of the neutralization of Red Mud by pyrolysis bio-oil using a design of experiments approach. *Energy & Environmental Science, 7*(3), 1125-1133.

Karimi, E., Gomez, A., Kycia, S., & Schlaf, M. (2010). Thermal Decomposition of Acetic and Formic Acid Catalyzed by Red Mud-Implications for the Potential Use of Red Mud as a Pyrolysis Bio-Oil Upgrading Catalyst. *Energy & Fuels, 24*(4), 2747-2757.

Karimi, E., Teixeira, I. F., Gomez, A., de Resende, E., Gissane, C., Leitch, J., & Schlaf, M. (2014). Synergistic co-processing of an acidic hardwood derived pyrolysis

bio-oil with alkaline Red Mud bauxite mining waste as a sacrificial upgrading catalyst. *Applied Catalysis B: Environmental, 145*, 187-196.

Karimi, E., Tiexeria, I. F., Ribeiro, L. P., Gomez, A., Lago, R. M., Penner, G., . . . Schlaf, M. (2012). Ketonization and deoxygenation of alkanoic acids and conversion of levulinic acid to hydrocarbons using a Red Mud bauxite mining waste as the catalyst. *Catalysis Today*(190), 73-88.

Kastner, J. R., Hilten, R., Weber, J. W., McFarlane, A. R., Hargreaves, J. S. J., & Batra, V. S. (2015). Continuous catalytic upgrading of fast pyrolysis oil using iron oxides in red mud. *RSC Advances, 5*, 29375-29385.

Kershenbaum, L. S. (1982). Chemical engineering kinetics (3rd edition) by J. M. Smith, McGraw Hill Book Company. *AIChE Journal, 28*(1), 298-322. doi:10.1002/aic.690280127

Miller, I., & Freund, J. E. (1985). *Probabilty and Statistics for Engineers* (3rd ed.). NJ: Prentice Hall.

Moulijn, J. A., Kreutzer, M. T., Nijhuis, T. A., & Kapteijn, F. (2014). Monolithic Catalysts and Reactors: High Precision with Low Energy Consumption. *Advances in Catalysis, 54*, 249-327.

Nakagawa, Y., Liu, S., Tamura, M., & Tomishige, K. (2015). Catalytic Total Hydrodeoxygenation of Biomass-Derived Polyfunctionalized Substrates to Alkanes. *ChemSusChem, 8*, 1114-1132.

Narayanan, S., & Unnikrishnan, R. (1998). Acetone hydrogenation over co-precipitated Ni/Al2O3 , Co/Al2O3 and Fe/Al2O3 catalysts. *Journal of the Chemical Society - Faraday Transactions, 94*(8), 1123-1128.

Olcese, R., Bettahar, M. M., Malamanc, B., Ghanbajac, J., Tibavizcoa, L., Petitjeana, D., & Dufour, A. (2013). Gas-phase hydrodeoxygenation of guaiacol over iron-based catalysts. Effect of gases composition, iron load and supports (silica and activated carbon). *Applied Catalysis B: Environmental, 129*, 528–538.

Olcese, R. N., Lardier, G., Bettahar, M., Ghanbaja, J., Fontana, S., Carro, V., . . . Dufour, A. (2013). Aromatic Chemicals by Iron-Catalyzed Hydrotreatment of Lignin Pyrolysis Vapor. *ChemSusChem, 6*, 1490 – 1499.

Perlack, R. D., Wright, L. L., Turhollow, A. F., & Graham, R. L. (2005). *Biomass as feedstock for a bioenergy and bioproducts industry: the technical feasibility of a billion-ton annual supply*: Oak Ridge National Laboratory.

Pestman, R., Koster, R. M., Boellard, E., Kraan, A. M., & Ponec, V. (1998). Identification of the Active Sites in the Selective Hydrogenation of Acetic Acid to Acetaldehyde on Iron Oxide Catalysts. *Journal of Catalysis, 174*, 142-152.

Pestman, R., Koster, R. M., van Duijne, A., Pieterse, J. A. Z., & Ponec, V. (1997). Reactions of Carboxylic Acids on Oxides: 2. Bimolecular Reaction of Aliphatic Acids to Ketones. *Journal of Catalysis, 168*(2), 265-272.

Pham, T. N., Sooknoi, T., Crossley, S. P., & Resasco, D. E. (2013). Ketonization of Carboxylic Acids: Mechanisms, Catalysts, and Implications for Biomass Conversion. *ACS Catalysis*(3), 2456-2474.

Piskorz, J., Majerski, P., Radlein, D., & Scott, D. S. (1989). Conversion of Lignins to Hydrogcarbon Fuels. *Energy and Fuels, 3*, 723-726.

Resasco, D. E. (2011). *Journal of Physical Chemistry Letters, 2*, 2294-2295.

Steele, P., Puettmann, M. E., Penmetsa, V. K., & Cooper, J. E. (2012). Life-Cycle Assessment of Pyrolysis Bio-Oil Production. *Forest Products Journal, 64*, 326-334.

Sushil, S., & Batra, V. S. (2008). Catalytic applications of red mud, an aluminium industry waste: A review. *Applied Catalysis B: Environmental, 81 (2008)*, 64-77.

Tishchenko, V., Meile, C., Scherer, M. M., Pasakarnis, T. S., & Thompson, A. (2015). Fe2+ catalyzed iron atom exchange and re-crystallization in a tropical soil. *Geochimica Et Cosmochimica Acta, 148*, 191-202.

Vispute, T. P., & Huber, G. W. (2009). Production of hydrogen, alkanes and polyols by aqueous phase processing of wood-derived pyrolysis oils. *Green Chemistry, 11*(9), 1433 -1445.

Witsuthammakula, A., & Sooknoi, T. (2015). Selective hydrodeoxygenation of bio-oil derived products: ketones to olefins. *Catalysis Science and Technology, 5*, 3639–3648.

Xu, C., & Teja, A. S. (2006). Supercritical water synthesis and deposition of iron oxide (-Fe2O3) nanoparticles in activated carbon. *Journal of Supercritical Fluids*(39), 135-141.

Zacher, A. H., Olarte, M. V., Santosa, D. M., Elliott, D. C., & Jones, S. B. (2014). A review and perspective of recent bio-oil hydrotreating research. *Green Chem., 16 (2014)*, 491-515.